

UNITED STATES AIR FORCE RESEARCH LABORATORY

Determination of Aircraft Sonic Boom Noise Penetration into Seas, Bays, and Lakes for Environmental Assessment

Victor W. Sparrow

The Pennsylvania State University
157 Hammond Building
University Park PA 16802

February 1998

Final Report for the Period April 1996 to February 1998

20000721 072

DTC QUALITY INSPECTED 4

Approved for public release; distribution is unlimited.

Human Effectiveness Directorate
Crew System Interface Division
2610 Seventh Street
Wright-Patterson AFB OH 45433-7901

NOTICES

When US Government drawings, specifications, or other data are used for any purpose other than a definitely related Government procurement operation, the Government thereby incurs no responsibility nor any obligation whatsoever, and the fact that the Government may have formulated, furnished, or in any way supplied the said drawings, specifications, or other data, is not to be regarded by implication or otherwise, as in any manner licensing the holder or any other person or corporation, or conveying any rights or permission to manufacture, use, or sell any patented invention that may in any way be related thereto.

Please do not request copies of this report from the Air Force Research Laboratory. Additional copies may be purchased from:

National Technical Information Service
5285 Port Royal Road
Springfield, Virginia 22161

Federal Government agencies and their contractors registered with the Defense Technical Information Center should direct requests for copies of this report to:

Defense Technical Information Center
8725 John J. Kingman Road, Suite 0944
Ft. Belvoir, Virginia 22060-6218

DISCLAIMER

This Technical Report is published as received and has not been edited by the Air Force Research Laboratory, Human Effectiveness Directorate.

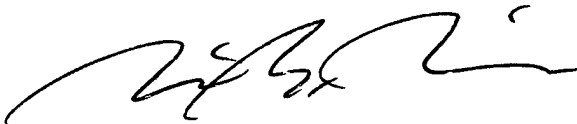
TECHNICAL REVIEW AND APPROVAL

AFRL-HE-WP-TR-2000-0064

This report has been reviewed by the Office of Public Affairs (PA) and is releasable to the National Technical Information Service (NTIS). At NTIS, it will be available to the general public.

This technical report has been reviewed and is approved for publication.

FOR THE COMMANDER



MARIS M. VIKMANIS
Chief, Crew System Interface Division
Air Force Research Laboratory

REPORT DOCUMENTATION PAGE			Form Approved OMB No. 0704-0188	
Public reporting burden for this collection of information is estimated to average 1 hour per response, including the time for reviewing instructions, searching existing data sources, gathering and maintaining the data needed, and completing and reviewing the collection of information. Send comments regarding this burden estimate or any other aspect of this collection of information, including suggestions for reducing this burden, to Washington Headquarters Services, Directorate for Information Operations and Reports, 1215 Jefferson Davis Highway, Suite 1204, Arlington, VA 22202-4302, and to the Office of Management and Budget, Paperwork Reduction Project (0704-0188), Washington, DC 20503.				
1. AGENCY USE ONLY (Leave blank)		2. REPORT DATE February 1998	3. REPORT TYPE AND DATES COVERED Final - April 1996 to February 1998	
4. TITLE AND SUBTITLE Determination of Aircraft Sonic Boom Noise Penetration into Seas, Bays, and Lakes for Environmental Assessment			5. FUNDING NUMBERS C - F41624-96-I-0006 PE - 63723F PA - 3037 TA - 08 WU - 03	
6. AUTHOR(S) Victor W. Sparrow				
7. PERFORMING ORGANIZATION NAME(S) AND ADDRESS(ES) The Pennsylvania State University 157 Hammond Building University Park PA 16802			8. PERFORMING ORGANIZATION REPORT NUMBER	
9. SPONSORING/MONITORING AGENCY NAME(S) AND ADDRESS(ES) Air Force Research Laboratory, Human Effectiveness Directorate Crew System Interface Division Aural Displays and Bioacoustics Branch Air Force Materiel Command Wright-Patterson AFB OH 45433-7022			10. SPONSORING/MONITORING AGENCY REPORT NUMBER AFRL-HE-WP-TR-2000-0064	
11. SUPPLEMENTARY NOTES				
12a. DISTRIBUTION AVAILABILITY STATEMENT Approved for public release; distribution is unlimited.			12b. DISTRIBUTION CODE	
13. ABSTRACT (Maximum 200 words) Sonic boom noise from overwater supersonic aircraft operations penetrates into the water. The present work developed an algorithm to simulate this penetrating sonic boom noise for realistically shaped sonic booms, predictions previously unavailable. The new algorithm assumes that the water surface is fairly flat and that the water is deep enough so that bottom reflections can be ignored. The algorithm was used to model the underwater sonic boom noise for the cases of incident sonic boom waves distorted by atmospheric effects and by common aircraft maneuvers. It was found that certain aircraft maneuvers and atmospheric effects can increase the penetration of the sonic boom noise, while others decrease it.				
14. SUBJECT TERMS sonic booms, supersonic aircraft, aircraft maneuvers			15. NUMBER OF PAGES 179	
			16. PRICE CODE	
17. SECURITY CLASSIFICATION OF REPORT UNCLASSIFIED	18. SECURITY CLASSIFICATION OF THIS PAGE UNCLASSIFIED	19. SECURITY CLASSIFICATION OF ABSTRACT UNCLASSIFIED	20. LIMITATION OF ABSTRACT UL	

This page intentionally left blank.

Table of Contents

	Page
1.0 Summary	1
2.0 Introduction	2
2.1 State of understanding prior to this study	2
2.2 Proposed goals	3
3.0 Methods, Assumptions, Procedures	5
3.1 Simulation methods	5
3.2 Modification of proposed goals	5
3.3 Summary of research tasks	7
4.0 Results and Discussion	8
5.0 Conclusions and Suggestions for Future Work	10
6.0 Research Personnel	12
7.0 Technical Publications Produced	13
8.0 Related Activities	15
9.0 References	16
10.0 Appendix:	
T. J. Ferguson, "The effect of aircraft maneuvers on sonic boom noise penetra- tion into a flat ocean," M. S. Thesis, The Pennsylvania State University, Graduate Program in Acoustics, December 1997.	
... begins on	19

This page intentionally left blank.

1.0 Summary

This document reports on the research performed under research grant F41624-96-1-0006, entitled "Determination of Aircraft Sonic Boom Noise Penetration into Seas, Bays, and Lakes for Environmental Assessment," a grant from the U.S. Air Force Material Command and the U.S. Air Force Armstrong Laboratory to The Pennsylvania State University. The project was undertaken by Dr. Victor W. Sparrow of the Penn State Graduate Program in Acoustics and his graduate students.

Since the U.S. Armed Forces often require that aircraft operate at supersonic speeds over water, concern has arisen regarding the resulting underwater noise that marine mammals and other underwater wildlife will experience. The purpose of the present research was to provide some first-pass answers to some of the research questions raised related to underwater sonic boom noise.

In the present work a new algorithm was developed to simulate the penetrating sonic boom noise from realistically shaped sonic booms. Such predictions were previously unavailable, and the new algorithm should provide a useful tool for predicting the underwater noise impact of typical military supersonic operations over water.

Once the new algorithm was developed, studies were undertaken to clearly understand how the sonic boom noise of real USAF aircraft were affected by penetration into the water. Although some sonic booms have a pressure-time waveform shaped like the letter N, most sonic booms are affected by atmospheric turbulence or by focusing from aircraft maneuvers. There is some existing theory, substantiated by experiments, to explain what happens when an N shaped sonic boom wave impacts an air-water interface. The major purpose of the present research, however, was to study the sonic boom noise penetration for the more realistic sonic boom waves. It was found that some aircraft maneuvers and atmospheric distortions of the sonic boom waves can enhance the noise penetration into the water. Further research needs to be performed, however, to more fully characterize the penetrating sonic boom noise, particularly for predicting the noise not underneath the aircraft flight path and for including the effects of bottom reflections for shallow bodies of water such as lakes and portions of the Gulf of Mexico.

2.0 Introduction

During routine training missions the U.S. Air Force operates aircraft which exceed the speed of sound and create sonic booms. Some flight paths take place either partially or totally over bodies of water such as seas, bays, and lakes. USAF training often takes place over the Atlantic or Pacific Oceans or over the Gulf of Mexico.

There is growing concern by some of the environmental noise impact of such supersonic operations over bodies of water. Marine mammals and other wildlife can be exposed to sonic boom noise while under the water, as evanescent acoustic energy penetrates the air – water interface. Schools of fish, sought after by commercial fishing vessels, can also experience the penetrating sonic boom.

2.1 State of understanding prior to this study

Prior to the present study, the understanding of this penetration of sonic boom noise from air into water, or its potential effects, was poor. Sawyers first developed a theory to predict the propagation of an N shaped sonic boom wave in air into a flat, homogeneous water surface in 1968.¹ This was later elaborated on by Cook in 1969.² Sawyers' theory was experimentally validated by the team of Waters and Glass,^{3,4} who examined the propagation of small spherical blasts into a pool of water, and the team of Intrieri and Malcolm,^{5,6} who studied the penetration of the booms from high speed projectiles into a small water tank.

Using Sawyers' theory, Sparrow at Penn State also observed that faster aircraft speeds imply greater penetration of the boom noise into the water.⁷ That result also depends on the aircraft being in level flight with no acceleration, deceleration, or turns as are common in USAF supersonic operations. Sparrow and Rochat also had investigated how common sonic boom metrics decay with distance below a flat ocean assuming that an N shaped sonic boom is incident on the surface.⁸

All previous studies assumed the water had a perfectly flat surface. The ocean surface is only rarely flat, however. More often than not the wind waves on the sea surface are between 1 and 2 meters high. These heights correspond to wind conditions of 0 to 20 knots and are based on 70,000 observations.⁹

Further, the previous studies all presuppose that the water is infinitely deep, a good assumption for the open ocean. However lakes or bays, including the Gulf of Mexico, are shallow enough that the previously cited theories do not apply. One expects that sonic boom noise will here penetrate the air – water interface and then reflect from the sediment/sandy bottom, creating a waveguide effect. In this case one may find that the penetrating sonic boom sound may “build up” in the water, created somewhat higher sound levels than in the open ocean.

2.2 Proposed goals

In this study it was proposed that research be instigated at Penn State to determine these penetrating sonic boom noise levels, since only by a thorough study of these sound levels can environmental noise impact assessments be made. The levels are expected to vary considerably due to many factors. The proposed objectives were to find first-pass estimates for

- the penetrating sonic boom noise levels for non-N wave shaped booms,
- the penetrating sonic boom focused by wind waves on the water surface,
- the penetrating sonic boom created in shallow bodies of water such as bays, lakes, and the Gulf of Mexico, and
- the penetrating sonic boom due to USAF aircraft accelerating, decelerating, and turning.

It was deemed that in one year of research, significant strides could be made in quantifying the underwater sonic boom sound levels from USAF aircraft. The knowledge of such sound levels would then allow for a complete assessment of the noise impact on marine mammals and other

underwater wildlife. The new understanding of these noise levels would then be available as inputs for USAF environmental noise planners.

It was thought that a several year effort would be needed to fully comprehend all of the nuances related to sonic boom noise penetration for U.S. military aircraft. The studies originally proposed, for one year of research, would center on obtaining first pass estimates of the penetrating sonic boom noise for use by USAF personnel. Future improvement in the theory could be developed in subsequent years, as separately negotiated research efforts.

3.0 Methods, Assumptions, Procedures

The approach taken in this project was not experimental, but computational and analytical, due to the prohibitively expensive cost of making underwater sound experiments in the vicinity of supersonic operations. The computational/analytical approach also eliminates any need for environmental permits.

3.1 Simulation methods

The penetrating sonic boom levels for non-N wave shaped booms and for sonic booms due to aircraft maneuvers was determined using the symbolic manipulation program *Mathematica*.¹⁰ Here Fourier synthesis was used, a natural extension of the approach Sawyers and Cook took. Reproducing the Sawyers and Cook analytical procedures required several weeks of work, as their methods are not straightforward. Once deciphered, however, we were able to implement their basic method for any desired sonic boom waveform. For the sonic booms due to aircraft maneuvers, the program PCBoom¹¹ was used to calculate the sonic boom waveform at the ground as well as the angles the boom intercept the air-water interface. Several weeks of work were spent interfacing PCBoom with the *Mathematica* Fourier synthesis method.

The other thrusts of the program, investigating the shallow water "waveguide effect" and the wind wave focusing, were studied using a finite difference method introduced by Sparrow¹² and later used in a study by Rochat and Sparrow.¹³ The specifics of the finite difference method are described there and in the Ph.D. thesis of Rochat.¹⁴

3.2 Modification of proposed goals

As will later be described in detail, the great majority of the goals proposed in this study were achieved. However, the questions about one of the proposed tasks were answered by a study

funded by NASA Langley Research Center, and another task proved more complex than was first thought.

Although it was originally proposed that a significant effort be spent on determining the penetrating sonic boom for U.S. military aircraft over ocean with significant ocean swell, it was determined from studies funded by NASA Langley Research Center for the High Speed Civil Transport (HSCT) that the effect of the swell should be negligible on the underwater sound levels.¹³⁻¹⁴ There it was found that a maximum of 12% increase in sound pressure in pascals could be achieved for the worst possible scenario due to focusing by ocean swell. This sound pressure increase corresponds to approximately 1 dB at most, certainly a minor effect. Hence with this new information unavailable at the time the present study was proposed, the principal investigator felt that calculating such negligible numbers would be a waste of time on the project. The time saved on the project made it possible to fully explore a wider range of aircraft maneuver situations and the resulting penetrating sonic boom noise.

The other originally proposed goal that was not investigated as fully as was desired was to understand the shallow water "waveguide effect" which occurs when a penetrating sonic boom sound energy interacts with an underwater bottom surface. It turned out that the models to account for bottom reflection of the penetrating sonic boom for shallow bays and lakes turned out to be much more complicated than was originally envisioned. The difficulty is that one must get the finite difference calculation into a "steady state" after a long run time before any useful data can be extracted. It was originally proposed that a matrix of computational simulation runs would be made to determine the extent to which "waveguide effects" need be considered for assessment. A wide number of sonic boom incident angles, water depths, and bottom characteristics were to be examined. Unfortunately, with the very long run times involved only a very few simulations were run successfully. It remains for future research to determine how to decrease the start up times for the simulations and then to determine the magnitude of the "waveguide effect." A buildup of

acoustic pressure was seen due to the bottom reflections, but many more simulations need to be made before one can clearly quantify the effect.

3.3 Summary of research tasks

- Determine the penetrating sonic boom noise levels for non-N wave shaped booms.
 - Completed, see Section 4.0.
- Determine the penetrating sonic boom focused by wind waves on the water surface.
 - Completed, results available from HSCT studies.¹³⁻¹⁴
- Determine the penetrating sonic boom created in shallow bodies of water such as bays, lakes, and the Gulf of Mexico.
 - Uncompleted, need more time/computing power or better algorithms.
- Determine the penetrating sonic boom due to USAF aircraft accelerating, decelerating, and turning.
 - Completed, see Section 4.0

4.0 Results and Discussion

The primary result of the present research study is the algorithm presented by Sparrow and Ferguson¹⁵ and by Ferguson.¹⁶ Reference 16, Ferguson's M.S. thesis, appears as an Appendix to this report. The algorithm allows one to calculate the sonic boom noise penetrating underwater for incident sonic booms of any shape, assuming that the water surface is flat and that the water is deep enough so that bottom reflections can be ignored. One also must know the incident angle at which the sonic boom hits the air-water interface. Although currently implemented in *Mathematica*, the algorithm can easily be converted into either Fortran, C, or another compiled language. Thus, one should be able to implement the algorithm directly in PCBoom¹¹ or any other sonic boom program. See Chapter 2 of Ferguson.¹⁶

The algorithm was tested against both the results of Rochat and Sparrow⁸ and the analytical solutions of Cook² for an incident N wave. Agreement was good. See Chapter 3 of Ferguson.¹⁶

The algorithm was used with a number of different input waveforms. The waveforms came from 1. analytical input spectra, 2. data from actual U.S. Air Force aircraft flights, and 3. simulated data from PCBoom¹¹. It was determined, for example, that the high frequencies present in spiked sonic boom waves or U-waves from USAF aircraft do not penetrate very far into the ocean. For this and other specific results, see Chapter 4 of Ferguson.¹⁶

Coupling PCBoom¹¹ and the new algorithm, a number of common military aircraft maneuvers were examined to determine the corresponding penetrating sonic boom noise above and beyond what would be experienced in straight, steady flight. The maneuvers studied included a linear acceleration, a 10 degree dive, a 30 degree dive, a pushover, and a constant g turn. For specific results for each of these cases, see Chapter 5 of Ferguson.¹⁶ There it is shown that some maneuvers can increase the underwater sonic boom noise, while other maneuvers can decrease it.

Lastly, using the new algorithm and a previous procedure developed by Gionfriddo¹⁷ to quantify the distortion of a sonic boom by atmospheric turbulence, the effect of atmospheric distortions on sonic boom penetration into the ocean was studied. It was determined that distortions, caused by atmospheric turbulence, can either increase or decrease the sonic boom noise penetration. See Chapter 6 of Ferguson.¹⁶

5.0 Conclusions and Suggestions for Future Work

This study has greatly improved the capability of the U.S. Air Force to determine the impact of sonic boom noise penetrating an air-water interface. We now have a quantitative tool for determining the underwater sonic boom noise for real Air Force aircraft, not from hypothetical N wave shaped sonic booms. Related studies have shown that focusing of the sonic booms due to ocean swell and wind waves is a minimal effect. The effect of several aircraft maneuvers on the penetrating sonic boom noise also has been thoroughly investigated. Clearly some maneuvers can increase the penetrating sonic boom noise, while others can decrease it. None of these findings were available prior to this present study, and the algorithm derived in this research is now ready for direct implementation in PCBoom or other sonic boom prediction models.

Although the project did not fully investigate the effect of bottom reflections from shallow bays and lakes, it was seen that **such reflections do have a strong effect** on the underwater noise. We have also ascertained the computational requirements for correctly modeling such bottom reflections. The simulation time needed for reaching a “steady state” for such calculations is substantial, and either improved computational algorithms or faster workstations are required.

In the future several additional research topics should be investigated to provide the U.S. Air Force with additional guidance in planning for sonic boom noise penetrating into Underwater Wildlife Areas (UWAs) which are often overflowed in Military Operations Areas (MOAs) and by Military Training Routes (MTRs). As was mentioned earlier, for supersonic fixed wing aircraft clearly the impact of the bottom reflections should be addressed. Such reflections have the potential to elevate the underwater sound levels by 6-10 dB, and a large number of simulations need to be performed to accurately predict these increases.

Since the present study primarily determined the penetrating sonic boom directly below the aircraft, further research should determine the underwater noise at positions NOT directly below the aircraft. Such predictions should be made for wide variety of maneuvers.

In earlier reports by the present author it was proposed that ocean bubbles near the water surface might be able to increase the penetrating sonic boom noise levels. However, recent studies¹⁴ have shown that the effects of ocean bubbles are very small, and the sound levels are enhanced by an amount even smaller than the effects of the ocean swell. Additional computations determining the effects of ocean bubbles on sound propagation into the ocean, therefore, will have little value. However, new experimental verifications of sound waves propagating through ocean bubbles should be undertaken to reinforce the findings of the computer simulations.

Another important additional study of interest to the U.S. Air Force is the prediction of the penetrating sonic boom noise due to Titan IV and other rocket launches. Since the Titan IV is launched near the ocean shore, one must account for the bottom interactions in calculating the underwater noise. Such predictions of the penetrating sonic boom should be made both directly under the flight path and also at other positions. A wide variety of Titan IV trajectories should be examined for comparison.

Lastly a good research study needs to be undertaken to clarify and contrast the findings of the present research with that of Cheng *et al.*¹⁸ Cheng and his colleagues have predicted substantially larger underwater sound levels due to ocean surface roughness effects. The present studies do not support Cheng's conclusions, and additional work should be performed to understand the discrepancies between the present work and Cheng's. Another study¹⁹ was unable to reconcile Cheng's work with the results of Rochat and Sparrow. However, a recent accidental experimental measurement of the underwater sonic boom from the Concorde supersonic passenger airplane found the underwater levels closely matched those predicted by the Cook/Sawyers/Sparrow/Rochat/Ferguson approach,²⁰ and the enhanced underwater levels predicted by Cheng were not observed.

6.0 Research Personnel

Principal Investigator:

Victor. W. Sparrow

Associate Professor of Acoustics

Graduate Program in Acoustics

The Pennsylvania State University

Graduate Student: (supported by Grant F41624-96-1-0006)

Tracie J. Ferguson

Research Assistant

Graduate Program in Acoustics

The Pennsylvania State University

Graduate Student: (supported by NASA Langley Research Center)

Judith L. Rochat

Research Assistant

Graduate Program in Acoustics

The Pennsylvania State University

7.0 Technical Publications Produced

The following research article directly stems from the present grant. It is being submitted, in a slightly modified form, to the AIAA Journal for possible publication:

- V. W. Sparrow and T. J. Ferguson, "Penetration of shaped sonic boom noise into a flat ocean," AIAA Paper 97-0486, 35th Aerospace Science Meeting and Exhibit, Reno, NV 1997.

The following two page abstract has been accepted for publication in the Proceedings of the International Congress on Acoustics/Acoustical Society of America '98 meeting to be held in Seattle, WA during June 1998:

- T. J. Ferguson and V. W. Sparrow, "Effect of waveform distortion on sonic boom noise penetration into a flat ocean."

The following technical presentations were made directly for the contract monitor, Dr. J. M. Downing, overseeing the present grant:

- V. Sparrow, Presentation at Kickoff Meeting held 4/30/96 at Science Applications International Corporation (SAIC), McLean, VA.
- V. Sparrow, T. Ferguson, and J. Rochat, Presentations held 6/11/97 at Armstrong Laboratory Noise Effects Branch, Wright Patterson AFB, OH.

The following related technical presentations at professional meetings were made during the duration of this grant:

- Victor W. Sparrow, "Algorithm for BEM calculations to simulate sonic boom noise penetration into the ocean," J. Acoust. Soc. Am., **102** (5, Pt. 2) 3148 (Fall 1997).

- J. Rochat and Victor W. Sparrow, "Focusing of sonic boom noise penetration into a homogeneous wavy ocean: Complex surfaces and wavelength comparisons," *J. Acoust. Soc. Am.*, **102** (5, Pt. 2) 3159 (Fall 1997).
- Victor W. Sparrow, INVITED KEYNOTE SPEECH: "SYSNOISE, Education, and Applied Research at Penn State," 4th Worldwide SYSNOISE Users Meeting, Leuven, Belgium, 15 September 1997.
- J. Rochat and Victor W. Sparrow, "Effects of wind-wave generated bubbles on sonic boom noise penetration into the ocean," *J. Acoust. Soc. Am.* **101** (5, Pt. 2) 3103 (Spring 1997).
- T. Ferguson and Victor W. Sparrow, "Effect of aircraft maneuvers on sonic boom penetration into the ocean," *J. Acoust. Soc. Am.* **101** (5, Pt. 2) 3103 (Spring 1997).
- Victor W. Sparrow and T. Ferguson, "Penetration of shaped sonic boom noise into a flat ocean," 35th Aerospace Sciences Meeting and Exhibit, Reno, NV, 8 January 1997.
- Victor W. Sparrow, J. Rochat, and T. Ferguson, "Sonic-boom penetration into the ocean: 1996 update," *J. Acoust. Soc. Am.* **100** (4, Pt. 2) 2566 (Fall 1996).
- Victor W. Sparrow and J. Rochat, "Two-dimensional focusing of evanescent sonic boom noise penetrating an air-water interface," 2nd AIAA/CEAS Aeroacoustics Conference (17th AIAA Aeroacoustics Conference), State College, PA, 7 May 1996.

8.0 Related Activities

During the grant period the following technical talks were given on sonic boom noise penetration into the ocean, at the recommendation of the grant contract monitor, Dr. J. M. Downing:

- V. Sparrow, Presentation to University of Southern California Department of Aerospace Engineering, Los Angeles, CA, 1/21/97.
- V. Sparrow, Presentation to The Aerospace Corporation and to Department of the Air Force, Space and Missile Systems Center (SMC), Los Angeles, CA, 1/22/97.
- V. Sparrow, Presentation to EDAW, Inc., Huntsville, AL, 12/18/97.

During the grant period, an additional graduate student Judith L. Rochat was funded by the NASA Langley Research Center under grant NAG 1 1638. Dr. Gerry L. McAninch is the technical monitor for that research, primarily directed toward determining the underwater noise due to sonic booms from a future commercial supersonic aircraft, the High Speed Civil Transport (HSCT). That study does not address sonic boom focusing for fighter aircraft, since the sonic boom durations are substantially longer for passenger aircraft, and since passenger aircraft are assumed to remain steady in flight.

Additionally, during the grant period the principal investigator, Victor W. Sparrow, began the planning for the 1998 Acoustical Society of America Sonic Boom Symposium. That Symposium will be held during the Norfolk, VA Acoustical Society of America meeting during October 12 – 16, 1998. Dr. Sparrow is the organizer and coordinator for that Symposium.

9.0 References

- ¹ K. Sawyers, "Underwater sound pressure from sonic booms," *J. Acoust. Soc. Am.* **44**, 523-524 (1968).
- ² R. K. Cook, "Penetration of a sonic boom into water," *J. Acoust. Soc. Am.* **47**, 1430-1436 (1970).
- ³ J. Waters, "Penetration of sonic boom energy into the ocean: an experimental simulation," in *Noise and Vibration Control Engineering*, M. Crocker, Ed., pp. 554-557, Proc. of the Purdue Noise Control Conference, July 14-16, 1971, (Purdue Univ., Lafayette, IN, 1972).
Condensed from:
- ⁴ J. F. Waters and R. E. Glass, "Penetration of sonic boom energy into the ocean: an experimental simulation," Hydrospace Research Corp. Final Report on Contract FA70WAI-185, HRC TR 288, (June 1970), available from NTIS/DTIC as AD 711 963.
- ⁵ P. Intrieri and G. Malcolm, "Ballistic range investigation of sonic-boom overpressures in water," *AIAA J.* **11**, 510-516 (1973). Revised from:
- ⁶ G. Malcolm and P. Intrieri, "Ballistic range investigation of sonic-boom overpressures in water," *AIAA Paper 72-657(654?)*, Presented at AIAA 5th Fluid and Plasma Dynamics Conference, Boston, MA (June 26-28, 1972).
- ⁷ V. Sparrow, "The effect of supersonic aircraft speed on the penetration of sonic boom noise into the ocean," *J. Acoust. Soc. Am.* **97**, 159-162 (1995).
- ⁸ J. Rochat and V. Sparrow, "Sound levels under the ocean surface due to sonic boom penetration," in *Proceedings of Inter-Noise 95*, 967-970 (1995).
- ⁹ W. Bascom, *Waves and Beaches*. (Anchor Books, Doubleday, New York, 1980), p. 48.

- ¹⁰ Wolfram Research Inc., *Mathematica*, Ver. 2.2 (Wolfram Research, Inc., Champaign, IL, 1993).
- ¹¹ K. Plotkin, M. Downing, and J. Page, "USAF single event sonic boom prediction model: PCBOOM," *J. Acoust. Soc. Am.* **95**, No. 5, Pt. 2, 2839 (1994).
- ¹² V. Sparrow, "Evanescent wave penetration of sonic boom noise into the ocean," presented at *2nd International Conference on Theoretical and Computational Acoustics*, Honolulu, HI, 22 August 1995.
- ¹³ J. Rochat and Victor W. Sparrow, "Two-dimensional focusing of sonic boom noise penetrating an air-water interface," *AIAA J.*, **35** (1) 35-39 (1997).
- ¹⁴ J. Rochat, "Effects of realistic ocean features on sonic boom penetration into the ocean: A computational analysis," Ph.D. Dissertation, The Pennsylvania State University, Graduate Program in Acoustics, University Park, PA, May 1998.
- ¹⁵ V. W. Sparrow and T. J. Ferguson, "Penetration of shaped sonic boom noise into a flat ocean," AIAA Paper 97-0486, 35th Aerospace Science Meeting and Exhibit, Reno, NV 1997.
- ¹⁶ T. J. Ferguson, "The effect of aircraft maneuvers on sonic boom noise penetration into a flat ocean," M. S. Thesis, The Pennsylvania State University, Graduate Program in Acoustics, University Park, PA, December 1997. Appears as an Appendix to this report.
- ¹⁷ T. A. Gionfriddo, "Quantification of sonic boom signature distortions from propagation through atmospheric turbulence," M.S. Thesis, The Pennsylvania State University, Graduate Program in Acoustics, University Park, PA, December 1992.
- ¹⁸ H. K. Cheng, C. J. Lee, M. M. Hafez, and W. H. Guo, "Sonic boom propagation and its submarine impact: A study of theoretical and computational issues," AIAA Paper 96-0755, 34th Aerospace Sciences Meeting and Exhibit, Reno, NV 1996.

- ¹⁹ H. K. Cheng, and C. J. Lee, "Submarine impact of sonic boom: A study comparing and reconciling results from two prediction approaches," in Proc. of NOISE-CON 97, The Pennsylvania State University, University Park, PA, (Noise Control Foundation, Poughkeepsie, NY, 1997), pp. 399–404.
- ²⁰ F. Desharnais and D. M. F. Chapman, "Underwater measurements of a sonic boom," in Proc. of OCEANS '97 MTS/IEEE, (Institute of Electrical and Electronics Engineers, Piscataway, NJ, 1997), pp. 592–596.

Appendix

T. J. Ferguson, "The effect of aircraft maneuvers on sonic boom noise penetration into a flat ocean,"

M. S. Thesis, The Pennsylvania State University, Graduate Program in Acoustics, December 1997.

The Pennsylvania State University
The Graduate School
Graduate Program in Acoustics

THE EFFECT OF AIRCRAFT MANEUVERS
ON SONIC BOOM NOISE PENETRATION
INTO A FLAT OCEAN

A Thesis in
Acoustics

by

Tracie J. Ferguson

Copyright 1997 Tracie J. Ferguson

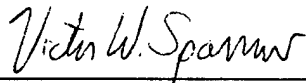
Submitted in Partial Fulfillment
of the Requirements
for the Degree of

Master of Science

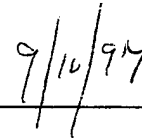
December 1997

We approve the thesis of Tracie J. Ferguson

Date of Signature

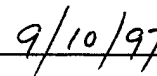


Victor W. Sparrow
Associate Professor of Acoustics
Thesis Advisor



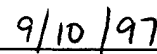


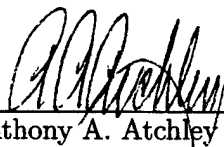
Philip J. Morris
Boeing/A. D. Welliver Professor of Aerospace Engineering



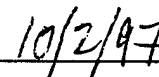


John S. Lamancusa
Associate Professor of Mechanical Engineering





Anthony A. Atchley
Professor of Acoustics
Chair of the Graduate Program in Acoustics



ABSTRACT

The penetrating underwater sound field due to an N-wave shaped sonic boom incident on a flat ocean surface is well described by existing theory. This thesis presents an algorithm which calculates the penetrating sound field from any arbitrarily shaped incident sonic boom by finding the frequency spectrum of the incident signature and superimposing the resulting penetrating waves for each frequency component. This method is implemented in the symbolic manipulation program *Mathematica*. It was verified by comparing results for an incident N wave with known analytical solutions. Underwater waveforms and sound exposure levels are given for several examples including hypothetical High Speed Civil Transport configurations and experimentally measured sonic booms from aircraft of the United States Air Force. It is shown that higher Mach numbers result in a greater penetration depth into the ocean. It is also seen that the perturbations in the incident waveforms caused by such things as atmospheric turbulence do not persist below depths of 16 meters.

The major portion of this thesis examines the effect of aircraft maneuvers on sonic boom noise penetration into a flat ocean. Using the sonic boom prediction model PCBoom3 and the present algorithm, examples of maneuvers such as accelerations, dives, climbs, and turns were investigated. Sonic boom footprints and focal zones were determined from PCBoom3 output files for each maneuver. The underwater sound field was calculated for various trajectory points. Each waveform was compared to a signature created by an identical aircraft engaged in straight flight to evaluate the effect of the maneuver on the noise penetration into water. It was seen that any maneuver containing an acceleration or a turn created focal zones. The U waves that were created had a higher penetration depth as compared with comparable N waves. Climb maneuvers were shown to create sonic booms with smaller amplitudes and diminished penetration depths compared to corresponding straight flight cases.

Finally, this thesis determines the effect of waveform distortions on sonic boom penetration into a flat ocean. Using experimental data, N waves were constructed that contain the same amount of energy as the measured waves. The underwater signatures were found for both waves at specified depths and were plotted on top of one another. From these plots, it was shown that the distortions in the waveform at the surface cause an increased penetration depth of the sonic boom noise.

Table of Contents

List of Figures	vi
List of Tables	ix
Acknowledgments	xi
Chapter 1. Introduction	1
1.1. Brief Overview	1
1.2. Research Objectives	2
1.3. Thesis Overview	3
Chapter 2. Background Review	4
2.1. Sonic Boom Overview	4
2.2. Review of Sonic Boom Noise Penetration Into Water	9
2.2.1. Propagating Waves	9
2.2.2. Penetrating Evanescent Waves	10
2.2.3. Work of Sawyers and Cook	10
2.2.4. Experimental Verification	16
2.2.5. Work of Rochat and Sparrow	17
Chapter 3. Arbitrarily Shaped Sonic Booms	20
3.1. Introduction	20
3.2. Sonic Boom Noise Penetration Into Water From Arbitrarily Shaped Sonic Booms	21
3.3. Verification	29
Chapter 4. Sonic Boom Data and Analysis	33
4.1. Introduction	33
4.2. Data Collection and Results	33
4.2.1. Data and Results From Published Spectra	33
4.2.2. Data and Results From Actual Aircraft Flights	38
4.2.3. Data and Results From PCBoom3	42
Chapter 5. Aircraft Maneuvers	48
5.1. Introduction	48
5.2. Methods	52
5.3. Maneuver Results	55
5.3.1. Linear Acceleration	55

5.3.2. 10 Degree Dive	59
5.3.3. 30 Degree Dive	64
5.3.4. Pushover	70
5.3.5. Constant g turn	76
Chapter 6. Effect of Waveform Distortion on Underwater Sound Levels	81
6.1. Introduction	81
6.2. Methods	81
6.3. Results	84
Chapter 7. Conclusions	91
7.1. Summary of Results	91
7.2. Recommendations	94
7.3. Conclusions	95
References	96
Appendix A. Tables of Sound Exposure Levels	98
Appendix B. Mathematica Code	124
Appendix C. PCBoom3 Files	139

List of Figures

Figure	page
1.1. An N wave with the points that the "cracks" occur marked with arrows. . .	2
2.1. Sonic boom terminology.	5
2.2. An illustration of a Mach and ray cone with respective hyperbolic ground intercepts.	6
2.3. The location of the Mach angle in both the Mach and ray cones.	6
2.4. The forward throw of a sonic boom.	7
2.5. The location of the primary and secondary carpets with respect to flight path.	8
2.6. The location of the incident, reflected, and transmitted evanescent waves. . .	11
2.7. The results using Cook's equations for sonic boom penetration into water. . .	15
2.8. The function mT in meters as a function of Mach number.	18
2.9. Waveforms underwater due to sonic boom penetration.	19
3.1. Comparison of an ideal N wave and a more realistically shaped sonic boom.	20
3.2. An N wave signal, sampled and zero padded.	22
3.3. The N wave in Fig. 3.2 normalized.	23
3.4. The spectrum of the N wave in Fig. 3.3.	24
3.5. The spectrum of the N wave from Fig. 3.4 rotated <i>samples/2</i> to the right. . .	25
3.6. An example of a sampled exponential function at a depth of 4 meters. . . .	25
3.7. Illustration of the N wave spectrum in Fig. 3.5 multiplied by the exponential function in Fig. 3.6.	26
3.8. The multiplied spectrum in Fig. 3.7 rotated <i>samples/2</i> to the left.	27
3.9. The inverse FFT of the rotated spectrum in Fig. 3.8.	27
3.10. Comparative results of a potential HSCT N wave at depths of 0, 4, 16, and 64 meters.	29
3.11. Results of a Mach 4.5 HSCT N wave at depths of 0, 4, 16, and 64 meters. . .	32
4.1. An expanded rise time sonic boom.	34
4.2. Underwater waveforms for a potential HSCT N wave with an expanded rise time.	35
4.3. A flat-top or minimized overpressure sonic boom.	36
4.4. Underwater signatures for a potential HSCT N wave flat-top sonic boom. . .	37
4.5. Underwater signatures for a surface measured F-15 rounded N wave.	39

4.6. Waveforms calculated underwater from a surface measured F-15 double-peaked wave.	40
4.7. Surface measured F-16 U wave.	42
4.8. Underwater waveforms from a potential F-22 N-shaped wave.	46
5.1. Ray patterns for aircraft in straight steady flight and accelerated flight. . .	48
5.2. A comparison of an N and U wave.	49
5.3. An example of a caustic caused by acceleration.	50
5.4. An example of focusing caused by an acceleration in three dimensions. . . .	51
5.5. A comparison of ray intercepts with the ground.	53
5.6. The representation of spherical coordinates.	54
5.7. Plot of Mach number and local Mach number versus time for a linear acceleration.	55
5.8. Isopemps created during a linear acceleration.	56
5.9. Underwater waveforms for a sonic boom predicted at trajectory time 19 seconds, $\phi = 0^\circ$ during a linear acceleration.	57
5.10. Signatures created underwater from trajectory time 90 seconds, $\phi = 0^\circ$ for a linear acceleration.	58
5.11. Trajectory for a 10° dive.	60
5.12. Plot of aircraft Mach number and local Mach number vs. time for a 10° dive.	60
5.13. Isopemps for a 10° dive.	61
5.14. Underwater waveforms for a sonic boom predicted at trajectory time 19 seconds, $\phi = 0^\circ$ during a 10° dive.	62
5.15. Signatures calculated underwater from trajectory time 23 seconds, $\phi = 0^\circ$ for a 10° dive.	63
5.16. The trajectory for a 30° dive.	64
5.17. Plot of aircraft Mach number and local Mach number vs. time for a 30° dive.	65
5.18. Isopemps created during a 30° dive.	65
5.19. Underwater waveforms for a sonic boom predicted at trajectory time 11 seconds, $\phi = 0^\circ$ during a 30° dive.	67
5.20. Signatures calculated underwater from trajectory time 16 seconds, $\phi = 0^\circ$ for a 30° dive.	68
5.21. Underwater wave shapes for a sonic boom predicted at trajectory time 22 seconds, $\phi = 0^\circ$ during a 30° dive.	69
5.22. Trajectory for a pushover.	71

5.23. Plot of aircraft Mach number and local Mach number vs. time for a pushover.	71
5.24. Isopemps generated during a pushover.	72
5.25. Underwater waveforms for a sonic boom predicted directly under the flight path for a pushover and straight flight at trajectory time 6 seconds.	73
5.26. Signatures calculated underwater for a sonic boom predicted directly under the flight path for a pushover and straight flight at trajectory time 10 seconds.	74
5.27. Underwater wave shapes for a sonic boom predicted 35° off the flight path for a pushover and straight flight at trajectory time 10 seconds.	75
5.28. Trajectory for a constant g turn.	77
5.29. Plot of isopemps for a constant g turn.	77
5.30. Underwater waveforms for a sonic boom predicted directly under the flight path for a constant g turn and straight flight at trajectory time 11 seconds.	78
5.31. Signatures calculated underwater for a sonic boom predicted -20° off the flight path for a constant g turn and straight flight at trajectory time 11 seconds.	79
6.1. Leading and trailing energy sections of an experimental signature.	82
6.2. Comparison of the F-15 rounded sonic boom and a corresponding N wave having the same energy content.	86
6.3. Comparison of the F-15 double peaked sonic boom and a corresponding N wave having the same energy content.	87
6.4. Comparison of the F-16 U wave and a corresponding N wave having the same energy content.	88
6.5. Semilog plot of peak pressure with respect to depth for an F-15 rounded sonic boom and a corresponding equal energy N wave.	89
6.6. Semilog plot of peak pressure with respect to depth for an F-15 double peaked sonic boom and a corresponding equal energy N wave.	89
6.7. Semilog plot of peak pressure with respect to depth for an F-16 U wave and a corresponding equal energy N wave.	90

List of Tables

Table	page
2.1. The $1/e$ "skin depth" of the sonic boom noise at specific frequencies.	16
3.1. HSCT N wave metrics calculated using the present algorithm.	30
3.2. HSCT N wave metrics from the work of Rochat and Sparrow.	30
3.3. HSCT N wave metrics from the present algorithm, relative to those at the surface of the water.	31
4.1. Metrics for a hypothetical HSCT N wave with an expanded rise time.	35
4.2. Metrics for a hypothetical HSCT N wave with an expanded rise time relative to those at the surface.	36
4.3. Metrics for a hypothetical HSCT flat-top boom.	37
4.4. Metrics for a hypothetical HSCT flat-top boom relative to those at the surface.	37
4.5. Metrics for a measured F-15 rounded wave.	39
4.6. Metrics for a measured F-15 rounded wave relative to those at the surface. .	39
4.7. Metrics for a measured F-15 double-peaked wave.	40
4.8. Metrics for a measured F-15 double-peaked wave relative to those at the surface.	41
4.9. Metrics for a measured F-16 U wave.	42
4.10. Metrics for a measured F-16 U wave relative to those at the surface.	42
4.11. Metrics for a potential F-22 N-shaped wave.	46
4.12. Metrics for a potential F-22 N-shaped wave relative to those at the surface. .	47
5.1. Metrics for trajectory time 19 seconds, $\phi = 0^\circ$ for a linear acceleration. . . .	57
5.2. Metrics for trajectory time 90 seconds, $\phi = 0^\circ$ for a linear acceleration. . . .	58
5.3. Metrics for trajectory time 19 seconds, $\phi = 0^\circ$ for a 10° dive.	62
5.4. Metrics for trajectory time 23 seconds $\phi = 0^\circ$ for a 10° dive.	63
5.5. Metrics for trajectory time 11 seconds, $\phi = 0^\circ$ for a 30° dive.	67
5.6. Metrics for trajectory time 16 seconds, $\phi = 0^\circ$ for a 30° dive.	68
5.7. Metrics for trajectory time 22 seconds, $\phi = 0^\circ$ for a 30° dive.	69
5.8. Metrics for trajectory time 6 seconds, $\phi = 0^\circ$ for a pushover and the corresponding straight flight boom.	73
5.9. Metrics for trajectory time 10 seconds, $\phi = 0^\circ$ for a pushover and the corresponding straight flight boom.	74
5.10. Metrics for trajectory time 10 seconds, $\phi = 35^\circ$ for a pushover and the corresponding straight flight boom.	75

5.11. Metrics for trajectory time 11 seconds, $\phi = 0^\circ$ for a constant $4g$ turn and the corresponding straight flight boom.	78
5.12. Metrics for trajectory time 11 seconds, $\phi = -20^\circ$ for a constant $4g$ turn and the corresponding straight flight boom.	79
6.1. Metrics for an F-15 rounded sonic boom and the corresponding equal energy N wave.	86
6.2. Metrics for an F-15 double peaked sonic boom and the corresponding equal energy N wave.	87
6.3. Metrics for an F-16 U wave and the corresponding equal energy N wave. . .	88

Acknowledgments

This research was funded through the Armstrong Laboratory, Air Force Material Command, United States Air Force, under grant F41624-96-1-0003. The author would like to thank the contract monitor Dr. Micah Downing for supporting this work.

The author would also like to thank many special people who made this thesis possible. First, I would like to thank Dr. Victor Sparrow for not only getting me involved in sonic boom research, but for also being a great advisor and a good friend. I thank committee members Dr. Philip Morris and Dr. John Lamancusa for their helpful comments to make the thesis better. I would like to thank all my parents, Daniel Ferguson, Bonnie Ferguson, Sue Matteson, and Bill Matteson, my sister Lisa Kelly, my brother Jason Matteson, and my whole family for giving me undying love and support throughout all my college years. I also am in gratitude to them for giving me the chance to leave the Mohawk Valley to learn what life is all about and for helping me cope along the way. I would like to thank the friends I have made here at Penn State for all the great support and laughter with special mention going to Judy Rochat, Ben Bard, Anderson Mills, Ellen Bradley, Brian Tuttle, and Brian Bennett. I would like to thank the crew at the Fashion Bug Nittany Mall in State College, for giving me a break from the acoustics life. I would especially like to thank Patty Weyman for being my Mom away from home and for feeding me mashed potatoes. Finally, I would like to give a special thank you so much to Bernie Sklanka who without his persistence, caring, and support, I would not have stayed at Penn State and received such an honorable degree.

Disclaimer: The views and conclusions contained herein are those of the author and should not be interpreted as necessarily representing the official policies or endorsements, either expressed or implied, of the Armstrong Laboratory Noise Effects Branch or the U.S. Government.

Chapter 1.

Introduction

1.1. Brief Overview

Sonic booms are impulsive sounds that are created by shock waves from objects traveling faster than the speed of sound. They are predominately associated with supersonic passenger and military aircraft, but can also be produced by launch vehicles (rockets) and projectiles (bullets). For rockets and objects such as a high speed civil transport, HSCT, a typical sonic boom will be heard on the ground as two "thumps" or "cracks" separated by some time.¹ The time between the two events is dependent on the characteristics of the object. For example, the time between the "cracks" for supersonic HSCT is between 50-300 ms while the delay time for a launch vehicle can be up to 1 second. For projectiles or most military aircraft, however, the delay time often is much smaller than for the HSCT. The shorter length of the objects makes the two sounds difficult to separate. Therefore, the typical sonic boom from these objects is only heard as one "crack." Figure 1.1 presents an ideal sonic boom, also called an N wave, and shows the times during the boom that a "crack" is heard.

Because of the impulsive nature of sonic booms, people generally find the noise annoying. Sonic booms have been reported to cause various problems, such as disturbed sleep and mental concentration. Supersonic flights over communities have also resulted in complaints of structure vibrations and property damage.² Because of these disturbances, supersonic passenger aircraft are restricted by U.S. and International law to only overwater flights. Many military training maneuvers are also practiced over water. This restriction is to ensure that the impact of sonic booms on humans is minimal.

Since most supersonic activities take place over water, there has been a growing concern about the effects of sonic boom noise on marine mammals. Marine mammals, such as dolphins and whales, spend a great deal of time near the surface of the ocean because they breathe air. As will be described later in this thesis, for most supersonic activities, the sonic boom wave is completely reflected off the air/water interface. But because of a pressure

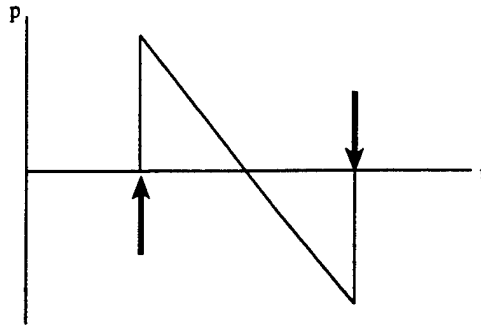


Figure 1.1: An N wave with the points that the “cracks” occur marked with arrows. The horizontal axis is time, the vertical axis is pressure.

continuity boundary condition at the interface, evanescent sonic boom noise does penetrate into the ocean. This noise may still be prevalent at a depth of 50 meters or larger for aircraft engaged in straight steady flight.³ It will be shown in this thesis that aircraft maneuvers, such as accelerations, dives, and turns, can cause focal zones at the surface of the water which can increase the depth that the sonic boom noise is found. Other maneuvers, such as a climb, can decrease the depth of sonic boom noise penetration. Since sonic boom noise can penetrate the water to significant depths, it is thought that US Air Force overwater supersonic operations may have an environmental noise impact on marine mammals close to the surface.

1.2. Research Objectives

To begin to discover the impact sonic boom noise has on marine mammals, an algorithm was developed to ascertain the underwater sound field for arbitrarily shaped waveforms incident on a flat ocean surface. This method is based on previous results by Cook⁵ and will be explained in detail in Chapter 3. In order to encompass all operations, sonic boom examples were analyzed from both supersonic passenger and military aircraft. Booms from aircraft in straight steady flight were examined to determine various sound exposure levels and waveforms at depths of 0, 4, 16, and 64 meters below the surface of the water. Then five different maneuvers, a 10 degree dive, a 30 degree dive, a constant g turn, a linear acceleration, and a pushover, were studied to learn the effect of maneuvers on sonic boom noise penetration into water. These booms were generated with PCBoom3,⁴ a sonic boom

prediction model. Again, sound exposure levels and waveforms were calculated for the depths stated above. Focal zones were also determined for each maneuver. Lastly, ideal N waves were created that have the same energy content as the arbitrarily shaped waves used before. Again, sound exposure levels and waveforms were found for these N waves. The levels and wave shapes from the N waves and the corresponding arbitrarily shaped waves were compared to see if they would be equivalent at some depth under the water. This helped to determine if waveform distortion creates pressure levels that are higher, lower, or the same as an N wave at any fixed depth.

1.3. Thesis Overview

Chapter 2 provides a general overview of sonic booms and key results from previous studies of sonic boom noise penetration into water. Chapter 3 discusses the creation of arbitrarily shaped sonic booms and introduces an algorithm which predicts wave shapes and sound exposure levels at various depths under a flat water surface. Using an N wave, this algorithm is also verified by comparing to known results. Chapter 4 describes the various methods by which sonic boom data was obtained. Predicted sound exposure levels and wave shapes are provided for several examples of each data type. Chapter 5 examines aircraft maneuvers and then effects on sonic boom noise penetrating the ocean. The method for predicting sonic boom waveforms during maneuvers via PCBoom3 is also described. Chapter 6 investigates creating incident N waves that have the same energy content as corresponding experimentally measured incident booms. The method used for determining the parameters for the N waves is provided. Finally, by comparing the noise penetration results for the experimentally measured incident waveforms to the idealized N wave incident signatures, it is determined if waveform distortions have any effect on pressure levels underwater at a fixed depth. Chapter 7 provides important conclusions regarding the analysis of sonic boom noise penetration into water, summarizing the effects of aircraft maneuvers and waveform distortion. Appendix A contains tables of sound exposure levels at different depths for many examples of incident sonic booms. Appendix B provides the *Mathematica* code used for data analysis. Finally, Appendix C presents examples of the PCBoom3 files used.

Chapter 2.

Background Review

2.1. Sonic Boom Overview

An object moving through air at a speed greater than the local speed of sound will create a system of shock waves. The characteristics of this system is dependent on the object. For a simple projectile, there is commonly only two waves at a given time. One shock wave emanates from the front of the projectile called the bow wave and the other emits from the rear called the tail wave. For more detailed geometries, such as an aircraft, the near field system of shock waves can be quite complex. However, as the nonlinear acoustic waves propagate away from the aircraft, they distort and ultimately converge into a bow and tail wave, like the basic projectile.² A compression occurs at the bow wave where the local pressure, p , rises quickly to some Δp above atmospheric pressure. The value Δp is called the *peak overpressure* of the wave and the time taken to go from local pressure to the peak overpressure is called the *rise time*. After the bow wave, a linear expansion transpires until a value is reached that is equal in magnitude to the peak overpressure, but below atmospheric pressure. This value $-\Delta p$ is called the *negative peak overpressure*. At the tail wave, a rapid recompression happens to return back to the local pressure. The time elapsed from the start of the compression to the return to local pressure is the *duration* of the wave. The shape that this process forms is the classic sonic boom signature called an N wave. Figure 2.1 shows an example of an N wave with an expanded rise time labeled with all the features discussed above.

During straight, steady, supersonic flight the N waves move with the object and are not only generated underneath the body, but on the sides and top as well. Over time, these shock waves travel outward from the object at the local speed of sound and form a *Mach cone*. The axis of the Mach cone represents the straight flight path and the angle from the axis to the edge of the cone is the *Mach angle*. The Mach angle is also given by the

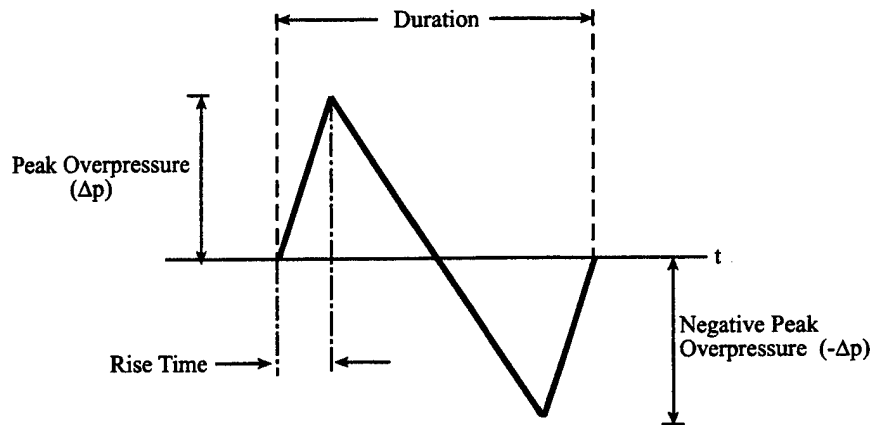


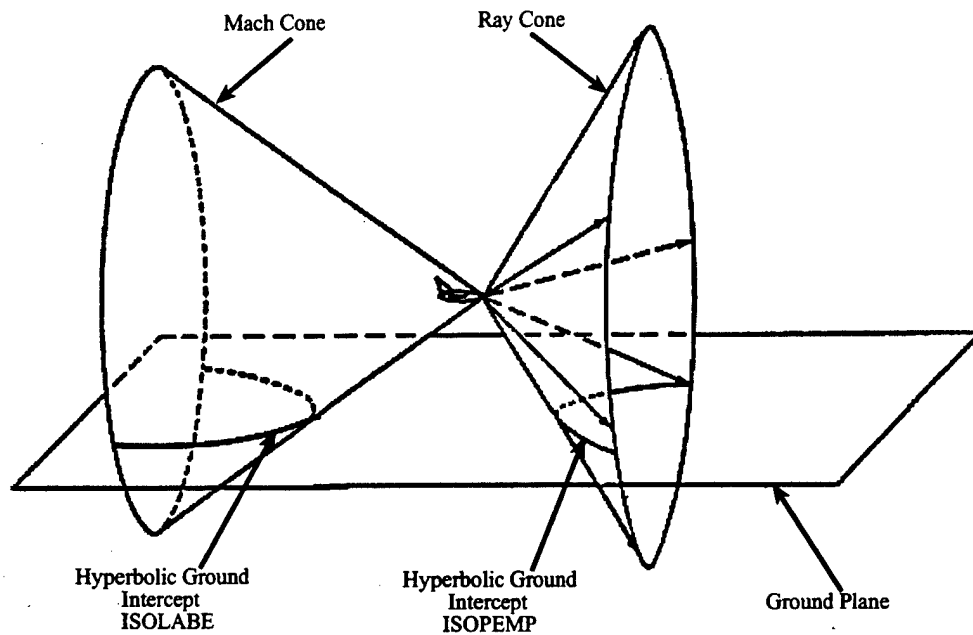
Figure 2.1: Sonic boom terminology. Acoustic pressure is plotted versus time. The rise time is exaggerated for clarity.

expression

$$\alpha = \sin^{-1} \left(\frac{1}{M} \right), \quad (2.1)$$

where M is the Mach number. Figure 2.3A illustrates the location of the Mach angle in the Mach cone. At the speed of sound, $M = 1$, the Mach angle is 90° . As the Mach number increases, the Mach angle decreases and the Mach cone becomes more narrow.

At a given time, after the Mach cone is generated, the corresponding *ray cone* is then established. The ray cone is perpendicular to the Mach cone and represents the path of the sonic boom energy generated at a certain time.⁴ Figure 2.2 illustrates the Mach cone and ray cone generated during straight flight. The angle from the edge of the cone to a vertical line joining the front of the body to the ground is the Mach angle. Figure 2.3B exhibits the location of the Mach angle in the ray cone. At $M = 1$, the Mach angle is again 90° , thus causing the ray cone to converge to a line that falls on the flight path. As the Mach number increases, the ray cone broadens. The ray cone intercepts the ground in a hyperbolic pattern which is always in front of the object. This pattern is called an *isopemp* and is also shown in Fig. 2.2. The distance measured along the flight path from the body position projected on the ground to the front of the isopemp is referred to as the *forward throw* of the boom, Fig. 2.4. Low Mach numbers (narrow ray cone) cause a long forward throw while high numbers (broad ray cone) cause a small forward throw.



Picture taken from PCBoom3 Manual

Figure 2.2: An illustration of a Mach and ray cone with respective hyperbolic ground intercepts. The plane is flying supersonic from left to right.

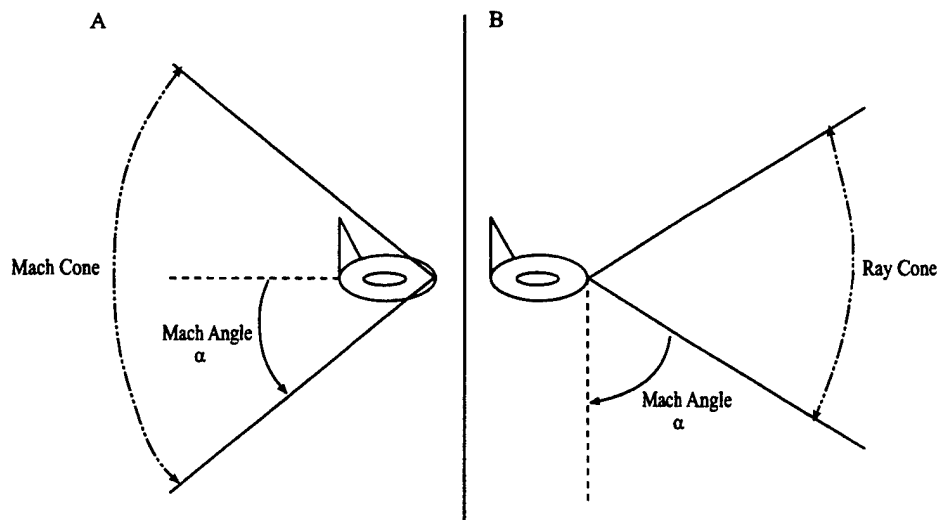


Figure 2.3: The location of the Mach angle in both the Mach and ray cones. The picture on the left, A, illustrates the Mach angle in the Mach cone. The picture on the right, B, shows the ray cone.

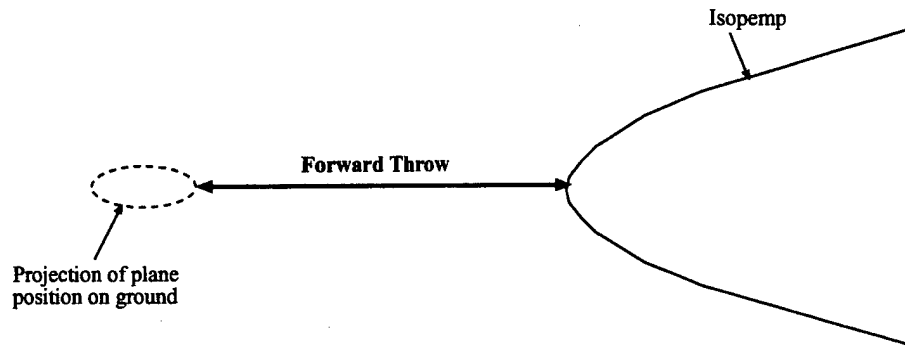
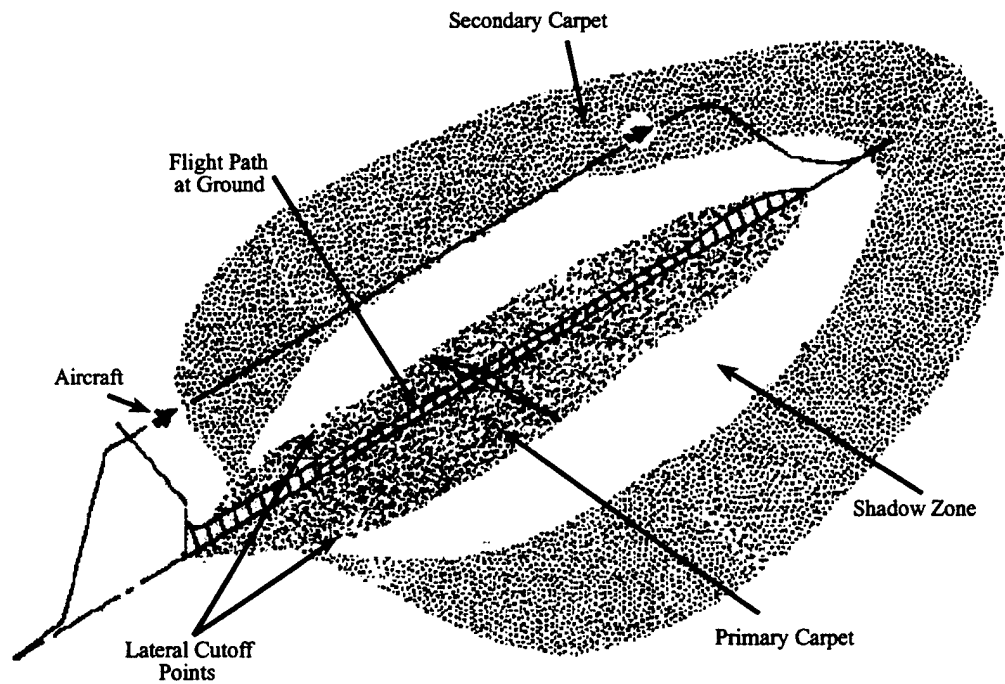


Figure 2.4: The forward throw of a sonic boom as viewed from a position above the aircraft looking down on the ground. The aircraft is flying from left to right.

The Mach cone also has a hyperbolic ground intercept that is sometimes called an *isolabe*. The isolabe is located behind the object and moves with the body. Figure 2.2 also illustrates an isolabe. During supersonic flight, the isolabe sweeps out an area on the ground. This area is commonly referred to as a *boom carpet*. There are two types of boom carpets, primary and secondary. The primary carpet is located directly under the flight path and contains only shock waves that are generated underneath the object. For straight steady flight, these are commonly the N-wave type sonic boom. The *lateral cutoff point* of the primary carpet is defined by the points where the outermost rays hit the ground and reflect away. Thus the lateral cutoff points define the width of the primary carpet. The cutoff points are independent of object type but dependent on Mach number, altitude, and atmospheric profile. As an example of the width of the primary carpet, measurements from XB-70 aircraft flights found the width to be at 37 km (23 miles) at an altitude of 6.1 km (20,000 ft) for $M=1.5$ and 111 km (69 miles) at an altitude of 18.3 km (60,000 ft) for $M=2.0$.² Near the lateral cutoff points, the waves deteriorate from N waves to weaker, more rounded shapes. The rounded waves are not heard as “cracks” but as low rumbles, like thunder. Overall, supersonic flights at high altitudes result in carpet widths that are broad and contain booms with lower peak overpressures, whereas at lower altitudes the width is narrower and higher peak overpressures are found.

The secondary boom carpet is located outside the primary carpet and contains shock waves that are generated from the sides and top of the object. These are sometimes called

“over the top” booms. The secondary carpet also contains reflections from rays in the primary boom carpet. The boom signatures that exist in the secondary carpet have peak overpressures that are much less than the ones in the primary carpet, but have a much greater duration. They are very rounded and thus have a very low frequency content. Because of these characteristics, the secondary booms are often inaudible. They are commonly noticed because they cause structure vibrations and rattling. The width of the secondary carpet is not well defined, but propagation distances of 161 km (100 miles) or greater are common.² Therefore, a very large area on the ground is exposed to some form of sonic boom noise. Between the primary and secondary carpets, there is an area where no sonic boom noise is present. This area is commonly called a *shadow zone*. Figure 2.5 exhibits the location of both types of sonic boom carpets relative to the flight path.



Picture taken from Ref. 2

Figure 2.5: The location of the primary and secondary carpets with respect to flight path. The aircraft is flying diagonally from left to right. The flight path in the air is represented by a solid line, the path at the ground is the lined area marked with an arrow.

2.2. Review of Sonic Boom Noise Penetration Into Water

Since many supersonic operations take place over water, the carpets generated also pass over water and the rays impinge on the surface. Depending on the angle that the incident sound wave makes with the water surface, a resulting propagating wave or penetrating evanescent wave exists. Usually for sonic booms, there is a penetrating evanescent wave, but there are extreme cases where a propagating wave is present. Therefore, both types of waves will be reviewed.

2.2.1. Propagating Waves

When a sinusoidal plane wave traveling in air encounters the boundary of the water, reflected and transmitted waves are generated.⁶ Whether the transmitted wave is a propagating or evanescent wave depends on the angle at which the sound is incident on the air/water interface. To get a propagating wave, the angle of incidence needs to be less than the critical angle. The critical angle is defined by the expression

$$\sin \theta_c = \frac{c_{\text{air}}}{c_{\text{water}}}, \quad (2.2)$$

where θ_c is the critical angle. The critical angle for the air/water case is about 13.2° which corresponds to the plane wave having a velocity along the surface of the water close to Mach 4.5.⁷ Therefore, for straight, level, supersonic flight above Mach 4.5, there will be a transmitted wave that propagates into the water. For this case, the incident wave p_i hits the air/water boundary at an angle θ_i . The reflected wave p_r comes off the boundary at an angle θ_r , which equals θ_i , and the transmitted wave p_t propagates through the surface of the water at an angle θ_t . Thus, for plane waves with $e^{i\omega t}$ time dependence

$$\begin{aligned} p_i &= P_i e^{i(\omega t - k_1 x \cos \theta_i - k_1 z \sin \theta_i)}, \\ p_r &= P_r e^{i(\omega t + k_1 x \cos \theta_r - k_1 z \sin \theta_r)}, \\ p_t &= P_t e^{i(\omega t - k_2 x \cos \theta_t - k_2 z \sin \theta_t)}, \end{aligned} \quad (2.3)$$

where P_i , P_r , and P_t are the respective complex pressure amplitudes, x is horizontal displacement and z is depth. Also, $k_1 = \omega/c_{\text{air}}$ and $k_2 = \omega/c_{\text{water}}$ with c_{air} being the speed of sound in air, 343 meters/second, and c_{water} being the speed of sound in water, 1500 meters/second. At the air/water interface, the boundary condition states the pressure must be

continuous. Therefore, $p_i + p_r = p_t$ and the angle of incidence equals the angle of reflection. These conditions lead to Snell's law which states

$$\frac{\sin \theta_i}{c_1} = \frac{\sin \theta_t}{c_2}, \quad (2.4)$$

from which one can calculate the angle of the transmitted propagating wave from the angle of the incident wave.

2.2.2. Penetrating Evanescent Waves

Since most supersonic flights are under Mach 4.4, the above case is considered extreme. More common cases involve an angle of incidence that is greater than the critical angle of 13.2° . Thus, the incident wave is completely reflected off the surface of the water. The transmitted wave still exists, but it exponentially decays in the direction perpendicular with the boundary into the water.⁶ Because $p_i + p_r = p_t$ still applies, the amplitude of the transmitted wave at the surface must be twice the amplitude of the incident wave. The decaying amplitude is called an evanescent wave. Therefore, for supersonic flights with speeds below Mach 4.4, the incidence angle will be greater than the critical angle and the evanescent wave will be present at the surface. Figure 2.6 diagrammatically shows an incident plane wave for the angle of incidence greater than the critical angle. The resulting reflected and transmitted evanescent waves are pictured. The rays are shown with arrows.

2.2.3. Work of Sawyers and Cook

There has been a considerable amount of previous work exploring the underwater sound field from the penetration of evanescent sonic boom noise into water. In 1968, Sawyers⁸ presented a theory that predicts the acoustic pressure underwater from a sonic boom. First, he assumed that a perfect N wave travels through a homogeneous atmosphere and impinges upon a flat water surface at a speed of V_{plane} . V_{plane} is less than the speed of sound in water, c_{water} . It is assumed that the aircraft is traveling less than $M = 4.4$. The N wave has a duration of T and a peak overpressure of p_o . From these assumptions, Sawyers showed that

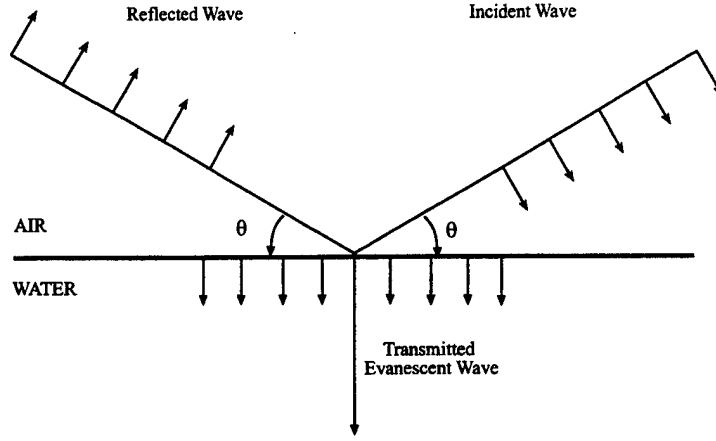


Figure 2.6: The location of the incident, reflected, and transmitted evanescent waves for incidence greater than the critical angle, $\theta_i = \theta_r = \theta$. The rays are shown with arrows.

the underwater acoustic pressure, p was a function of several dimensionless parameters

$$\begin{aligned} \pi \hat{p}(\xi, \zeta, \tau) = & \tan^{-1} \left(\frac{\tau + \xi - 1}{\zeta} \right) + \tan^{-1} \left(\frac{\tau + \xi}{\zeta} \right) + 2(\tau + \xi - 1) \tan^{-1} \left(\frac{\tau + \xi - 1}{\zeta} \right) \\ & - 2(\tau + \xi) \tan^{-1} \left(\frac{\tau + \xi}{\zeta} \right) + \zeta \log \left(\frac{\zeta^2 + (\tau + \xi)^2}{\zeta^2 + (\tau + \xi - 1)^2} \right), \end{aligned} \quad (2.5)$$

where

$$\begin{aligned} \hat{p} &= \frac{p}{p_o}, \\ \tau &= \frac{t}{T}, \\ \xi &= \frac{x}{(TV)}, \\ \zeta &= \frac{z}{(mT)}, \end{aligned} \quad (2.6)$$

and

$$m = V_{\text{plane}} \left(1 - V_{\text{plane}}^2 / c_{\text{water}}^2 \right)^{-1/2}. \quad (2.7)$$

Here, τ is scaled time, ξ is scaled horizontal distance, ζ is scaled depth, and \hat{p} is the acoustic pressure scaled by the peak overpressure. In summary, Sawyers showed that with increasing depth, the N wave loses its discontinuities. The wave shape becomes more rounded and diminishes in amplitude.

In 1969, Cook⁵ also addressed the problem of sonic boom noise penetration into water. His findings expanded on the results of Sawyers and is the work on which the present research is based. Cook's analysis had two main purposes. First to find the underwater pressure caused by an incident sonic boom. Second was to find the reflected waveform from the water surface. Only the analysis of the underwater sound field will be addressed here.

To start, Cook solved the Cauchy problem for the penetration of a single sinusoidal plane wave by calculating the reflected and transmitted waves. The plane wave traveled through a homogeneous atmosphere and hit a flat water surface at the Mach angle, α , Eq. (2.1). The Mach angle was assumed to be greater than the critical angle of 13.2° . Therefore, the sound pressure in the atmosphere was the sum of the incident and reflected waves. The sound pressure immediately underwater was a penetrating evanescent wave whose amplitude was also equal to the sound pressure amplitude in air just above the surface. For $e^{i\omega t}$ time dependence, the pressures were represented by the following expressions

$$p_{\text{air}} = Ae^{i(\omega t - k_o x - k_z z)} + Be^{i(\omega t - k_o x + k_z z)}, \quad (2.8)$$

$$p_{\text{water}} = Ce^{i(\omega t - k_o x)} e^{-Kz}.$$

Notice the exponential decay with depth term, e^{-Kz} , in the expression for p_{water} .

Here,

$$\begin{aligned} k_o &= \frac{k}{M} = k \sin \alpha, \\ k_z &= \left(1 - \frac{1}{M^2}\right)^{\frac{1}{2}} k = k \cos \alpha, \\ K &= \left(\frac{1}{M^2} - \frac{1}{W^2}\right)^{\frac{1}{2}} k, \end{aligned} \quad (2.9)$$

and

$$k = (k_o^2 + k_z^2)^{\frac{1}{2}} = \frac{\omega}{c_{\text{air}}}. \quad (2.10)$$

Also, M is the Mach number of the aircraft, $W = c_{\text{water}}/c_{\text{air}}$ which is the ratio of the speed of sound in water to that in the atmosphere (≈ 4.5), z is depth and x is horizontal position. A , B , and C are calculated from the boundary conditions at the air/water interface. Because pressure and the z -component of the velocity is continuous on the boundary, Cook showed

$$B = \frac{(1 + i\delta)}{(1 - i\delta)} \times A,$$

$$C = \frac{2}{(1 - i\delta)} \times A, \quad (2.11)$$

and

$$\delta = \left(\frac{\rho_{\text{air}}}{\rho_{\text{water}}} \right) \frac{(1 - M^2/W^2)^{\frac{1}{2}}}{(M^2 - 1)^{\frac{1}{2}}},$$

where ρ_{air} and ρ_{water} are the respective densities of air and water. For most cases of supersonic flight where M is less than 4.5, δ is insignificant. Therefore, we can assume, $|B| \approx |A|$ and $|C| \approx 2|A|$.

The next step was to write an expression for the simplified N wave in terms of an inverse Fourier transform in k_o , the transverse wavenumber, as

$$N(x) = \frac{1}{2\pi} \int_{-\infty}^{\infty} f(k_o) e^{-ik_o x} dk_o. \quad (2.12)$$

$N(x)$ represents the incident N wave and is defined by

$$N(x) = \begin{cases} 0, & \text{if } x > 1; \\ \frac{1}{2}, & \text{if } x = 1; \\ x, & \text{if } -1 < x < 1; \\ -\frac{1}{2}, & \text{if } x = -1; \\ 0, & \text{if } x < -1. \end{cases} \quad (2.13)$$

The spectrum of $N(x)$,

$$f(k_o) = -2i \frac{d}{dk_o} \left(\frac{\sin k_o}{k_o} \right), \quad (2.14)$$

turns out to be an odd function of k_o . Thus, by using the Fourier integral theorem, Eq. (2.12) is written as,

$$N(x) = \frac{-i}{\pi} \int_0^{\infty} f(k_o) \sin(k_o x) dk_o. \quad (2.15)$$

The last step was to finally calculate the underwater pressure field due to the incident N wave. An N wave is made up of many sinusoidal components each having a unique incident, reflected, and penetrating wave. Therefore, to find the underwater sound field from an N wave, all the sinusoidal components are weighted with the spectrum, $f(k_o)$ then superimposed. First Eq. (2.8) and Eq. (2.11) are combined, choosing $A = 1$. From this, the underwater pressure from the sinusoidal components is written as,

$$p_w = 2 \cos \Delta \sin(k_o x - \Delta) e^{-k_o \mu z}, \quad (2.16)$$

where

$$\Delta = \arctan \delta \approx \delta,$$

and

$$\mu = \sqrt{1 - \frac{M^2}{W^2}} = \sqrt{1 - \frac{V_{\text{plane}}^2}{c_{\text{water}}^2}}. \quad (2.17)$$

The term, $e^{-k_o \mu z}$, accounts for the exponential decay of the incident wave with respect to depth, z . Note that $\mu = mV_{\text{plane}}$ from Eq. (2.7). To find the total sound pressure from the N wave, Eq. (2.16) is multiplied by the spectrum of $N(x)$, Eq. (2.14) and integrated over all k_o , using Eq. (2.15):

$$p_w(x, z) = -\frac{4 \cos \Delta}{\pi} \int_0^\infty e^{-k_o \mu z} \sin(k_o x - \Delta) \frac{d}{dk_o} \left(\frac{\sin k_o}{k_o} \right) dk_o. \quad (2.18)$$

Expanding the sine function yields the final expression for the sound pressure underwater due to an incident N wave,

$$p_w(x, z) = 2p_o \cos \Delta (I_1 \cos \Delta + I_2 \sin \Delta), \quad (2.19)$$

where

$$\begin{aligned} \pi I_1 &= -2 \int_0^\infty e^{-k_o \mu z} \sin k_o x \frac{d}{dk_o} \left(\frac{\sin k_o}{k_o} \right) dk_o, \\ \pi I_2 &= 2 \int_0^\infty e^{-k_o \mu z} \cos k_o x \frac{d}{dk_o} \left(\frac{\sin k_o}{k_o} \right) dk_o. \end{aligned} \quad (2.20)$$

The equations for I_1 and I_2 are in the forms of Laplace transforms. With the help of integral tables,⁹ analytical expressions can be found for each,

$$\begin{aligned} I_1 &= -\frac{\mu z}{2\pi} \log \left[\frac{(\mu z)^2 + (x+1)^2}{(\mu z)^2 + (x-1)^2} \right] + \frac{x}{\pi} \arctan \left[\frac{2\mu z}{(\mu z)^2 - 1 + x^2} \right], \\ I_2 &= \frac{x}{2\pi} \log \left[\frac{(\mu z)^2 + (x+1)^2}{(\mu z)^2 + (x-1)^2} \right] + \frac{\mu z}{\pi} \arctan \left[\frac{2\mu z}{(\mu z)^2 - 1 + x^2} \right] - 2. \end{aligned} \quad (2.21)$$

These are Cook's primary results. There are two things to mention when using these equations for the underwater sound pressure. First, the correct branch of the arctan is between 0 and π radians and not between $-\pi/2$ and $\pi/2$. Second, we are assuming δ is negligible and hence the value Δ is a small number. Since the $\cos \Delta \approx 1$ and $\sin \Delta \approx \Delta$, I_2 almost always can be ignored. Therefore, the sound pressure underwater due to an incident N wave, Eq. (2.19), can be written as,

$$p_w(x, z) = 2p_o I_1. \quad (2.22)$$

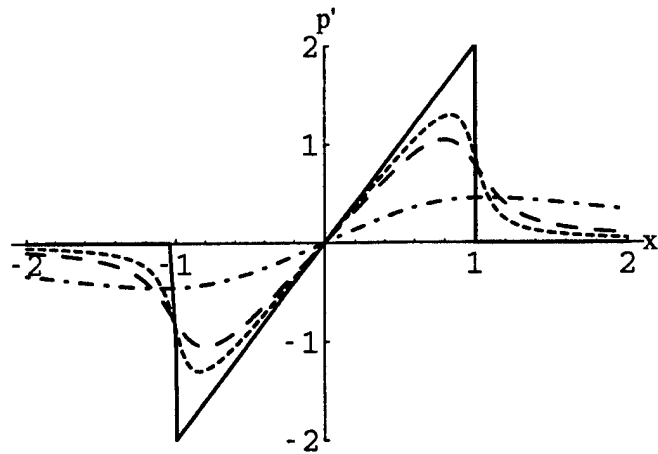


Figure 2.7: The results using Cook's equations for sonic boom penetration into water. The horizontal axis is scaled sonic boom length $x' = x/L$; the vertical axis is scaled peak overpressure $p' = p/p_o$. Signatures are shown at depths of 0 (solid), 6 (short dashes), 12 (long dashes), and 62 (dash/dot) meters.

In conclusion, Cook also showed that with increasing depth, the N-wave shape becomes more rounded and diminishes in amplitude. Figure 2.7 illustrates the results of using Cook's equations. The incident N wave was produced by an aircraft flying at Mach 2.7. Signatures are shown at the surface and at depths of 6, 12, and 62 meters. The waveforms are also scaled relative to peak overpressure in pascals and sonic boom length in meters.

Another key result of Cook's and Sawyers' analyses was that the higher frequency components of the incident sonic boom noise penetrate less far into the ocean. If one takes the $e^{-k_o \mu z}$ term in Eq. (2.21) and rewrites it in frequency instead of wavenumber, it becomes $e^{-\frac{|\omega|}{M c_{\text{air}}} \mu z}$. Here, ω is radian frequency, M is the Mach number, and c_{air} is the speed of sound in air. It is in this term that the frequency spectrum dependence is contained. One can see the frequency/depth dependence from Tbl. 2.1 by using the exponential term and the definition for m given in Eq. (2.7). For each frequency in Tbl. 2.1, the corresponding $1/e$ skin depth is calculated. The skin depth, or penetration depth into water for any frequency is the the depth at which the sound pressure is less than that at the surface by a factor of $1/e$.⁵ Just by looking at these frequencies, it is again noticeable that the higher frequencies decay more rapidly with increasing depth.

Table 2.1: The $1/e$ “skin depth” of the sonic boom noise at specific frequencies.

Frequency (Hz)	Depth (m)
3.33	47.0
33.3	4.70
333.0	0.470

2.2.4. Experimental Verification

Both Sawyers’ and Cook’s work was experimentally verified. The first of such experiments was performed by Waters and Glass in 1970.¹⁰ To validate the theory, dynamite caps were exploded over water to produce spherically spreading N waves which impinged on the surface. The N waves were all under total reflection conditions, or for M less than 4.5. The body of water used was a flooded quarry, 91.5 m (300 ft) wide and 24.4 m (80 ft) deep. Hydrophones placed at depths of .6 m (1.9 ft), .9 m (2.9 ft), and 1.5 m (4.9 ft) were used to measure the underwater pressure field due to the N waves. Microphones were also placed near the surface of the water to measure the incident N wave. Results from the experiment were then scaled and compared to the work of Sawyers. Agreement between the two methods was found to be generally good.

The next experiment was executed by Malcom and Intrieri in 1972.¹¹ Again, to verify theory, small cone-cylinder models were gun-launched over water at Mach numbers of 2.7, and 5.7 in air. A pressure transducer was mounted flush in a aluminum plate and placed in a plexiglass tank 61.0 cm long, 30.5 cm wide, and 61.0 cm deep. Then, by changing the level of water in the tank, measurements of the underwater pressure were taken at depths of 0, 0.32, 2.54, 5.08, and 15.25 cm. For the $M = 2.7$ case, the resulting underwater disturbance was found to be an evanescent wave whose amplitude decreased rapidly with depth. For the $M = 5.7$ case, it was shown that the incident shock wave propagated into the water and did not attenuate with depth. The $M = 2.7$ case was also compared to the work of Sawyers and was found to be in good agreement, hence, showing that sonic boom noise penetration into a flat ocean is well defined by existing theory.

More recently, in 1996 while performing an ambient noise experiment on the Scotian Shelf, Desharnais and Chapman recorded underwater signals from an unexpected sonic boom created by the Air France Concorde.¹² During the experiment, the sea was calm with

a 0.25 swell and 10 knot winds. The signatures were measured in a water depth of 76 meters with a vertical array of eleven hydrophones ranging from 16.5 to 65 meters. In order to verify the waveforms with the theory of Sawyers, certain variables needed to be estimated. This is first because no microphone was at the surface to measure the incident wave and second because the exact altitude and speed of the Concorde was not known. Using the data from the full set of hydrophones and a curve fitting algorithm, it was assumed that the aircraft was flying at Mach 2 and produced an N wave with a duration of 0.16 seconds. Sawyers equations were then used to produce signatures at depths of 16.5, 33, and 57 meters. The experimental data was multiplied by a correction factor, 0.6 relative units per 1.909 pascals, and then compared with the analytical solutions. It was discovered that the evanescent N-shaped waveform was recognizable and did decay with depth. The amplitude of the corrected data agreed well with Sawyers theory however, oscillations followed the experimental sonic boom. This was speculated to be due to bottom reflections or from distortions in the incident wave.

2.2.5. Work of Rochat and Sparrow

Expanding the study of sonic boom noise penetration into the ocean in 1995, Sparrow investigated the effect of aircraft speed on the penetration depth.⁷ Basically, he combined Sawyers' theory with a relationship between aircraft speed and sonic boom duration. First, it was assumed that the aircraft was flying at a constant velocity at a fixed altitude through a homogeneous atmosphere. Then it was shown that the sonic boom duration, T , depended on the aircraft speed by the following expression^{2,15}

$$T = \kappa \frac{M}{(M^2 - 1)^{3/8}}, \quad (2.23)$$

where M is the Mach number of the aircraft and κ is a constant which depends on the plane's shape, altitude, and other parameters. Then using the symbolic manipulation program *Mathematica*,¹⁶ Eq. (2.23) was combined with Eq. (2.6) and a plot of mT versus M was created (Fig. 2.8) where m is again defined in Eq. (2.7).

The data obtained by Sparrow for this plot was for an SR-71 aircraft which produced a nearly perfect N wave of duration 200 ms, Mach 2.6, altitude of 20 km and $\kappa = 0.1483$.⁷ This plot displayed that faster aircraft speeds produced higher peak pressures at a fixed

depth. This is because the product mT appears in the denominator of the last equation in Eq. (2.6), so a larger mT indicates a farther penetration of the sound. Next, plots of a waveform from an aircraft flying at Mach 1.4, 2.4, and 3.4 were examined at depths of 1, 10, and 100 meters below the water surface (Fig. 2.9). Finally, it was determined that at higher aircraft speeds, there is a greater sound penetration into the ocean.

Since Sparrow's work did not account for the change in spectral content of the penetrating sound wave with depth, in 1995 Rochat and Sparrow examined N waves at different depths using several sound descriptors.¹³ By applying these sound descriptors, they showed how measures of loudness change with depth. Rochat and Sparrow also hoped by using these human derived sound descriptors, some realistic measure of annoyance could be determined for marine mammals. Ultimately, the changes in loudness may help determine the effect of sonic boom noise penetration on marine mammals. The sound descriptors used for the research were peak decibel level; unweighted sound exposure level, L_{UE} ; C-weighted sound exposure level, L_{CE} ; A-weighted sound exposure level, L_{AE} ; and Stevens' Mark VII perceived level, PLdB. Using an incident N wave of 50 pascals from an aircraft flying at Mach 2.4, it was shown that there is a significant diminished noise impact with weighted levels. More specifically, L_{CE} , L_{AE} , and PLdB all diminish more rapidly with depth than the peak dB or unweighted levels. Details on the method used to obtain these values and specific results are discussed in Chapter 3.

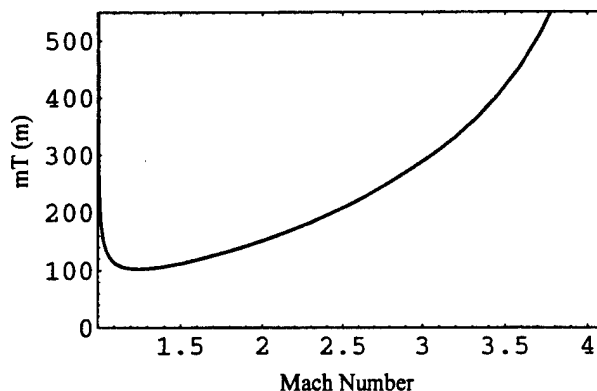


Figure 2.8: The function mT in meters as a function of Mach number.

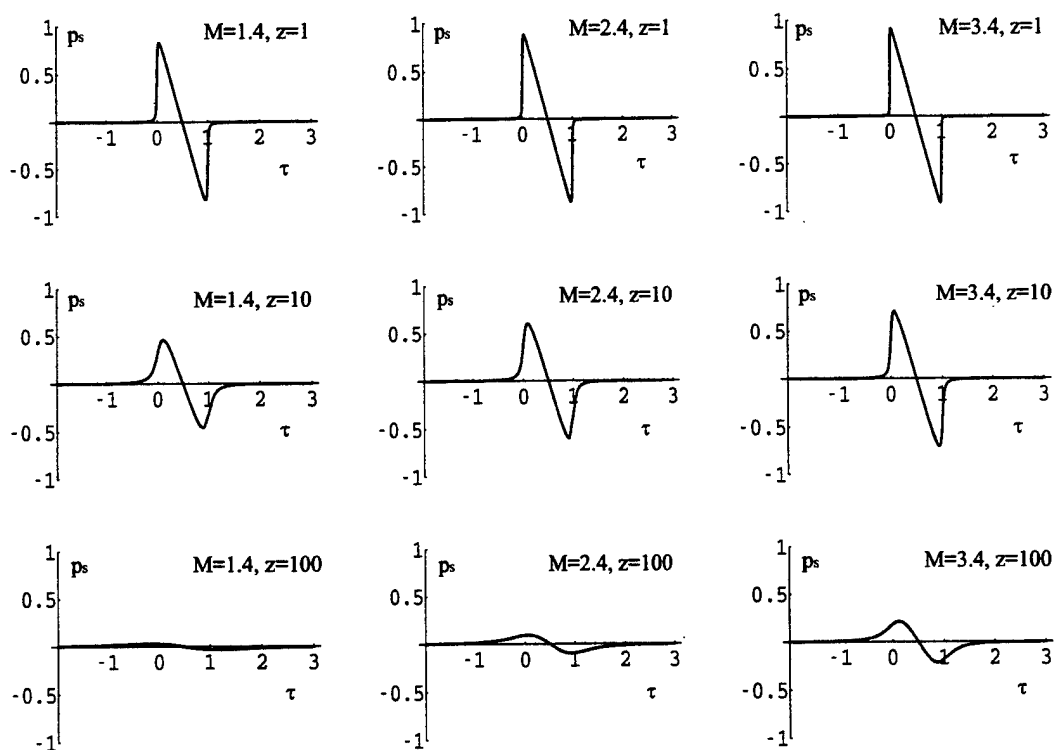


Figure 2.9: Waveforms underwater due to sonic boom penetration. The horizontal axes are scaled time $\tau = t/T$. The vertical axes are scaled acoustic pressure $p_s = p/p_o$. Signatures are shown at depths of 1, 10, and 100 meters for Mach numbers of 1.4, 2.4, and 3.4.

Rochat and Sparrow also recently looked at the effects of ocean swell on sonic boom noise penetration.¹⁴ It is assumed everywhere in this thesis that the ocean is homogeneous and perfectly flat.

Chapter 3.

Arbitrarily Shaped Sonic Booms

3.1. Introduction

All the work described already assumes that a perfectly shaped N wave traveling through a homogeneous atmosphere impinges on the air/water interface. But, in realistic situations most of the waves that hit the surface of the water are not perfect N waves, but are spiked or rounded. The cause of these distortions is believed to be caused by atmospheric processes.¹⁸ Deformations of the waveforms can also be caused by aircraft maneuvers. Aircraft maneuvers will be discussed in detail in Chapter 5. Some of the atmospheric processes include dissipation and turbulence. Dissipation is a mechanism that absorbs acoustic energy, particularly at higher frequencies. This causes a sonic boom with a greater rise time and a more rounded shape. Turbulence resulting from temperature gradients or wind can cause booms with random ripples and peaks, thus making the waveform arbitrarily shaped. It is thought that atmospheric turbulence is the dominant cause of waveform spiking and rounding. Figure 3.1 exhibits the difference between an ideal N wave and a realistically shaped sonic boom.

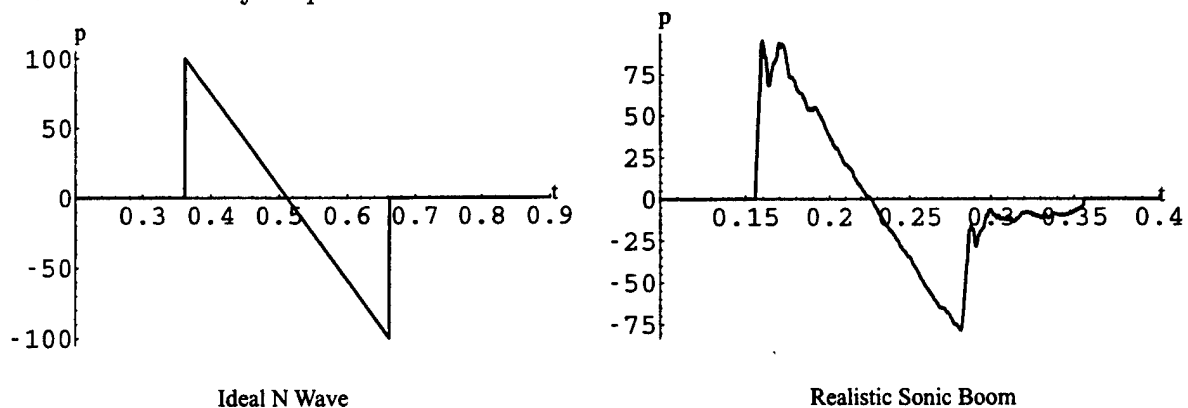


Figure 3.1: Comparison of an ideal N wave and a more realistically shaped sonic boom. The horizontal axes are time in seconds, the vertical axes are pressure in pascals.

3.2. Sonic Boom Noise Penetration Into Water From Arbitrarily Shaped Sonic Booms

To expand on the previous work of sonic boom penetration into a flat ocean, the underwater sound field from more realistic waveforms needs to be considered. In other words, an algorithm was desired that determined the underwater sound pressure for arbitrarily shaped sonic booms. The scope of the present research involves creating such an algorithm. It expands on the work of Cook⁵ and uses the symbolic manipulation program *Mathematica*.¹⁶

The procedure used for finding the underwater sound field from an arbitrarily shaped wave first recalls the N wave work of Cook, Eq. (2.18), taking δ to be 0,

$$p_w(x, z) = -\frac{4}{\pi} \int_0^\infty e^{-k_o \mu z} \sin(k_o x) \frac{d}{dk_o} \left(\frac{\sin k_o}{k_o} \right) dk_o. \quad (3.1)$$

Again, because Eq. (3.1) assumes a perfect N wave, analytical solutions can be found. Modifications to this equation were made to consider random waveforms. More specifically, instead of using a Laplace transform, a Fourier synthesis using discrete Fourier transforms (DFTs) was implemented. Actually, the discrete Fourier transforms were performed as fast Fourier transforms (FFTs). Using the discretized method, the spectrum of the random waveform at the surface is,

$$[\text{spectrum}] = \sum_{X=1}^{N_{\text{samp}}} p_w(x, z=0) e^{-j \frac{2\pi}{N_{\text{samp}}} (K-1)(X-1)}. \quad (3.2)$$

In this expression, X is the spatial sampling variable, K is the wavenumber sampling variable, and N_{samp} is the number of samples in the spectrum. In a similar fashion to Eq. (3.1), the spectrum is used to find the underwater sound pressure,

$$p_w(x, z) = \frac{2}{N_{\text{samp}}} \sum_{K=1}^{N_{\text{samp}}} [\text{spectrum}] e^{-z \mu k_o} e^{j \frac{2\pi}{N_{\text{samp}}} (K-1)(X-1)}. \quad (3.3)$$

Again, the $e^{-z \mu k_o}$ term accounts for the exponential decay of the incident wave with respect to depth. The factor of 2 in front of the equation comes from the pressure doubling at the surface due to the boundary conditions. Rather than performing the Fourier transform in space-wavenumber, the current research uses radian frequency-time. This is achieved by changing K to Ω , a radian frequency sampling variable and X to T , a time sampling

variable. Also, $e^{-z\mu k_o}$ is changed to $e^{-z\mu \frac{|\omega|}{(c_{air}M)}}$ where ω is the radian frequency, M is the Mach number and c_{air} is the speed of sound in air. Thus, rewriting Eq. (3.3),

$$p_w(t, z) = \frac{2}{N_{\text{samp}}} \sum_{\Omega=1}^{N_{\text{samp}}} [\text{spectrum}] e^{-z\mu \frac{|\omega|}{(c_{air}M)}} e^{j \frac{2\pi}{N_{\text{samp}}} (\Omega-1)(T-1)}. \quad (3.4)$$

This form of the expression for the underwater sound pressure with respect to depth is used for all the present research.

Now that an expression for the underwater sound field for any arbitrarily shaped sonic boom was found, the equation was implemented in *Mathematica*,¹⁶ and the *Mathematica* code is found in Appendix B.

Algorithm:

1. Create a data file of pressure values over time by simply reading in data or sampling an existing or created incident waveform. For the algorithm to work, the number of samples needs to be an even number. Since discrete Fourier transforms are performed only on lists of numbers in *Mathematica*, the data file needs to be read in as a list, e.g.,

$$\text{datalist} = \text{ReadList}[\text{"datafile"}, \text{Number}]; \quad (3.5)$$

The function `ReadList["file"]` reads all objects in the specified file and returns a them in a list. Different methods and types of data collection used in the present research will be discussed in detail in Chapter 4.

2. Zero pad the sampled time incident waveform to be a power of 2 to facilitate implementing the FFT. Zero padding permits the computation of the linear convolution of two finite length signals using an FFT.¹⁹ To zero pad in *Mathematica*, first a list of zeros is created.

$$\text{zeros} = \text{Table}[0i, \{i, 1, \text{zerosamples}/2\}] \quad (3.6)$$

The number of zeros, `zerosamples`, is determined by the total number of samples desired minus the number of samples in the signal. The function `Table[expr, {i, imax}]`, generates a list of values of `expr` from 1 to `imax`. The list is only sampled to `zerosamples/2` because half of the zeros are joined to the beginning and half to the end of the waveform samples to create the zero padded sample.

$$\text{zeropad} = \text{Join}[\text{zeros}, \text{datalist}, \text{zeros}] \quad (3.7)$$

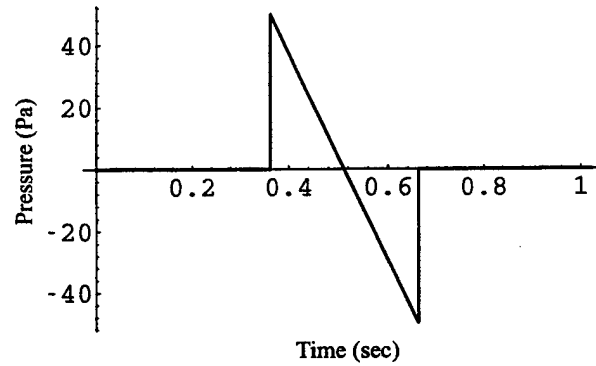


Figure 3.2: An N wave signal, sampled and zero padded. The horizontal axis is time in seconds, and the vertical axis is pressure in pascals.

3. Normalize the zero padded list by dividing the entire list by the maximum pressure value.

$$\text{normlist} = \text{zeropad} / \text{Max}[\text{zeropad}] \quad (3.8)$$

Normalizing the list is necessary to follow the theory of Cook.⁵ Recalling Eq. (2.22), I_1 represents the wave at the surface with a peak amplitude of 1. To get the true dimensions of the boom, p_o , the amplitude of the incident wave, is multiplied by $2I_1$.

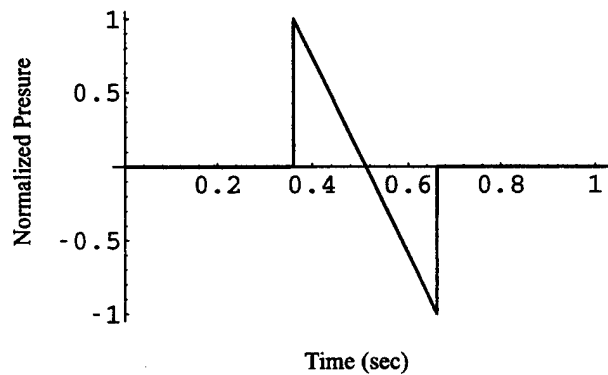


Figure 3.3: The N wave in Fig. 3.2 normalized to have a peak pressure of 1. The horizontal axis is time in seconds, the vertical axis is normalized pressure.

4. Obtain the spectrum of the zero padded, normalized list by using an FFT. In *Mathematica*, to perform an “engineer’s” FFT defined by

$$X[\omega] = \sum_{T=0}^{N_{samp}} x[t] e^{-j \frac{2\pi}{N_{samp}} (\Omega-1)(T-1)}, \quad (3.9)$$

one must use the following expression²⁰:

$$\text{transform} = N[\text{Sqrt}[\text{total number of samples}] * \text{InverseFourier}[\text{normalized list}]]. \quad (3.10)$$

This is because the InverseFourier function is defined as,

$$\frac{1}{\sqrt{N_{samp}}} \sum_{t=0}^{N_{samp}} x[t] e^{-j \frac{2\pi}{N_{samp}} (\Omega-1)(T-1)}. \quad (3.11)$$

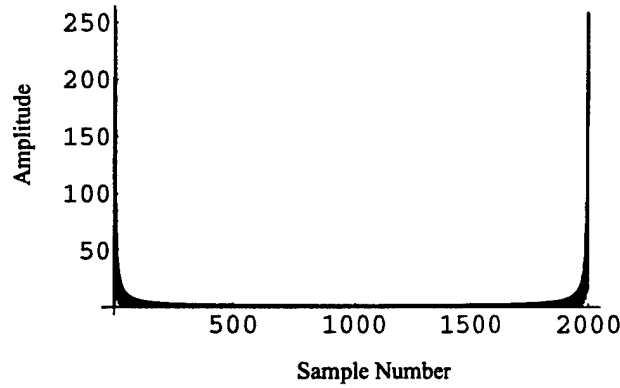


Figure 3.4: The spectrum of the N wave in Fig. 3.3. The vertical axis is amplitude and the horizontal axis is sample number. The samples from 1025 to 2048 represent the negative frequency components of the spectrum.

5. When *Mathematica* performs an FFT, the resulting list contains the positive frequency components on the right and the negative frequency components on the left. In order to properly multiply or window the list by the exponential decay, the negative components must precede the positive. To do this in *Mathematica* use,

$$\text{listswitch} = N[\text{RotateRight}[\text{transform}, \text{samples}/2]]. \quad (3.12)$$

The function `RotateRight[expr, n]`, cycles the elements in *expr*, *n* positions to the right.

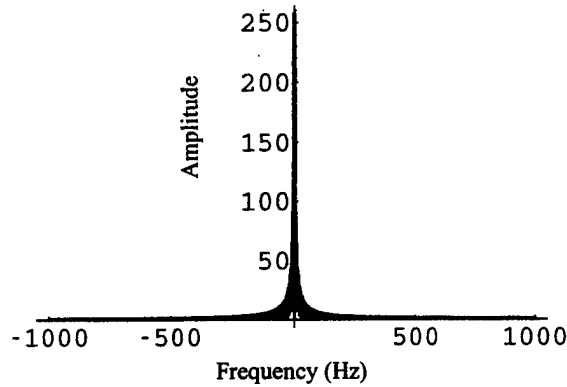


Figure 3.5: The spectrum of the N wave from Fig. 3.4 rotated *samples/2* to the right. The horizontal axis is frequency in hertz, the vertical axis is amplitude.

6. Create a list by sampling the function $e^{-\mu z \frac{|\omega|}{c_{\text{air}} M}}$ from Eq. (3.4). To assure that the exponential function and spectrum lists are the same size, sample the exponential function from $\omega = -\pi f_s$ to $\omega = \pi f_s - \frac{2\pi f_s}{\text{samples}}$ in a step size of $\frac{2\pi f_s}{\text{samples}}$ where f_s is the sampling frequency.

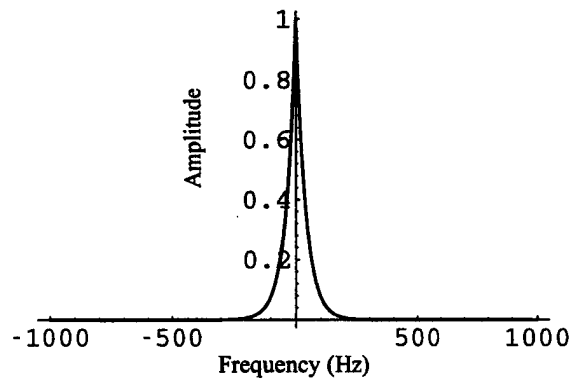


Figure 3.6: An example of a sampled exponential function at a depth of 4 meters ($z=4$). The horizontal axis is frequency in hertz; the vertical axis is amplitude.

The sampling frequency is found by the signal samples/signal duration. A point to notice when sampling the exponential function is that the ω in this function is not the same ω that is involved in the FFT. The FFT ω has the units of radian/sample and is represented

by the expression,¹⁹

$$\omega = 2\pi \frac{f}{f_s}. \quad (3.13)$$

The exponential ω has units of radians and is represented by the expression,

$$\omega = 2\pi f. \quad (3.14)$$

Therefore, to guarantee that the list created from the FFT and the list from the exponential are the same units, the exponential must be sampled from $-\pi f_s$ to πf_s . This sampling also guarantees that the frequencies of the two lists line up.

7. Multiply the spectrum created in step 5 by the exponential list in step 6 ensuring that the multiplication is done by multiplying the n^{th} element in one list by the n^{th} element in the other. This creates the windowed spectrum of the new waveform.

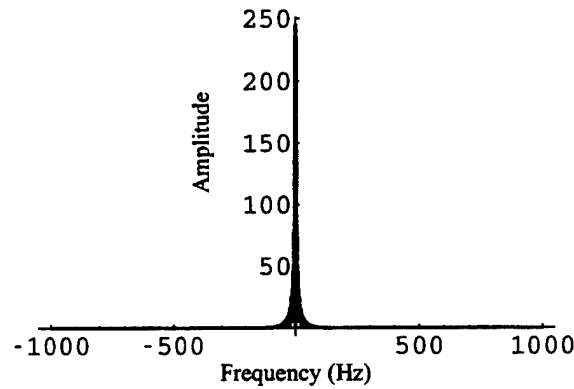


Figure 3.7: Illustration of the N wave spectrum in Fig. 3.5 multiplied by the exponential function in Fig. 3.6. The horizontal axis is frequency in hertz; the vertical axis is amplitude.

8. Switch negative/positive frequency components again by using the function RotateLeft. This places the windowed spectrum in a form to take the inverse FFT.

9. Obtain the waveform of the multiplied spectrum by using an inverse FFT. In *Mathematica*, to perform an inverse FFT defined by

$$x[t] = \frac{1}{N_{\text{samp}}} \sum_{\Omega=0}^{N_{\text{samp}}} X[\omega] e^{+j \frac{2\pi}{N_{\text{samp}}} (\Omega-1)(T-1)}, \quad (3.15)$$

one must use the following expression²⁰:

$$\text{invtrans} = N [(2/\text{Sqrt}[\text{total number of samples}]) * \text{Fourier}[\text{multiplied spectrum}]]. \quad (3.16)$$

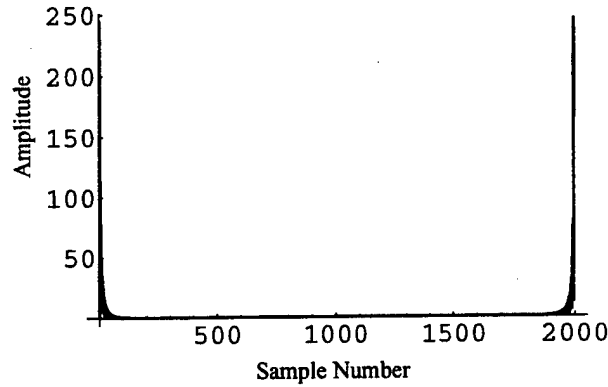


Figure 3.8: The multiplied spectrum in Fig. 3.7 rotated *samples/2* to the left. The vertical axis is amplitude; the horizontal axis is sample number. The samples from 1025-2048 represent the negative frequency components of the spectrum.

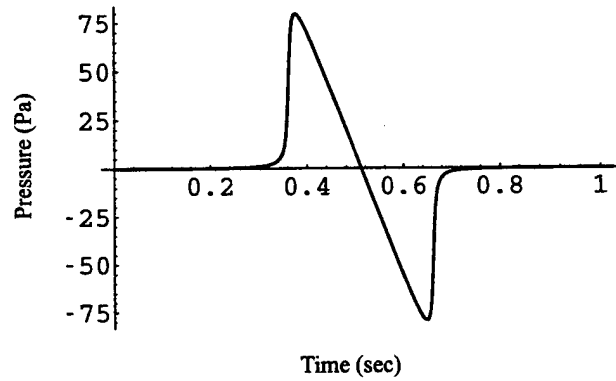


Figure 3.9: The inverse FFT of the rotated spectrum in Fig. 3.8. The waveform is at a depth of 4 meters. The horizontal axis is time in seconds and the vertical axis is pressure in pascals.

This is because the Fourier function is defined as,

$$\frac{1}{\sqrt{N_{\text{samp}}}} \sum_{\Omega=0}^{N_{\text{samp}}} X[\omega] e^{+j \frac{2\pi}{N_{\text{samp}}} (\Omega-1)(T-1)}. \quad (3.17)$$

The factor of 2 in this expression accounts for the pressure doubling at the surface of the water caused by the boundary conditions.

10. Multiply the resulting waveform in step 9 by the peak pressure value of the incident wave to get the true dimensions of the boom.

11. Repeat steps 6-10 for each depth of interest.

End of Algorithm

Because the present research is based on the work of Cook, some of the same assumptions are still valid. In the preceding algorithm, the surface of the water is assumed to be flat. Also, the Mach number of the wave at the ground cannot exceed 4.5. This is because in Cook's work, the incident angle of the waves is assumed to be greater than the critical angle of 13.2° . Therefore, from using Eq. (2.1), the Mach number at the ground must be less than 4.5. If the Mach number is greater than 4.5, a propagating wave exists as described in Section 2.2.1.

In addition to finding the waveform and pressure values at various depths, sound exposure levels were found using the method described in the work of Rochat and Sparrow.¹³ The different sound descriptors were applied to find how the relative measures of loudness change with depth for arbitrarily shaped sonic booms. The physical description of sonic booms is better represented by an unweighted (L_{UE}) or C-weighted (L_{CE}) sound exposure level rather than A-weighted (L_{AE}) levels.²¹ This is because A-weighting roughly accounts for the characteristics of human hearing while C-weighting emphasizes lower frequencies. The predominant frequency content of a typical sonic boom is below several hundred hertz. Therefore, the algorithm used for the present research calculates peak decibel level (dB peak), L_{UE} , L_{CE} , and L_{AE} for each waveform.

First, the peak decibel level was found by using the maximum pressure value of the waveform created in step 10:

$$\text{dBpeak} = 20 \log \frac{\text{max pressure}}{20 \times 10^{-6} \sqrt{2}}. \quad (3.18)$$

The unweighted, A-weighted, and C-weighted sound exposure levels were all calculated in the same manner. First, a Fourier transform of the list of pressure values from step 10 is taken. Second, the transformed list is changed to dB. Third, appropriate A- or C- weighted filters were applied for the respective sound exposure level.²² Fourth, an inverse Fourier transform is performed on the weighted or unweighted list. Finally, sound exposure levels are calculated in dB for each waveform.²³

In summary, the algorithm developed for finding the underwater sound pressure from any arbitrary shaped sonic boom is a function that allows the user to specify an incident waveform data file in pascals, depth in meters, Mach number of the incident wave, and

signal length in seconds. From this input, waveforms and values for peak dB, L_{UE} , L_{CE} , and L_{AE} are output.

3.3. Verification

Now that an algorithm has been developed for any shape sonic boom, it needs to be verified. The procedure used a perfect N wave for the incident wave. The waveform plots were checked against the results of Sawyers⁸ and the sound descriptor results were compared with those of Rochat and Sparrow.¹³ Sound descriptor values for the unweighted sound exposure level at the surface were also checked with existing theory.

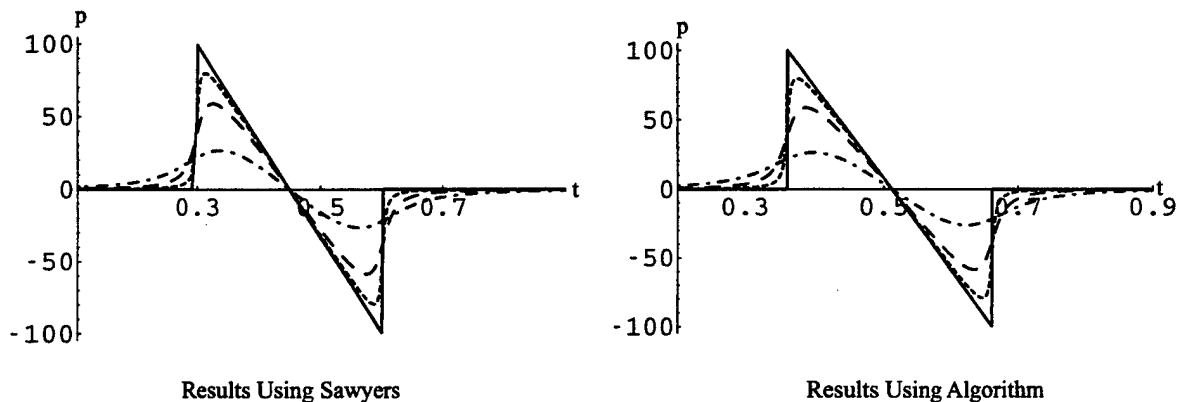


Figure 3.10: Comparative results of a potential HSCT N wave at depths of 0 (solid), 4 (short dashes), 16 (long dashes), and 64 meters (dash/dot). The left graph represents the theory of Sawyers and the right is the new algorithm. The horizontal axis is time in seconds and the vertical axis is pressure in pascals.

To validate the resulting waveform shapes from the algorithm, an incident N wave from a potential High Speed Civil Transport (HSCT) was used. The plane was hypothetically flying at Mach 2.4 and the boom had a signal length of 0.3 seconds and a peak pressure of 100 pascals (2.1 psf). The peak pressure accounts for the pressure doubling at the surface. In the algorithm, a 2048-point FFT was used for the N wave input. The N wave was sampled every 0.5 ms which corresponds to a sampling frequency of 2000 Hz. This rough sampling is sufficient for the research and for common sonic booms since most of the energy is below a few hundred hertz. Also, the high frequency components that do exist do not

penetrate into the water very far and do not contribute greatly to the underwater sound field. The results of using the N wave in the algorithm is shown in Fig. 3.10. Also seen in Fig. 3.10 is the outcome of using the same parameters for the N wave in Sawyers' equations. Four curves are shown for depths of 0, 4, 16, and 64 meters. The curves from the algorithm clearly agree well with the existing theory of Sawyers.

Next, the sound descriptor results were validated by comparing them to the findings of Rochat and Sparrow.¹³ Their calculated results were compared with a Fortran program provided by NASA Langley Research Center, and hence, have been verified themselves.

Table 3.1: HSCT N wave metrics calculated using the present algorithm.

Depth(m)	peak dB	L_{UE} (dB)	L_{CE} (dB)	L_{AE} (dB)
0	131.0	118.0	104.2	91.2
4	129.0	117.1	97.0	61.0
16	126.3	115.2	88.6	38.4
64	119.4	109.8	76.7	8.0

Table 3.2: HSCT N wave metrics from the work of Rochat and Sparrow.

Depth(m)	peak dB	L_{UE} (dB)	L_{CE} (dB)	L_{AE} (dB)
0	131.0	118.0	108.0	94.4
4	129.0	117.1	96.7	61.1
16	126.4	115.3	87.9	38.2
64	119.4	109.9	75.0	9.6

As seen from Tbl. 3.1 and Tbl. 3.2, the peak and unweighted values agree well, but the C- and A- weighted values do not coincide. This is because the process to find these sound exposure levels is extremely frequency sensitive. The method of creating the incident N wave in the algorithm is different than that of the method of Rochat and Sparrow. Therefore, certain frequencies could be present in one calculation, but not in the other. This is causing the sound exposure levels to be different. One point to notice about the various sound metrics is that the L_{AE} levels drop off the fastest with depth and then the L_{CE} , peak dB values, and finally the L_{UE} levels decrease the least. This is discovered to be a consistent result throughout the research.

The tables were then normalized relative to the values at the water surface to create Tbl. 3.3. This is done because even though all the tables in this thesis that are not normalized to the surface are referenced to 20 μPa and 1 second, this algorithm can be used with any other reference values. Plus, in this form it is easy to notice the amount of decay of the dB values relative to depth.

Table 3.3: HSCT N wave metrics from the present algorithm, relative to those at the surface of the water.

Depth(m)	peak dB	L_{UE} (dB)	L_{CE} (dB)	L_{AE} (dB)
0	0.0	0.0	0.0	0.0
4	-2.0	-0.9	-7.2	-30.2
16	-4.7	-2.8	-15.6	-52.8
64	-11.6	-8.2	-27.5	-83.2

As another check, the unweighted sound exposure level at the surface, $z = 0$, was confirmed with an analytical expression. The sound exposure level L_{UE} is defined as

$$L_{UE} = 10 \log \left(\frac{\int_{-\infty}^{\infty} p^2(t) dt}{2p_{ref}^2 T_{ref}} \right) - 3, \quad (3.19)$$

where p_{ref} is 20×10^{-6} for air and T_{ref} is 1 second. The 2 in the denominator is to convert $p^2(t)$ to an RMS quantity, and the 3 dB subtraction is a psychological adjustment to account for the fact that in a single boom, people may hear two audible cracks.³ For the case of an incident N wave, Eq. (3.19) reduces to,

$$L_{UE} = 10 \log \left(\frac{(2p_o/T)^2}{p_{ref}^2} \frac{1}{3} \left(\frac{T}{2} \right)^3 \right) - 3,$$

which equals

$$L_{UE} = 10 \log \left(\frac{T p_o^2}{6 p_{ref}^2} \right) - 3. \quad (3.20)$$

Here, T is the duration of the sonic boom in seconds and p_o is the peak pressure of the wave at the surface of the water. Using the parameters for the N wave listed above, the analytical unweighted sound exposure level at the surface was 118.0 dB which matches exactly with the algorithm method.

The last test examined a case where the Mach number of the aircraft was 4.5. In Cook's theory, when the Mach number was equal to 4.5, the incident ray was at the critical angle.

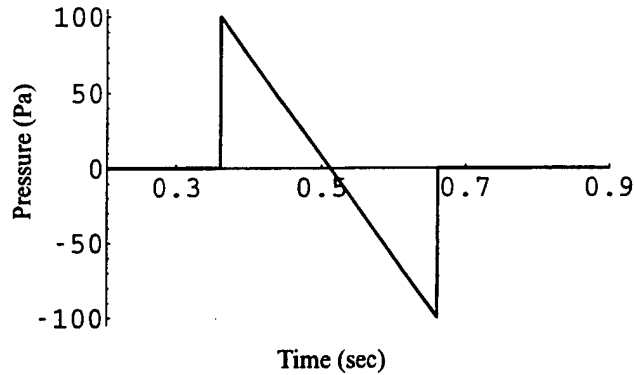


Figure 3.11: Results of a Mach 4.5 HSCT N wave at depths of 0 (solid), 4 (short dashes), 16 (long dashes), and 64 (dash/dot) meters. The horizontal axis is time in seconds and the vertical axis is pressure in pascals. Only the surface wave is seen because the sonic boom does not decay with depth, therefore all curves coincide.

The sound field consisted of equal-intensity incident and reflected waves in the atmosphere and an infinite plane wave in the water⁵. Therefore, from the algorithm, one should see a wave that does not decay with depth, but continues at the same level, even at a depth of 64 meters. An incident N wave from a potential High Speed Civil Transport (HSCT) was used, however the plane was hypothetically flying at Mach 4.5. The sonic boom had a signal length of 0.3 seconds and a peak pressure of 100 pascals (2.1 psf). Again, a 2048-point FFT was used for the N wave input and it was sampled every 0.5 ms which corresponds to a sampling frequency of 2000 Hz. The results of this run for all depths are shown in Fig. 3.11. From Fig. 3.11, one can clearly see the wave has not decayed and the levels at the four depth values line up exactly upon each other as predicted.

Chapter 4.

Sonic Boom Data and Analysis

4.1. Introduction

Once the algorithm of Chapter 3 was validated with known results, other shaped sonic booms were examined. There were several sources from which the input data for the algorithm was obtained. Slightly different steps were taken to get the various data types into a form that could be used. This chapter describes the data types, how each data set was obtained, and the respective underwater waveforms and sound exposure levels at depths of 0, 4, 16, and 64 meters below the water surface.

4.2. Data Collection and Results

4.2.1. Data and Results From Published Spectra

In 1991 Shepherd and Sullivan presented a procedure to find the loudness of sonic booms.²⁴ This work was motivated by the efforts to design a supersonic airplane that would produce a minimized sonic boom at the ground, thus being less annoying to people and animals. This altered sonic boom could theoretically be produced by changing the lift distributions and the volume of a supersonic aircraft. Some examples of these sonic boom shapes include a boom with an expanded rise time and one with a flat top. Analytical spectra are given for each of the boom shapes. These analytical spectra easily can be input to the algorithm described in Chapter 3, yielding predictions of these shaped sonic booms underwater.

In order to find the underwater sound field from the spectra, the corresponding waveforms first needed to be obtained. This was achieved by entering the expression for the spectrum into *Mathematica* and then performing an inverse Fourier transform.

$$\text{waveform} = \frac{\text{peak pressure}}{2\pi} \int_{-\infty}^{\infty} [\text{spectrum}] e^{i\omega t} d\omega \quad (4.1)$$

Next, the waveform was sampled over the wave duration using the Table function, Eq. (3.6), thus creating a list of pressure values over time. The list was then displayed in a column and copied and pasted into BBEdit, a high performance text editor.²⁶ The column was saved to a file and then read back into *Mathematica* as the incident wave in the present algorithm. Finally, the underwater waveforms and sound pressure levels at any depth could be calculated.

The first shape examined was an N wave with an expanded rise time. Figure 4.1 displays an example of this sonic boom.

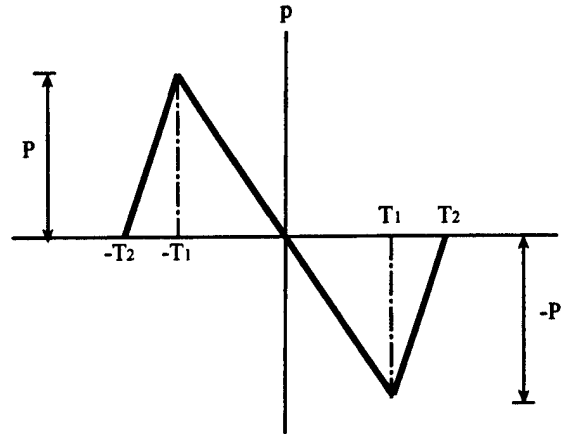


Figure 4.1: An expanded rise time sonic boom. The horizontal axis is time and the vertical axis is pressure.

Defining $\tau = T_2 - T_1$ and $D = T_1 + T_2$ Shepherd and Sullivan give the following expression for the frequency spectrum of the expanded rise time boom,

$$F(\omega) = \frac{i4P(\tau \sin \frac{\omega D}{2} \cos \frac{\omega \tau}{2} - D \sin \frac{\omega \tau}{2} \cos \frac{\omega D}{2})}{\omega^2 \tau (D - \tau)}. \quad (4.2)$$

In order to compare results from this wave to the hypothetical HSCT N wave in Chapter 3, the same sonic boom parameters were used. It was assumed that the HSCT was flying at Mach 2.4 and produced this expanded rise time boom with a duration of 0.3 seconds and a peak pressure of 100 pascals (2.1 psf) after pressure doubling. Therefore, $T_2 = 0.15$ sec, and $T_1 = 0.1$ sec. The waveform was sampled every 0.5 ms which corresponds to a sampling frequency of 2000 Hz.

Comparing the expanded rise time boom in Fig. 4.2 and the HSCT N wave in Fig. 3.10, the increased rise time has little effect on the peak amplitude of the waveforms. This result is more clearly shown by noting the peak dB value in Tbl. 4.2 and Tbl. 3.3. Here, one observes that there is less than 1 dB change between the two waves at all depths examined. The only significant change that occurs by expanding the rise time happens in the C- and A- weighted sound exposure levels. The expanded rise time levels at the surface are lower than the N wave levels, but they decay noticeably less. Therefore, building an aircraft that creates this type of sonic boom may be helpful in diminishing the effect on humans at the surface, but will have the same or worse effect as a comparable N wave with increased depth.

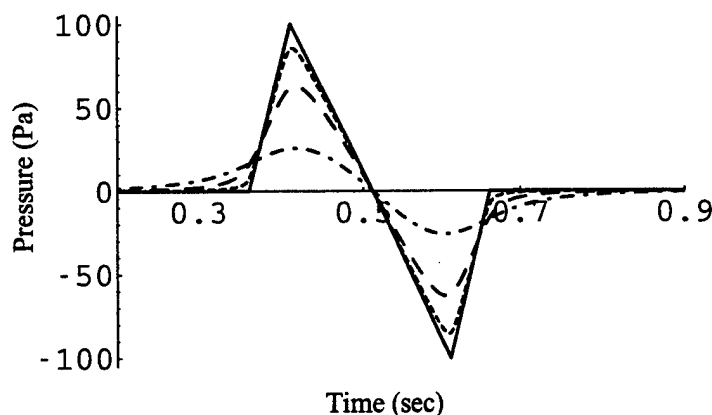


Figure 4.2: Underwater waveforms for a potential HSCT N wave with an expanded rise time at depths of 0 (solid), 4 (short dashes), 16 (long dashes), and 64 (dash/dot) meters. The horizontal axis is time in seconds the vertical axis is pressure in pascals.

Table 4.1: Metrics for a hypothetical HSCT N wave with an expanded rise time.

Depth(m)	peak dB	L_{UE} (dB)	L_{CE} (dB)	L_{AE} (dB)
0	131.0	118.0	94.6	56.3
4	129.6	117.3	92.5	43.9
16	127.0	115.4	88.1	29.9
64	119.2	109.3	77.5	8.5

Table 4.2: Metrics for a hypothetical HSCT N wave with an expanded rise time relative to those at the surface.

Depth(m)	peak dB	L_{UE} (dB)	L_{CE} (dB)	L_{AE} (dB)
0	0.0	0.0	0.0	0.0
4	-1.4	-0.7	-2.1	-12.4
16	-4.1	-2.6	-6.5	-26.4
64	-11.8	-8.7	-17.1	-47.8

The next waveform examined was a modified N wave with minimized overpressure, also called a flat-top boom. Figure 4.3 shows an example of a flat-top sonic boom.

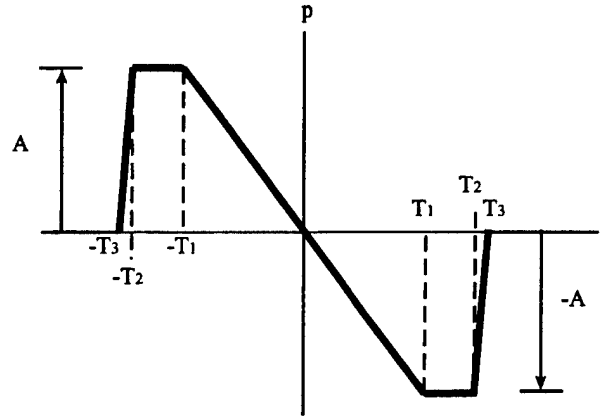


Figure 4.3: A flat-top or minimized overpressure sonic boom. The horizontal axis is time and the vertical axis is pressure.

The frequency spectrum of the flat-top signature is given by Shepherd and Sullivan as,

$$F(\omega) = \frac{i2A [(T_3 - T_2) \sin \omega T_1 - T_1 (\sin \omega T_3 - \sin \omega T_2)]}{\omega^2 T_1 (T_3 - T_2)}. \quad (4.3)$$

Again to compare the results from the flat-top boom to the HSCT N wave, the same parameters were used. It was assumed the HSCT was flying at Mach 2.4 and created the flat top boom with a duration of 0.3 seconds and a peak pressure of 100 Pa (2.1 psf). Therefore, $T_3 = 0.15$ sec, $T_2 = 0.14$ sec, and $T_1 = 0.1$ sec. This wave was also sampled every 0.5 ms which again corresponds to a sampling frequency of 2000 Hz.

Using Fig. 4.4 and Fig. 3.10 to compare the peak amplitudes of the wave shapes, it is noticeable that the flat top boom diminishes less rapidly than the N wave. This is also

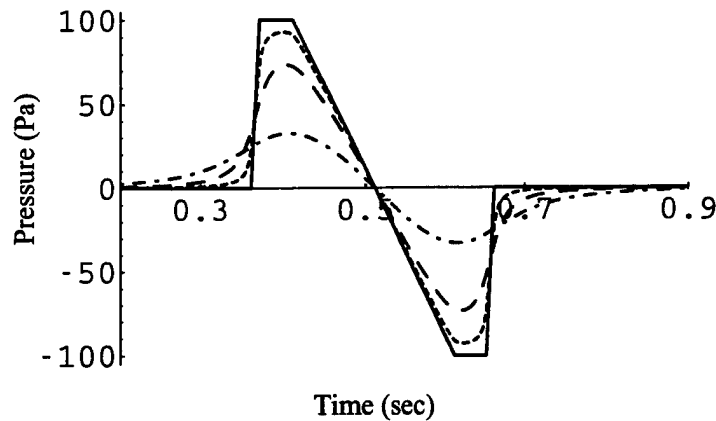


Figure 4.4: Underwater signatures for a potential HSCT flat-top sonic boom at depths of 0 (solid), 4 (short dashes), 16 (long dashes), and 64 (dash/dot) meters. The horizontal axis is time in seconds the vertical axis is pressure in pascals.

Table 4.3: Metrics for a hypothetical HSCT flat-top boom.

Depth(m)	peak dB	L_{UE} (dB)	L_{CE} (dB)	L_{AE} (dB)
0	131.0	119.8	101.2	70.5
4	130.3	119.1	96.7	56.6
16	128.3	117.3	89.9	37.5
64	121.3	111.7	79.0	9.8

Table 4.4: Metrics for a hypothetical HSCT flat-top boom relative to those at the surface.

Depth(m)	peak dB	L_{UE} (dB)	L_{CE} (dB)	L_{AE} (dB)
0	0.0	0.0	0.0	0.0
4	-0.7	-0.7	-4.5	-13.9
16	-2.7	-2.5	-11.3	-33.0
64	-9.7	-8.1	-22.2	-60.7

seen in Tbl. 4.4 and Tbl. 3.3 where at a depth of 64 meters, the peak dB level of the N wave is -11.6 dB relative to the surface level, while the flat top wave has only decreased 9.7 dB. Another detail to point out is that the A-weighted level at the surface for the flat top boom is actually higher than the N wave. Therefore, configuring a plane so that it produced

flat-top-shaped sonic booms might not be a desirable idea to minimize the impact of the sonic boom on underwater noise levels.

Another key result to mention when examining the HSCT N wave, expanded rise time boom, and flat-top boom is the value of the peak overpressure at a depth of 64 meters. Since the values only decay approximately 10 dB relative to the surface, there is still a substantial amplitude sonic boom at 64 meters. Therefore, this result implies that the sonic boom noise can still be prevalent even at substantial depths under the ocean surface.

4.2.2. Data and Results From Actual Aircraft Flights

With the algorithm of Chapter 3, one can also determine experimentally measured underwater sonic boom signatures using incident sonic booms from actual flights. This is an important feature because the underwater sound field can be found from waveforms that have been distorted by processes such as atmospheric turbulence. As an example, actual incident sonic booms were taken from the United States Air Force *BoomFile* database.²⁵ The signatures were measured from flights performed in August 1987 over the Mojave Desert near Edwards Air Force Base. The data was taken by a Boom Event Analyzer Recorder (BEAR) and recorded in files of pressure in pounds per square foot, psf, over time in seconds.¹ In order to find the underwater sound field from these waveforms, the existing measured list of pressure values was simply multiplied by 47.85 to convert to pressure in pascals and read into BBEdit. The BBEdit file was then used as the incident waveform in the algorithm.

The first of the experimentally measured signatures analyzed was an example of a rounded waveform. This boom was created by an F-15 Eagle engaged in straight, steady flight at Mach 1.45 and an altitude of 13.1 kilometers (42,979 ft). It was recorded on August 4th, 1987 from Flight 21, BEAR 61 and had a signal length of 0.2465 seconds and a peak pressure just below the surface of the water of 86.2 Pa (1.8 psf). The existing pressure file was sampled at 0.5 ms for a sampling frequency of 2000 Hz.

The first point to notice is that compared with the HSCT N wave in Fig. 3.10, the rounded wave in Fig. 4.5 decays more rapidly with depth. This is also seen by comparing the peak decibel levels in Tbl. 4.6 and Tbl. 3.3. An explanation for why the rounded wave decays faster is that the F-15 is flying at a lower Mach number than the HSCT. Recalling

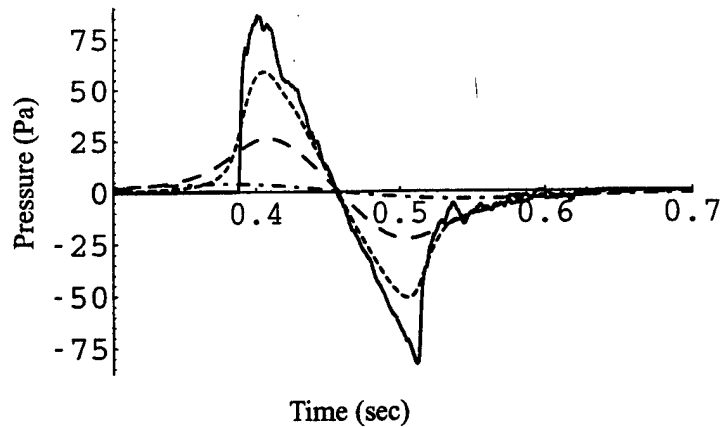


Figure 4.5: Underwater signatures for a surface measured F-15 rounded N wave at depths of 0 (solid), 4 (short dashes), 16 (long dashes), and 64 (dash/dot) meters. The horizontal axis is time in seconds the vertical axis is pressure in pascals.

Table 4.5: Metrics for a measured F-15 rounded wave.

Depth(m)	peak dB	L_{UE} (dB)	L_{CE} (dB)	L_{AE} (dB)
0	129.7	113.8	100.1	76.4
4	126.3	111.4	92.7	48.2
16	119.3	106.1	82.6	24.6
64	102.7	93.6	61.1	-7.9

Table 4.6: Metrics for a measured F-15 rounded wave relative to those at the surface.

Depth(m)	peak dB	L_{UE} (dB)	L_{CE} (dB)	L_{AE} (dB)
0	0.0	0.0	0.0	0.0
4	-3.4	-2.4	-7.4	-28.2
16	-10.4	-7.7	-17.5	-51.8
64	-27.0	-20.2	-39.0	-84.3

the work of Sparrow,⁷ it was determined that at higher aircraft speeds, there is a greater sound penetration into the water. Another result to point out is that the waveform loses its discontinuities and becomes more smooth with increased depth. In other words, the perturbations that are noticeable in the wave at the surface are not seen in the signatures

at depths of 16 or 64 meters. Distortions in the wave have higher frequency components associated with them which are greater than the normal frequency content of an N wave. From the work of Sawyers and Cook it was discovered that higher frequency components of the incident sonic boom penetrate less far into water.^{8,5} Therefore, with increased depth the high frequencies decay faster than the lower ones, thus causing a smoother waveform.

Next of the experimental signatures examined was an example of a double-peaked sonic boom. It was created by an F-15 Eagle in straight, steady flight at Mach 1.45 and an altitude of 13.1 kilometers (42,979 ft). It was again recorded on August 4th, 1987 from Flight 21, BEAR 01. The double-peaked boom had a signal length of 0.1998 seconds and a peak pressure of 95.3 Pa (2.0 psf) after pressure doubling. This existing pressure file was sampled every 0.25 ms for a sampling frequency of 4000 Hz.

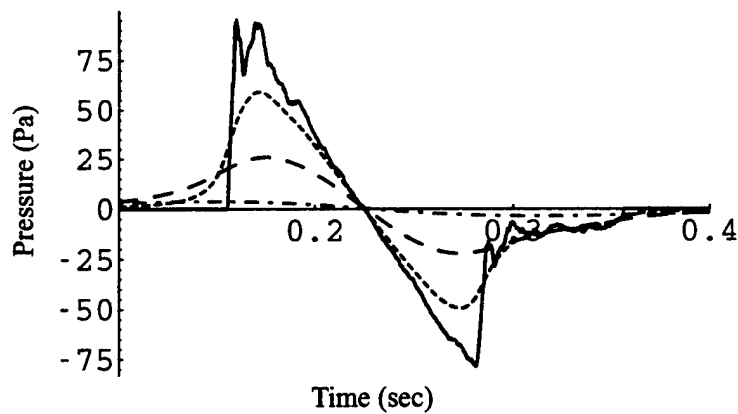


Figure 4.6: Waveforms calculated underwater from a surface measured F-15 double-peaked wave at depths of 0 (solid), 4 (short dashes), 16 (long dashes), and 64 (dash/dot) meters. The horizontal axis is time in seconds the vertical axis is pressure in pascals.

Table 4.7: Metrics for a measured F-15 double-peaked wave.

Depth(m)	peak dB	L_{UE} (dB)	L_{CE} (dB)	L_{AE} (dB)
0	130.6	113.7	101.7	79.7
4	126.4	111.2	94.1	49.8
16	119.2	105.9	84.6	27.4
64	102.5	92.5	65.0	-2.2

Table 4.8: Metrics for a measured F-15 double-peaked wave relative to those at the surface.

Depth(m)	peak dB	L_{UE} (dB)	L_{CE} (dB)	L_{AE} (dB)
0	0.0	0.0	0.0	0.0
4	-4.2	-2.5	-7.6	-29.9
16	-11.4	-7.8	-17.1	-52.3
64	-28.1	-21.2	-36.7	-81.9

From the F-15 double peaked signatures in Fig. 4.6, it is seen that the results for this wave are similar to the ones for the rounded wave. Again, the wave decays faster than the HSCT N wave because the Mach number of the F-15 is 1.45 while the number for the HSCT is 2.4. Therefore, there is a less significant sonic boom at 64 meters. However, in this waveform, it is easier to notice that the high frequency components of the wave decay faster than the low components. Even at a depth of 4 meters, the distortions in the signature have evened out.

The last experimental waveform to be investigated was an example of a U wave. U waves will be discussed in detail in Chapter 5. This boom was created by an F-16 Fighting Falcon again in straight, steady flight at Mach 1.2 and an altitude of 5.6 kilometers (18,372 ft). It was recorded on August 5th, 1987 from Flight 26, BEAR 54. The U wave had a signal length of 0.2995 seconds and a peak pressure of 305.8 Pa (6.4 psf) just below the surface. The sampling frequency for this existing pressure file was 2000 Hz.

Once again, similar results are found compared to the previously mentioned cases. From the waveform results in Fig. 4.7, one can very clearly see that spikes evident in the incident wave do not persist to the 16 or 64 meter wave shapes. This again verifies that the high frequency components do not persist in the underwater sound field. Also since the Mach number is 1.2, the U wave again decays more quickly than the HSCT N wave. Comparing the F-16 signature with the F-15 waves, one notices from examining the waves at 64 meters that the U wave even diminishes faster than the F-15 cases. The peak amplitude at 64 meters for the F-15 runs is nearly two times greater than that for the U wave.

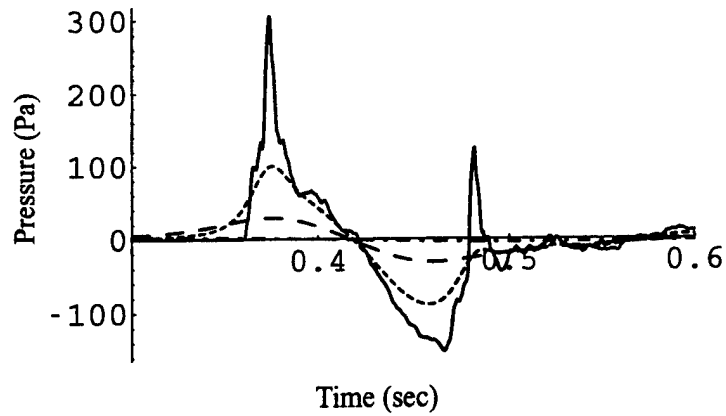


Figure 4.7: Signatures created underwater from a surface measured F-16 U wave at depths of 0 (solid), 4 (short dashes), 16 (long dashes), and 64 (dash/dot) meters. The horizontal axis is time in seconds the vertical axis is pressure in pascals.

Table 4.9: Metrics for a measured F-16 U wave.

Depth(m)	peak dB	L_{UE} (dB)	L_{CE} (dB)	L_{AE} (dB)
0	140.7	119.3	110.8	89.7
4	131.0	115.1	98.9	56.5
16	120.3	107.9	85.1	27.3
64	99.1	93.7	59.5	-11.2

Table 4.10: Metrics for a measured F-16 U wave relative to those at the surface.

Depth(m)	peak dB	L_{UE} (dB)	L_{CE} (dB)	L_{AE} (dB)
0	0.0	0.0	0.0	0.0
4	-9.7	-4.2	-11.9	-33.2
16	-20.3	-11.4	-25.7	-62.4
64	-41.6	-25.6	-51.3	-100.9

4.2.3. Data and Results From PCBoom3

Another way one can exploit the power of the present method is by finding the underwater noise signatures from waveforms created from the sonic boom prediction model PCBoom3.⁴ PCBoom3 is a PC-based program that calculates sonic boom footprints from

any supersonic vehicle. The program is useful for planning missions that will involve supersonic flight, or reviewing sonic boom incidents. An advantage to PCBoom3 is that the vehicle can be exercising any maneuver while flying in a real atmosphere.

To begin an analysis with PCBoom3, one must first specify the options listed below through the menu interface:

The aircraft. PCBoom3 uses the type of aircraft to determine the overall magnitude of the sonic boom. The user can either choose an aircraft from the list given in the aircraft menu, or give a description of the plane in F-function format, through various parameters related to aircraft design. Also, any default parameters for the planes given in the aircraft menu can be changed. Examples of such parameters include the weight and length of the aircraft.

The atmosphere. PCBoom3 uses the atmospheric profile to account for the effects of winds and temperature gradients on the sonic boom location and shape. This information is important in cases such as determining how far the aircraft must go out over the ocean to avoid impacting the shore. The user can again specify or edit an existing atmospheric profile in the atmosphere menu, or create a new file. If the CREATE NEW FILE option is chosen, a dialog box appears where the new atmospheric profile is created. The parameters entered by the user include units for altitude in kilofeet or kilometers, units for temperature either in Fahrenheit, Centigrade, Kelvin, or Rankine, number of temperatures to be input from 2 to 99, the altitude measured from sea level, and the corresponding temperature at that altitude. Other details that are input include ambient pressure at the ground in psf, wind units either in feet/sec or meters/sec, number of X- and Y-wind values from 0 to 99, and altitude and wind values for X- and Y-winds. This creates temperature gradients and winds for use in the analysis. An example of an atmospheric profile is given in Appendix C. This profile describes a U.S. standard atmosphere with no winds.

The elevation of the local ground measured from sea level. PCBoom3 uses the local ground to determine if the sonic boom in question will hit the surface. This value can be different than the ground altitude in the atmospheric profile specified.

The aircraft maneuver. This is usually the most important input. From this, PCBoom3 predicts the sonic booms associated with the designated maneuver. The user can again select or edit an existing maneuver file from the maneuver menu, or create a new

file. If the user chooses to create a new trajectory file, another dialog box appears. The parameters entered first include the trajectory name and a descriptive title line about it. Next, various initial flight parameters are recorded including Mach number, time in seconds, altitude measured from sea level, X, Y, location, heading angle in degrees clockwise from north, climb angle in degrees up from the horizontal, and the first and second derivatives of the Mach number, heading angle, and climb angle. Finally, a series of "advance time" specifications are created. These serve to progress the trajectory at specified time increments chosen by the user. At each of these increments there is the opportunity to change the second derivative of the Mach number, heading angle, and climb angle. Entering a zero, completes the trajectory file. An example of a trajectory file is given in Appendix C. This file characterizes straight flight with no acceleration.

The case title. PCBoom3 uses the title to help the user refer to the current case. It also allows one to save the file and recall it at a later time.

After defining the necessary parameters and saving the current case, PCBoom3 is ready to execute a full ray trace analysis. Selecting the full ray trace analysis in the FILE/EXECUTE menu causes the main sonic boom calculation to enact. In order to monitor progress, a message is displayed each time a boom calculation is started at a new trajectory time. The message is also followed by a series of periods or asterisks with the periods denoting a normal N-wave shaped sonic boom and an asterisk denoting a focus condition. After the boom calculations, the boom footprint is processed. During this procedure, the same time messages are shown and followed by a another series of symbols. An N-wave shaped boom, or a carpet boom, at the ground is denoted by a ".", "*" denotes a focus boom, and a post-focus boom is denoted by a "o." Again, focus conditions will be reviewed in Chapter 5.

PCBoom3 then takes the footprint created in the ray trace analysis and allows it to be viewed in many ways. The first being contour plots of peak overpressures, C-weighted sound exposure levels, loudness, A-weighted sound exposure levels, peak levels, or overall sound pressure levels. Up to six contour levels can be graphed alone or with the corresponding isopemps. The isopemps can also be viewed alone. All of these diagrams also include the ground track of the aircraft. There is also an option which allows the creation of an ASCII file which contains the number of trajectory points, the x-y pairs that first define the

contours, and then the x-y pairs that define the isopemps. An example of this contour file is shown in Appendix C. Another useful feature generates an HPGL, postscript, or DXF file by selecting the plot device type. From this, the graphs can be saved and imported to another program.

Second, PCBoom3 also generates plots of individual sonic boom signatures or its energy spectral density. To look at these, the user must first scroll through a list of trajectory points, which gives the aircraft time, Mach number, position, and altitude. By selecting one of these points, the signature at the end of the computed ray will be shown. If one wishes to see a waveform at any location, there is an option to permit the entry of specific coordinates. After choosing a trajectory point, a list of boom values at the end of a ray defined by the aircraft time, t , and the azimuthal angle, ϕ is displayed. The list also shows the ground intercept points, the arrival time, the maximum overpressure (psf), and the type of boom. After a ϕ value is picked, the user can view the signature or energy spectral density of the sonic boom. One important feature of this output is the ability to create a tabular output of the signature and send it to a file. This feature creates a file which contains the ray involved, the type of signature, and various metrics such as A-weighted sound exposure levels. After this information, a list of pressure values in psf versus time in seconds is displayed. An example of this signature file is again given in Appendix C.

To find the underwater sound field from the output of PCBoom3, the steps outlined above were followed. Then, after creating a case, performing a full ray trace analysis, and choosing a sonic boom signature, the output of the signature was saved to a file. The file was copied to a floppy disk and opened in BBEdit.²⁶ In BBEdit, the header information and time data were removed and the file was saved as simply a list of pressure values in psf. This list of pressure values was then read in as the incident waveform in the *Mathematica* algorithm in Chapter 3. For all cases involving PCBoom3 output, the list of pressure values needed to be changed from psf to pascals. Therefore, every element in the incident waveform list was multiplied by 47.85. Finally, waveforms and sound exposure levels were found at the depths of 0, 4, 16, and 64 meters for each case in question.

The first case examined involved an F-22 Raptor engaged in straight, steady flight over water at Mach 1.2. The PCBoom3 input parameters had the aircraft flying north at 6096 meters (20,000 ft) through a U.S. standard atmosphere with no winds. The trajectory file

and atmospheric profile are again shown in Appendix C. PCBoom3 produced a nearly N-wave shaped signature at trajectory time, $t = 0$ sec, and azimuthal angle, $\phi = 0^\circ$. The plane is already assumed to be flying at Mach 1.2 at time 0. When the waveform was saved to a file, it was sampled every 1.3 ms which corresponds to a sampling frequency of 769 Hz. Again, this coarse sampling works because the predominant frequency content of a sonic boom is under 400 Hz. The peak pressure just below the surface of the water was 274.8 Pa, and the duration was 0.134 sec.

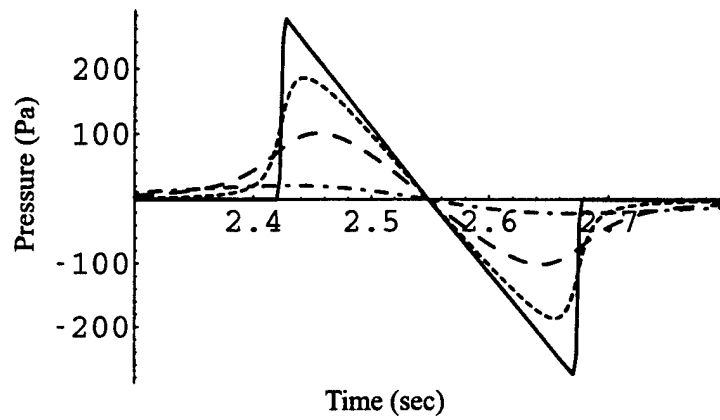


Figure 4.8: Underwater waveforms from a potential F-22 N-shaped wave at depths of 0 (solid), 4 (short dashes), 16 (long dashes), and 64 (dash/dot) meters. The horizontal axis is time in seconds, the vertical axis is pressure in pascals.

Table 4.11: Metrics for a potential F-22 N-shaped wave.

Depth(m)	peak dB	L_{UE} (dB)	L_{CE} (dB)	L_{AE} (dB)
0	139.8	123.3	112.6	93.4
4	134.5	120.0	100.9	57.2
16	126.1	113.5	88.1	28.4
64	107.7	99.4	61.9	-10.0

This initial signature was input into the present algorithm and wave shapes and sound exposure levels were calculated. A point to notice from Fig. 4.8, Tbl. 4.11, and Tbl. 4.12 is that the F-22 wave has a substantial peak overpressure being almost three times the amplitude of the HSCT N wave. The F-22 wave also has a lower Mach number than the

Table 4.12: Metrics for a potential F-22 N-shaped wave relative to those at the surface.

Depth(m)	peak dB	L_{UE} (dB)	L_{CE} (dB)	L_{AE} (dB)
0	0.0	0.0	0.0	0.0
4	-5.3	-3.3	-11.7	-36.2
16	-13.7	-9.8	-24.5	-65.0
64	-32.1	-23.9	-50.7	-103.4

HSCT N wave, causing the F-22 signature to decay faster than the HSCT N wave with increasing depth. At a depth of 64 meters, the peak dB values of the F-22 wave is 11.7 dB less than the HSCT N wave. Therefore even though the sonic boom created by the F-22 is larger at the surface, it penetrates less far into the ocean.

Chapter 5.

Aircraft Maneuvers

5.1. Introduction

The work and results from the previous chapters assume that the aircraft was flying straight and level with no acceleration. However, most supersonic activities associated with Air Force training operations involve maneuvers such as dives, turns, or accelerations. When an airplane is maneuvering, it is better to analyze the sonic booms in terms of rays rather than wavefronts.⁴ Therefore, one would use the ray cone, rather than the Mach cone, to find the sonic booms associated with a certain maneuver, (Fig. 2.2).

Any deviation an aircraft makes from straight steady flight can cause considerable modifications in the location, number, and intensity of the ray pattern emanating from the body.² Figure 5.1 illustrates this result of maneuvering.

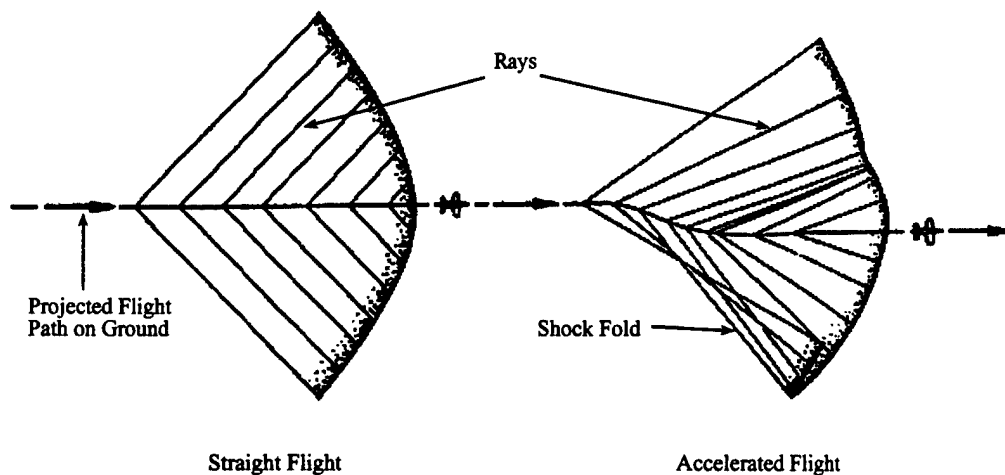


Figure Taken from Ref. 2

Figure 5.1: Ray patterns for aircraft in straight steady flight and accelerated flight. This picture is viewed as if looking down upon the flight path. The aircraft is flying from left to right.

The picture on the left represents the ray pattern below an aircraft in straight steady flight. The emitted rays are generally straight lines which are parallel to each other. Upon ground intersection, the rays create a hyperbolic shape represented by the thick line on the figure. The picture on the right shows the ray pattern for an aircraft which is accelerating. Immediately, one observes that the rays are no longer parallel, converging in some areas, diverging in others. The distortion of the ray pattern also can cause slight variations in the ground intersection shape. The configuration is no longer hyperbolic, but contains irregularities. One of the deformations is a *shock fold* which is shown at the bottom of the ray pattern. In the shock fold, the rays tend to cross which corresponds to a buildup of acoustic pressure at the intersection points. An increase of pressure is also present where the rays cluster, as shown toward the top of the ray pattern. The pressure buildups that occur are a function of the type of maneuver and the acceleration involved. Instead of the common carpet wave, or N wave, developing at these points, the pressure buildup creates a focused sonic boom, or U wave.

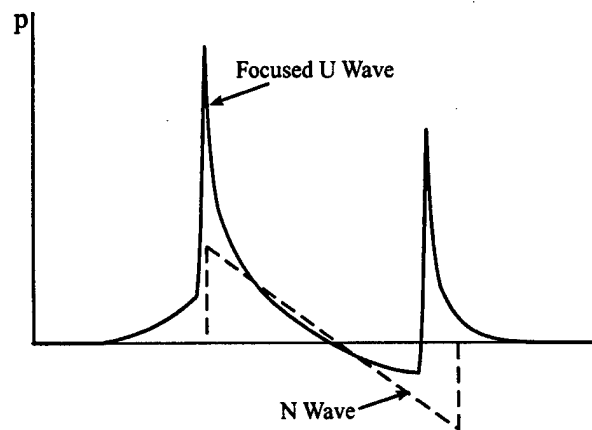


Figure 5.2: A comparison of an N and U wave. The U wave is shown with a solid line and the N wave with a dashed line. The horizontal axis is time and the vertical axis is pressure.

Again, a U wave is a type of sonic boom that is associated with focus conditions. It tends to have a more spiked shape than that of an N wave. A comparison of an N wave and a U wave is displayed in Fig. 5.2. The spikes of the U wave are located at the maximum peak and minimum peak overpressure points of the N wave. This causes most of the U

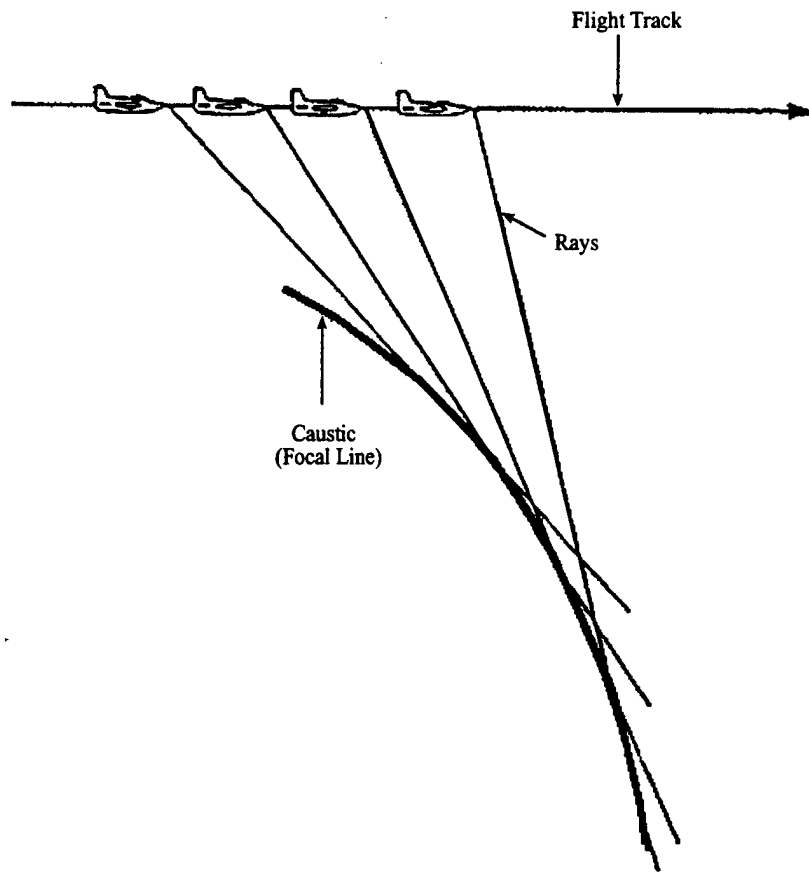


Figure Taken from Ref. 2

Figure 5.3: An example of a caustic caused by acceleration. The aircraft is flying from left to right.

wave to be above ambient pressure. Also, the pressure expansion between the two spikes is no longer linear. Another significant difference between the two waves is in the amplitude. The peak overpressure of a U wave is typically two to five times higher than that of a carpet boom produced with the same conditions. Because of this high amplitude, U waves are also referred to as focused “superbooms.”

Another consequence of distorting ray patterns are *caustics*. A caustic is also known as a focal line. It is created over time and contains the areas in which the rays cross or focused U waves exist. An example of a caustic caused by an acceleration is illustrated in Fig. 5.3. When an aircraft accelerates, the Mach number increases, thus causing the Mach angle to decrease. As the Mach angle decreases, the rays come off the aircraft increasingly

more perpendicular to the ground. This causes the rays to cross at a given point. As the aircraft continues accelerating, the Mach number again increases, and the focus point tends to move farther away from the plane. The caustic is the line that connects the focus points as they move away from the plane.

However, in three dimensions, the rays emit from not only the bottom of the aircraft, but on the top and sides as well creating the ray cone. Maneuvers can also cause the ray cones to intersect. This creates a caustic that is a two-dimensional surface. An example of focusing caused by an acceleration in three dimensions is viewed in Fig. 5.4. Again, when an aircraft accelerates, the Mach angle decreases, causing the ray cone to broaden. This produces successive ray cones which intersect. Since there is a reduction in the forward throw, the hyperbolic ground intercepts of the ray cones, or isopemps, also converge at the ground. The areas where the isopemps intersect is referred to as a *focal zone*. It is within this focal zone that the spiked U-wave shaped sonic booms exist.

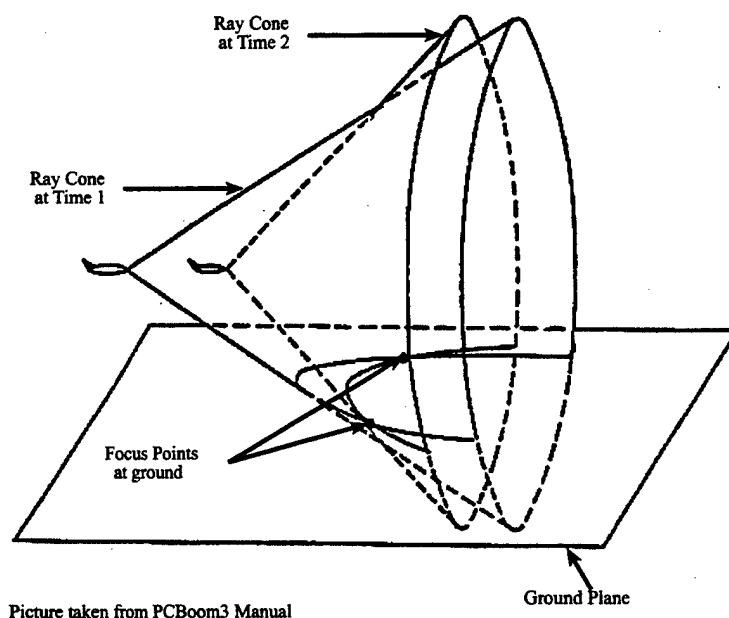


Figure 5.4: An example of focusing caused by an acceleration in three dimensions. The aircraft is flying from left to right.

A very important point to remember is that although the aircraft and the waves are traveling, the focal zones are fixed and do not move with the aircraft. The width of the

localized focus areas are on the order of only 305 meters (1000 ft) rather than on the order of hundreds of kilometers.

5.2. Methods

Next, the effect of select aircraft maneuvers on sonic boom noise penetration into the ocean was investigated. This was accomplished through many steps again using PCBoom3,⁴ *Mathematica*,¹⁶ BBEdit,²⁶ and the algorithm introduced in Chapter 3. Five maneuvers were chosen for analysis; a linear acceleration, a 10° dive, a 30° dive, a pushover, and a constant g turn. Each maneuver's trajectory file was used in PCBoom3 to predict the respective sonic boom footprint. One of the outputs of performing a full ray trace analysis in PCBoom3 is the file *case title*.OUT. An example of a .OUT file is listed in Appendix C. Despite the suggestions of the PCBoom3 manual, the .OUT file should not be deleted. This file is the main output file and contains much useful information. At each trajectory time the following data is specified: x , y , z , location of the aircraft, airplane Mach number, climb angle, heading angle, and the first and second derivatives of the Mach number, heading angle and climb angle. After this information is listed, each trajectory time is broken up into the various ϕ components. For each ϕ value, the type of sonic boom and the number of points in the signature are some of the things listed.

Another key piece of information in the .OUT file is the x , y , z , components of the ray-direction unit vector at the ground for each ϕ value. From this vector, the local ground Mach number can be found. The local Mach number needs to be calculated because it is the Mach number that is perceived at the ground and is used in the current algorithm to find the underwater sound field. To explain further, when an aircraft is in straight steady flight and assuming a flat water surface, the angle which the ray makes with the vertical as it comes off the plane is the same at which it intersects the surface. This case is shown on the left in Fig. 5.5.

The picture on the right shows a diving aircraft. Here, the angle which the ray makes with the vertical as it comes off the plane is not the same at which it intersects the surface. Up to this point in this thesis, it has been assumed that these two angles are the same. In Chapter 2, this angle was defined as the Mach angle, α , for the ray cone. Therefore for a maneuvering aircraft, the Mach number of the aircraft is different from that perceived at

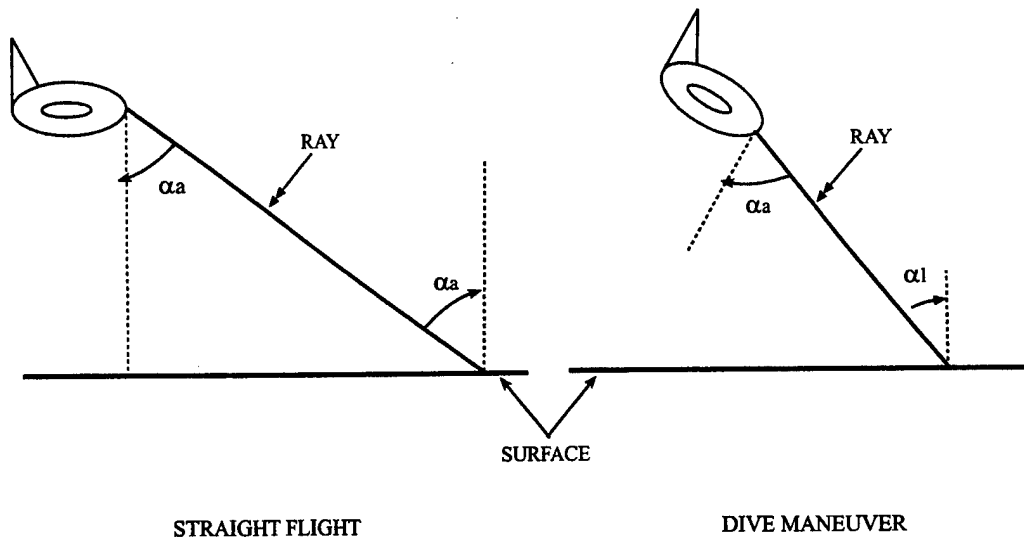


Figure 5.5: A comparison of ray intercepts with the ground. The case on the left is for straight steady flight, and the one on the right is for a diving aircraft. The aircraft Mach angle is represented by α_a while the local Mach number is α_l .

the ground. The local ground Mach number is also calculated by Eq. (2.1),

$$M = \frac{1}{\sin \alpha_l},$$

where now α_l specifically denotes the angle with respect to the ground. However, the .OUT file doesn't explicitly give a value for this Mach angle, and it needs to be calculated from the components of the unit vector. Using the definition for spherical coordinates shown in Fig. 5.6, the angle from the vertical to the ray is given by the expression,²⁷

$$\alpha_l = \cos^{-1} \left[\frac{z}{r} \right]. \quad (5.1)$$

Since a unit vector is the ray being used, the value of r is 1. Therefore, Eq. (5.1) reduces to,

$$\alpha_l = \cos^{-1} [z]. \quad (5.2)$$

By using Eq. (2.1) and Eq. (5.2) the local ground Mach number can be determined

$$M = \frac{1}{\sin [\cos^{-1} [z]]}. \quad (5.3)$$

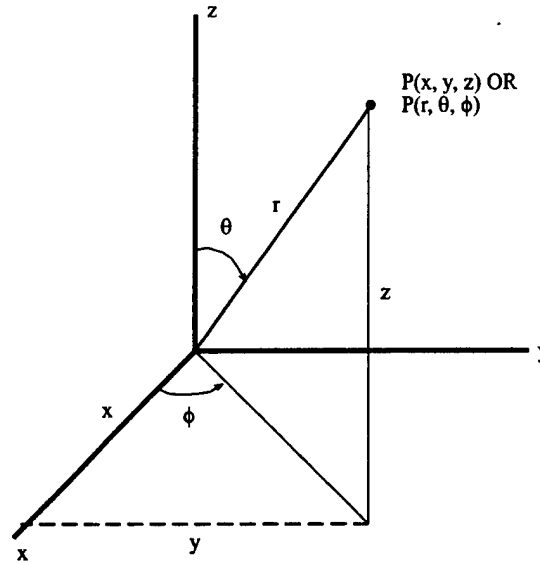


Figure 5.6: The representation of spherical coordinates.

After defining the local Mach number for each trajectory time, a plot of aircraft and local Mach number versus time was generated for each maneuver. A diagram of each trajectory was also created. The final graph that was produced was a plot of the isopemps for each maneuver. This was accomplished through PCBoom3 by viewing the isopemps alone after the full ray trace analysis. By mapping out the isopemps, focal zones for each maneuver were ascertained. From the various figures, waveforms were chosen to be input into the algorithm of Chapter 3. The underwater wave shapes and sound exposure levels were found at the surface of the water and at depths of 4, 16, and 64 meters. Finally, each waveform was compared to a signature created by an identical aircraft engaged in straight flight. This case used all the same initial parameters as the corresponding maneuver, but generated the sonic boom footprint as if the aircraft were in straight steady flight. From this comparison, the effect of the maneuver on sonic boom noise penetration into water can be predicted.

5.3. Maneuver Results

5.3.1. Linear Acceleration

The first maneuver analyzed was a linear acceleration. The parameters used in PC-Boom3 include an F-15 Eagle flying east through a U.S. standard atmosphere with no winds. The trajectory file, a 0.31 g linear acceleration where g is the acceleration due to gravity, places the fighter initially at 3,048 m (10,000 ft), flying at Mach 0.9. A plot of the aircraft and local Mach number versus time is seen in Fig. 5.7. From this figure, one first observes that there is no local ground Mach number for the first 18 seconds of the trajectory. This is due to the fact that no sonic boom reaches the ground because the plane is mainly subsonic. When a sonic boom reaches the ground, the local Mach number is slightly lower than the aircraft Mach number. Because the aircraft is parallel with the surface, the difference in Mach number is not caused by the maneuver. It results from the effects of the atmosphere on the ray as it travels from the aircraft to the ground.

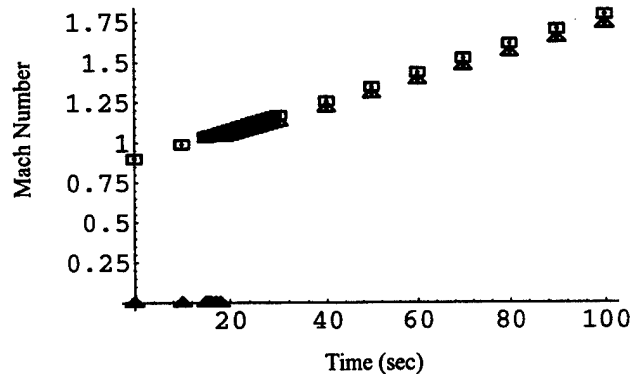


Figure 5.7: Plot of aircraft Mach number and local Mach number versus time for a linear acceleration. The aircraft Mach number is represented by squares and the local Mach number by triangles. A symbol at $M=0$ means there is no sonic boom at the ground for that time. The horizontal axis is time in seconds and the vertical axis is Mach number.

Next, the respective isopemps were generated and are shown in Fig. 5.8. The isopemps begin where the booms intersect with the ground or 19 seconds into the trajectory. The isopemps located on the left are spaced one second apart while the ones on the right are

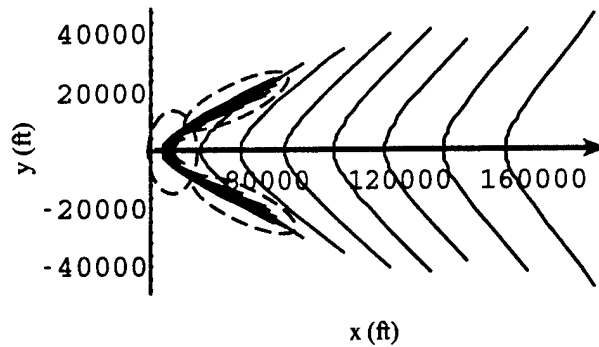


Figure 5.8: Isopemps created during a linear acceleration. The horizontal and vertical axes are x and y ground positions in ft, $1 \text{ ft} = 0.3 \text{ m}$. The view shown is as if one was looking down upon the flight path which is shown with an arrow. The plane is flying from left to right.

spaced every ten seconds. A point to note concerning all the isopemp figures is the flight path shown with an arrow is not the actual one. Since the isopemps are hyperbolic ground intercepts of the ray cone, the actual flight path would be located before the isopemps. In the particular case of the linear acceleration, the flight path would be to the left of the isopemps. To clearly demonstrate how the isopemps relate to the trajectory, the flight path is superimposed on the figure. The focal zones for this maneuver are developed during the beginning of the acceleration and are inside the circled areas. It is clearly noticed that the isopemps cluster and intersect within these regions. Again, the reason for the focusing is that when the aircraft accelerates, the ray cone broadens causing consecutive isopemps to intersect. Starting 40 seconds into the trajectory, the ray cone flattens to a point where the isopemps fail to cross and only carpet booms exist.

To determine the effects of a linear acceleration on sonic boom noise penetration into the ocean, a straight flight case was created for comparison. It also assumed an F-15 Eagle was flying east through a U.S. Standard atmosphere with no winds. However, instead of accelerating the aircraft remained in straight steady flight at 3,048 m (10,000 ft), flying at Mach 0.9. No sonic booms were created during this trajectory because the aircraft remained subsonic. Therefore, the booms that are created from the flight including the linear acceleration are a direct result of the maneuver.

The first waveform chosen as an incident wave in the algorithm was the signature created directly below the flight path at $t = 19$ seconds. This time was chosen primarily because

it was the first time a sonic boom reached the ground. This point was also contained in a focal zone. The aircraft was flying at Mach 1.1 and the resulting local ground Mach number was 1.0. From PCBoom3, a focused U wave was predicted with a signal length of 0.2558 seconds and a peak acoustic pressure of 420.2 Pa (8.8 psf) after pressure doubling. The wave was sampled every 1.3 ms which is a sampling frequency of 796 Hz.

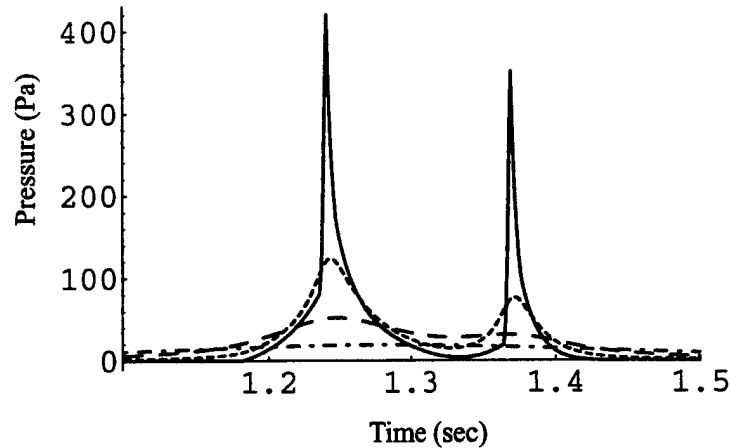


Figure 5.9: Underwater waveforms for a sonic boom predicted at trajectory time 19 seconds, $\phi = 0^\circ$ during a linear acceleration at depths of 0 (solid), 4 (short dashes), 16 (long dashes), and 64 (dash/dot) meters. The horizontal axis is time in seconds, the vertical axis is pressure in pascals.

Table 5.1: Metrics for trajectory time 19 seconds, $\phi = 0^\circ$ for a linear acceleration.

Depth(m)	peak dB	L_{UE} (dB)
0	143.4	120.4
4	132.8	116.7
16	125.4	113.7
64	116.6	110.3

This initial signature was input into the present algorithm and wave shapes and sound exposure levels were calculated. The waveform results are viewed in Fig. 5.9 and peak dB values and unweighted sound exposure levels are listed in Tbl. 5.1. The first aspect to notice about this sonic boom is that it is of a substantial size at the surface. However, because of

the low Mach number, the wave has decreased to less than half of its original amplitude by a depth of four meters. The high frequency components do diminish rapidly, but evidence of the spikes is still present at 16 meters. Therefore, because the aircraft accelerated, this focused sonic boom was created and prevails underwater, even at depths of 64 meters.

The next trajectory time chosen for investigation was at $t = 90$ seconds. At this time, the ray cone has broadened enough such that only carpet (N-wave shaped) booms exist. At this point, the aircraft was flying at Mach 1.7 with the local ground Mach number being 1.6. A carpet boom located directly under the flight path was predicted by PCBoom3 with a duration of 0.0843 seconds and a peak pressure of 638.9 Pa (13.4 psf), a substantial size boom. This wave was sampled at 1,235 Hz or every 0.81 ms.

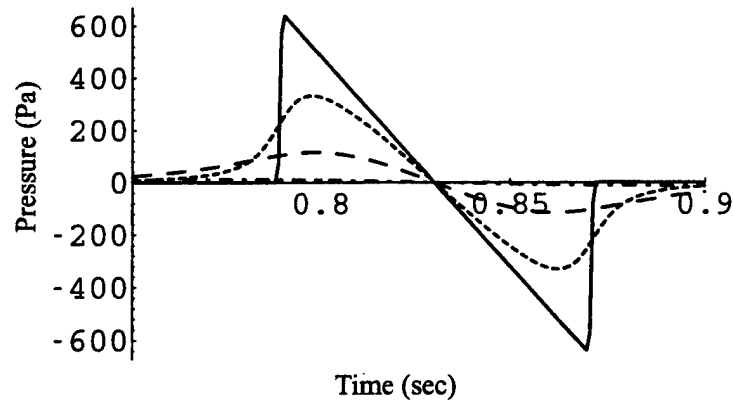


Figure 5.10: Signatures created underwater from trajectory time 90 seconds, $\phi = 0^\circ$ for a linear acceleration at depths of 0 (solid), 4 (short dashes), 16 (long dashes), and 64 (dash/dot) meters. The horizontal axis is time in seconds, the vertical axis is pressure in pascals.

Table 5.2: Metrics for trajectory time 90 seconds, $\phi = 0^\circ$ for a linear acceleration.

Depth(m)	peak dB	L_{UE} (dB)
0	147.1	128.6
4	141.4	125.0
16	132.2	117.8
64	113.1	103.2

From the underwater signatures displayed in Fig. 5.10, one can see that even though a carpet boom was predicted, it clearly has an amplitude that is 34 percent greater than the focused wave at 19 seconds. However, Tbl. 5.2 shows that by the time the waves are 64 meters below the surface, the N wave is smaller than the U wave. It should also be noted that the N wave decays faster while being at a higher Mach number. Therefore, even though the N wave has the larger amplitude at the surface, focusing effects are more prevalent at greater depths and cause a greater acoustic pressure underwater.

From this example, it was shown that a subsonic aircraft performing a linear acceleration while maintaining a constant altitude, will cause sonic booms upon going supersonic. Early in the supersonic acceleration, focal zones will be produced, causing focused U waves and a greater penetration of sonic boom noise into the ocean. The focusing will persist until the plane has accelerated to a point where the ray cone has flattened enough to only produce carpet booms. A way to counter the focusing effects of the linear acceleration would be to fly at higher altitudes. This makes the ray path from the plane to the ground greater and thus gives the atmosphere a better chance to diminish the amplitude of the signature. Along the same idea, another countering action would be to climb while accelerating. Not only does this increase altitude and make the ray path longer, but the resulting local ground Mach number would be lower. This causes the wave to penetrate less far into the ocean.

5.3.2. 10 Degree Dive

The next maneuver examined was a 10 degree dive. This case involved an F-15 Eagle flying west through a U.S. standard atmosphere with no winds. The plane was initially flying at Mach 0.9 at an altitude of 5,578 m (18,300 ft). The trajectory taken by the fighter is displayed in Fig. 5.11. The aircraft begins to dive at a 10° angle two seconds into the flight path. This dive continues until an altitude of 4,398 m (14,429 ft) achieved at $t = 23$ seconds. Next, the plane climbs at a 5° angle to the final altitude of 5,103 m (16,742 ft). The aircraft and local Mach number achieved over time is seen in Fig. 5.12. The only time a sonic boom intersects the ground is between 19 and 23 seconds. During this short time, the local Mach number is slightly higher than the aircraft number while diving and lower while climbing. The difference in local Mach number is due to the fact that the aircraft is

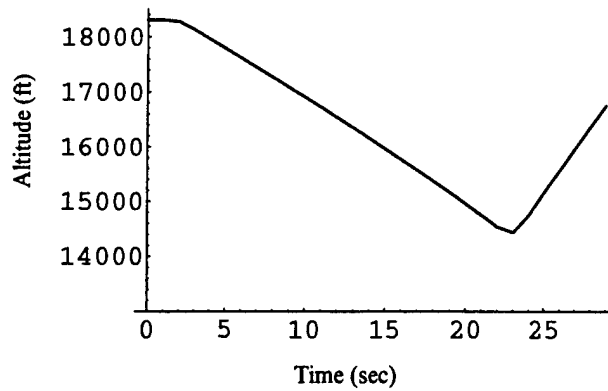


Figure 5.11: Trajectory for a 10° dive. The horizontal axis is time in seconds. The vertical axis is altitude in feet, $1 \text{ ft} = 0.3 \text{ m}$.

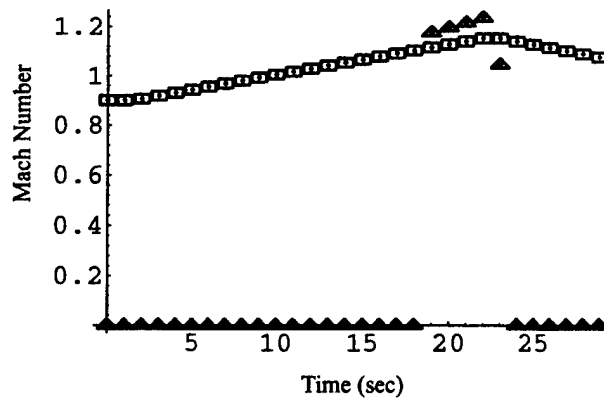


Figure 5.12: Plot of aircraft Mach number and local Mach number vs. time for a 10° dive. The horizontal axis is time in seconds, the vertical axis is Mach number. The aircraft Mach number is represented by squares and the local Mach number by triangles. A symbol at $M=0$ means there is no sonic boom at the ground for that time.

not parallel with the ground. Again, this causes the Mach angle to change from the plane to the surface, resulting in different Mach numbers.

The five isopemps created during this dive are displayed in Fig. 5.13. All the isopemps are spaced one second apart. The only focal zone created from this maneuver is developed during the dive section of the trajectory. This focusing exists over the entire isopemp and is a result of acceleration during the dive. The one isopemp which is separated from the

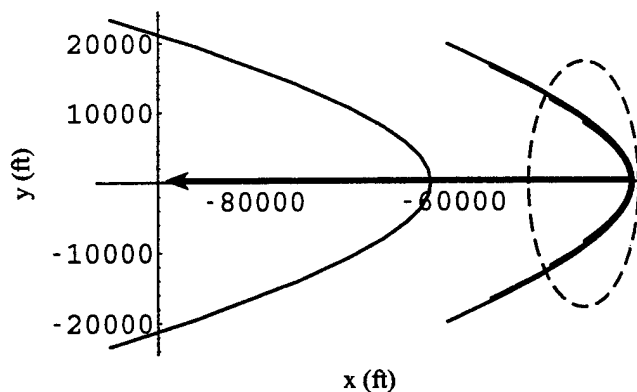


Figure 5.13: Isopemps for a 10° dive. The horizontal and vertical axes are x and y ground positions in ft, 1 ft = 0.3 m. The figure is shown as if looking down on the flight path which is shown with an arrow. The plane is flying from right to left.

cluster is a result of climbing. In this example climbing causes a decrease in the aircraft speed, thus producing an increased forward throw and diverging isopemps.

A straight flight trajectory was used to determine the effect of a 10° dive on sonic boom noise penetration into water. This case also had an F-15 Eagle flying west through a U.S. standard atmosphere with no winds. The aircraft was flying at Mach 0.9 at an altitude of 5,578 m (18,300 ft). Since the straight flight trajectory was flown at a subsonic Mach number, no sonic booms existed. Therefore, the ones that are that are created in the flight with the maneuver are a direct result of the 10° dive.

The underwater sound field was first calculated for $t = 19$ seconds. This time was chosen primarily because it was the first time that a sonic boom reached the ground. This point was also contained within a focal zone. The F-15 was at an altitude of 4,621 m (15,162 ft) flying at Mach 1.1 with the corresponding local Mach number being 1.2. PCBoom3 predicted a focused sonic boom directly under the flight path with a peak pressure of 518.3 Pa (10.8 psf) and a signal length of 0.2485 seconds.

The waveform results of this point in the 10° dive are displayed in Fig. 5.14. This focused wave is similar to the one produced during the linear acceleration. From the peak dB values in Tbl. 5.3 it is again noticed that there is a substantial amplitude at the surface. However, the wave decreases to less than half of the original amplitude by a depth of four meters. The spikes in the wave shape are noticeable at 16 meters and there still is a

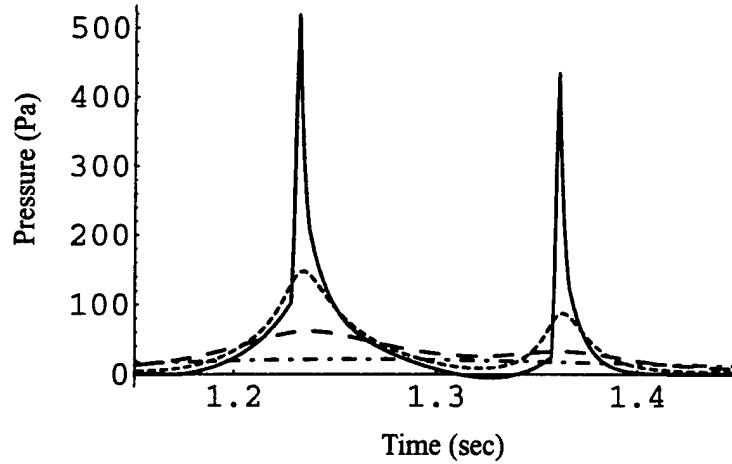


Figure 5.14: Underwater waveforms for a sonic boom predicted at trajectory time 19 seconds, $\phi = 0^\circ$ during a 10° dive at depths of 0 (solid), 4 (short dashes), 16 (long dashes), and 64 (dash/dot) meters. The horizontal axis is time in seconds, the vertical axis is pressure in pascals.

Table 5.3: Metrics for trajectory time 19 seconds, $\phi = 0^\circ$ for a 10° dive.

Depth(m)	peak dB	L_{UE} (dB)
0	145.3	121.4
4	134.4	117.5
16	126.8	114.3
64	117.7	110.8

significant acoustic pressure at 64 meters below the surface. One again sees that focusing effects produce a greater penetration depth of sonic boom noise into the ocean.

The next time examined underwater was at trajectory time, $t = 23$ seconds. At this time, the aircraft had completed the dive and was engaged in a 5° climb. The fighter was flying at an altitude of 4,398 m (14,429 ft) at Mach 1.2. The calculated local ground Mach number was 1.0. PCBoom3 predicted an N-wave shaped sonic boom right under the flight path with a duration of 0.1816 seconds and a peak pressure 167.1 Pa (3.5 psf). As compared with the dive portion of the trajectory, the wave that is predicted here has a smaller amplitude. More specifically, the N wave has a peak dB value that is 9.9 dB less than the focused wave. Also because of the low local Mach number, the signature decays

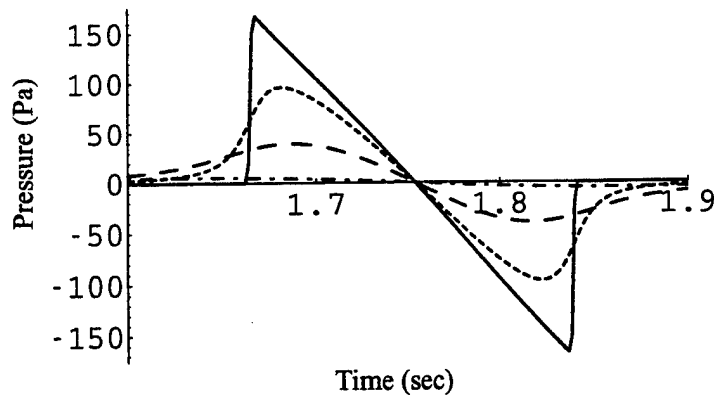


Figure 5.15: Signatures calculated underwater from trajectory time 23 seconds, $\phi = 0^\circ$ for a 10° dive at depths of 0 (solid), 4 (short dashes), 16 (long dashes), and 64 (dash/dot) meters. The horizontal axis is time in seconds, the vertical axis is pressure in pascals.

Table 5.4: Metrics for trajectory time 23 seconds, $\phi = 0^\circ$ for a 10° dive.

Depth(m)	peak dB	L_{UE} (dB)
0	135.4	120.2
4	130.6	117.3
16	122.9	111.3
64	105.5	97.9

quickly, being reduced by 29.9 dB at 64 meters below the surface. Therefore, a climb maneuver will have a decreasing effect on the underwater sound field as compared with a dive.

Therefore, it was seen that a subsonic airplane engaged in a dive at an angle of 10 degrees will accelerate and eventually will go supersonic. Because the plane is accelerating while diving, focused sonic booms will be produced that have a higher local Mach number than the aircraft Mach number. The focusing causes the wave to decay less quickly and thus causes a greater penetration of sonic boom noise into the ocean. A way to counter the effects of focusing during a dive would be to perform the dive at a higher amplitude. This would again give the atmosphere a greater opportunity to diminish the amplitude of the wave. In addition, when the aircraft climbs, the waves that are created are considerably

less in amplitude. Climbing also causes the local Mach number to be lower than the aircraft speed therefore causing the sonic boom noise to penetrate less far into the water.

5.3.3. 30 Degree Dive

The third maneuver that was investigated for its effect on sonic boom noise penetration into water was a 30 degree dive. It also was used to compare with the 10 degree dive discussed above. The 30° dive was performed by an F-15 Eagle initially flying west at an altitude of 5,578 m (18,300 ft) through a U.S. standard atmosphere with no winds. The trajectory taken by the fighter is illustrated in Fig. 5.16. At $t = 0$ seconds, the plane is flying level at Mach 0.9. Starting eight seconds into the path, the aircraft begins to dive at a 30° angle. The dive continues until $t = 17$ seconds where an altitude of 3,043 m (9,983 ft) is reached. At this time, the F-15 first levels and then climbs at a 15° angle until the end of the trajectory and a final altitude of 3,603 m (11,820 ft). A comparison of the aircraft and local Mach numbers is represented in Fig. 5.17. From this figure it is noted that no sonic booms are generated until eleven seconds into the flight path. This is due to the fact that the aircraft is subsonic. When the aircraft accelerates to supersonic speed causing sonic booms to intersect the ground, the local Mach number of the waves increases to almost twice that of the aircraft Mach number. However, during the climb portion of the trajectory, the local Mach number recedes to a point that is lower than the aircraft Mach number. This is again a result of the plane not being level with the ground causing the Mach angle to vary.

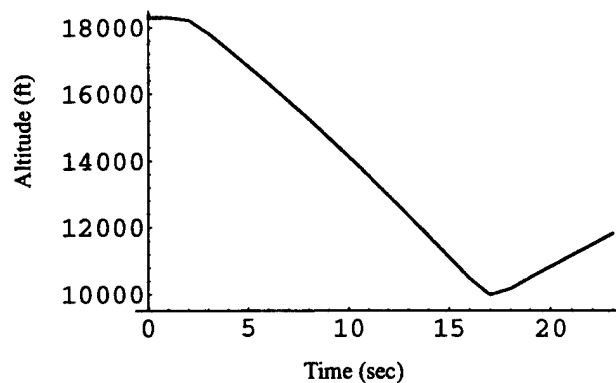


Figure 5.16: The trajectory for a 30° dive. The horizontal axis is time in seconds. The vertical axis is altitude in feet, 1 ft = 0.3 m.

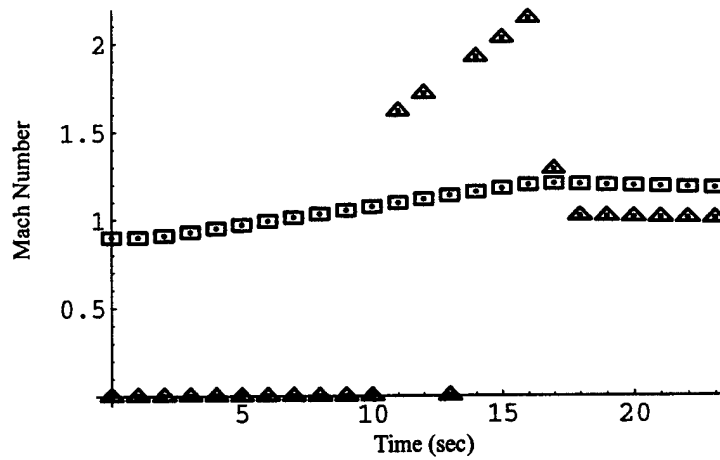


Figure 5.17: Plot of aircraft Mach number and local Mach number vs. time for a 30° dive. The horizontal axis is time in seconds, the vertical axis is Mach number. The aircraft Mach number is represented by squares and the local Mach number by triangles. A symbol at $M=0$ means there is no sonic boom at the ground for that time.

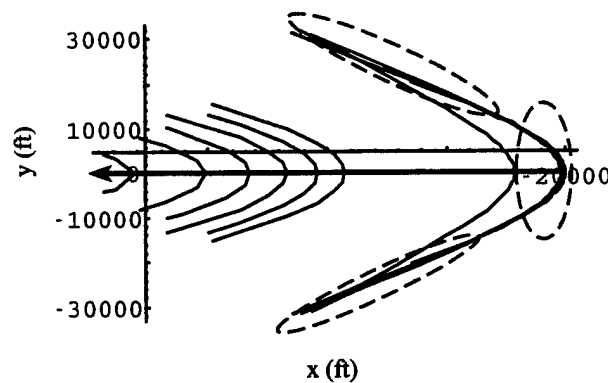


Figure 5.18: Isopemps created during a 30° dive. The horizontal and vertical axes are x and y ground positions in ft, $1 \text{ ft} = 0.3 \text{ m}$. The figure is shown as if looking down on the flight path which is shown with an arrow. The plane is flying from right to left.

The isopemps that are generated during this maneuver are mapped out in Fig. 5.18. All the separate patterns are spaced one second apart. A point to notice is that there are over twice as many isopemps created during the 30° dive as compared with the dive at a 10 degree angle. The focal zones that are created occur during the beginning of the dive. As the aircraft dives and accelerates, the isopemps first intersect over the whole hyperbolic pattern. After a time of continued acceleration, the focal zones only exist at the edges of the isopemps. Finally, during climbing, the isopemps are spread farther apart thus discouraging focus conditions.

Using the initial parameters of the maneuver, a straight flight case was examined to help determine the effects of a 30° dive on the signatures calculated underwater. For this trajectory, an F-15 was engaged in straight steady flight through a U.S. atmosphere with no winds. The aircraft was at an altitude of 5,578 m (18,300 ft) flying at Mach 0.9. During the whole flight path, the plane remains subsonic, thus creating no sonic booms. Therefore, the sonic booms that are created from the aircraft making a 30° dive are again a direct result of the maneuver.

The first underwater sound field calculated was at $t = 11$ seconds. At this time in the flight path, the sonic booms first intersect with the ground. Also, this point was contained within a focal zone, resulting in focus conditions all along the corresponding isopemp. The aircraft was well into the dive, flying Mach 1.1 at an altitude of 4,128 m (13,544 ft). The local ground Mach number was calculated at 1.7, a considerable difference. PCBoom3 predicted a focused U wave directly under the flight path with a signal length of 0.2197 seconds and a peak pressure of 675.4 Pa (14.1 psf). This waveform was sampled every 1.1 ms, a sampling frequency of 909 Hz. From comparing the underwater wave shapes for the 30° dive in Fig. 5.19 to the 10° dive in Fig. 5.14, one notices that the initial 30° dive signature is larger by 2.3 dB. Also, due to the slightly higher Mach number and lower altitude, at a depth of 64 meters below the surface the 30° dive wave has decreased 25 dB while the 10° dive has decreased 27.6. Therefore, the focusing effects during the 30° dive create a greater penetration depth than the 10° dive.

The next wave chosen for examining the resulting underwater waveforms and sound metrics was produced 16 seconds into the flight path. At that time the aircraft was at the end of the dive portion of the trajectory. This point was selected to demonstrate the large

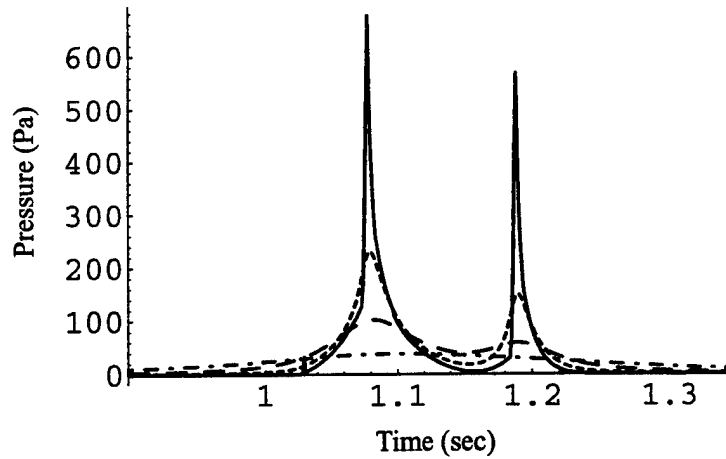


Figure 5.19: Underwater waveforms for a sonic boom predicted at trajectory time 11 seconds, $\phi = 0^\circ$ during a 30° dive at depths of 0 (solid), 4 (short dashes), 16 (long dashes), and 64 (dash/dot) meters. The horizontal axis is time in seconds, the vertical axis is pressure in pascals.

Table 5.5: Metrics for trajectory time 11 seconds, $\phi = 0^\circ$ for a 30° dive.

Depth(m)	peak dB	L_{UE} (dB)
0	147.6	123.7
4	138.2	120.5
16	131.2	117.6
64	122.6	114.3

difference between the local and aircraft Mach number that could be developed. The F-15 was flying Mach 1.2 at an altitude of 3,195 m (10,483 ft). Because of the aircraft speed and the angle at which the ray comes off the plane, the local Mach number was calculated at 2.1, a very significant difference. Right under the flight path, PCBoom3 predicted a carpet boom with a peak pressure of 885.6 Pa (18.5 psf) and a duration of 0.0988 seconds. This wave was sampled at 1,053 Hz or every 0.95 ms. From the various signatures in Fig. 5.20, and peak dB levels in Tbl. 5.6, it is seen that even though this is an N-wave shaped sonic boom, because of the high local Mach number and amplitude, it is larger than the focused U wave at a depth of 64 meters. Therefore, besides focusing effects having a greater sonic

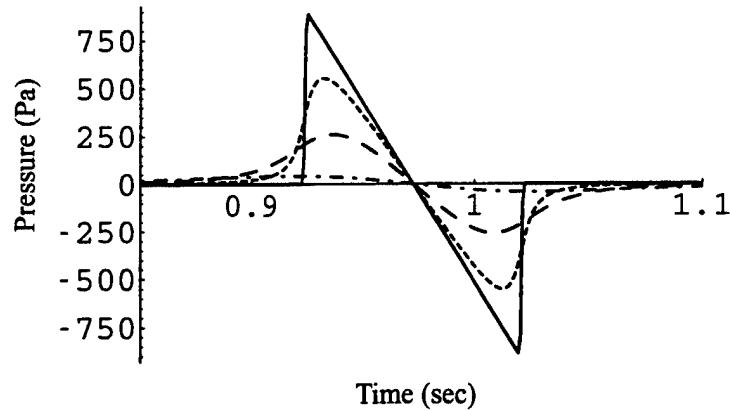


Figure 5.20: Signatures calculated underwater from trajectory time 16 seconds, $\phi = 0^\circ$ for a 30° dive at depths of 0 (solid), 4 (short dashes), 16 (long dashes), and 64 (dash/dot) meters. The horizontal axis is time in seconds, the vertical axis is pressure in pascals.

boom penetration depth into water, a large difference in local Mach number can yield the same result.

Table 5.6: Metrics for trajectory time 16 seconds, $\phi = 0^\circ$ for a 30° dive.

Depth(m)	peak dB	L_{UE} (dB)
0	149.9	132.2
4	145.8	129.7
16	139.3	124.7
64	123.5	112.5

The final initial waveform investigated was taken directly under the flight path 22 seconds into the trajectory. This point is during the climb portion of the trajectory. The aircraft was at Mach 1.2 and a local ground Mach number of 1.0. The local Mach number is again lower than the aircraft number because of a 15° climb angle. At an altitude of 3,503 m (11,493 ft) PCBoom3 predicted an N-wave shaped boom that was sampled every 1.3 ms or at 767 Hz. The carpet boom had a peak pressure of 193.9 Pa (4.1 psf) and a duration of 0.1381 seconds. Comparing the underwater sound field from the 15° climb signature in Fig. 5.21 to the 5° climb wave in Fig. 5.15, the amplitude of the incident wave in Fig. 5.21 is 14 percent larger than the 5° case. The increase in amplitude is due to the lower altitude

Table 5.7: Metrics for trajectory time 22 seconds, $\phi = 0^\circ$ for a 30° dive.

Depth(m)	peak dB	L_{UE} (dB)
0	136.7	120.3
4	130.8	116.5
16	121.2	109.0
64	101.7	94.1

of the aircraft. However, since the aircraft is engaged in a 15° climb angle, the incident wave decreases faster with depth and by 64 meters, is the smaller of the two signatures. This demonstrates that a steeper climb angle could diminish the penetration depth of the sonic boom noise.

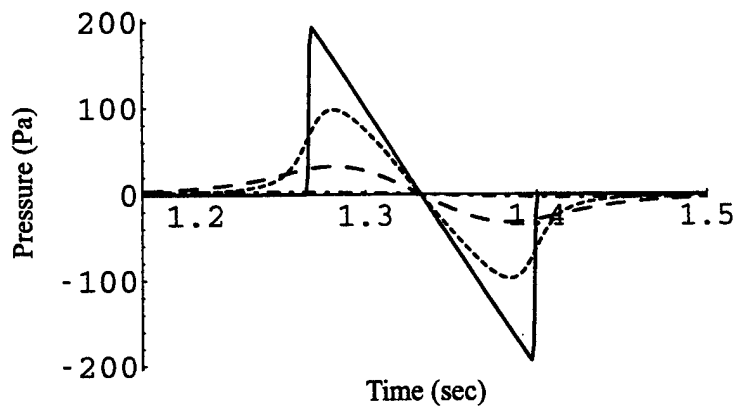


Figure 5.21: Underwater wave shapes for a sonic boom predicted at trajectory time 22 seconds, $\phi = 0^\circ$ during a 30° dive at depths of 0 (solid), 4 (short dashes), 16 (long dashes), and 64 (dash/dot) meters. The horizontal axis is time in seconds, the vertical axis is pressure in pascals.

From investigating this maneuver, it was seen that a subsonic airplane engaged in a 30° degree dive will accelerate and eventually become supersonic. As seen before, accelerating aircraft cause focal zones upon going supersonic. The focusing first occurs at all points where a sonic boom intersects with the ground. Then when the ray cone flattens enough, it exists only on the isopemp edges. These focused U waves will have a higher local Mach number, being close to twice that of the airplane toward the end of the dive. This again causes a greater penetration depth of sonic boom noise into the ocean. Again, a way to

counter this focusing effect would be to perform the dive at higher altitudes. As compared with a 10 degree dive, the 30 degree dive creates sonic booms with amplitudes which can be 20 percent larger and Mach numbers which can be 50 percent greater, therefore having an increased influence on the underwater sound field. However, as compared with a 5 degree climb, a 15 degree climb has the same or a decreased noise impact. This section of the flight path can produce sonic booms with a slightly higher amplitude, but because of the climb angle penetrate less far into water.

5.3.4. Pushover

The fourth maneuver analyzed was a pushover. This maneuver is of particular interest because it is the path taken by the Concorde SST after take-off. A pushover involves a supersonic climb to a desired altitude and then a leveling off to straight flight. An example of this trajectory is illustrated in Fig. 5.22. This example involved an F-15 Eagle flying west through a U.S. Standard atmosphere with no winds. The aircraft initially was at Mach 1.2 at an altitude of 3,048 m (10,000 ft). Two seconds into the flight path, the fighter climbs at a 10 degree angle until an altitude of 3,527 m (11,570 ft) is achieved at eight seconds. For the rest of the time, there is a leveling off until $t = 23$ seconds where at 4,025 m (13,206 ft), the aircraft finally dives at a 0.3 degree angle. This entire maneuver is performed at a constant Mach number of 1.2. A comparison of the aircraft Mach number to the local ground number is shown in Fig. 5.23. It is seen that the local ground Mach number is the smaller of the two for the entire flight path. During the first eight seconds, or while the plane is climbing, the local Mach number decreases. However, while leveling off, it increases to a value of approximately 1.15 which is still below the aircraft Mach number. This variance in local ground Mach number is also due to the fact that the airplane is not parallel with the ground, thus changing the Mach angle.

The isopemps generated during the pushover are mapped out in Fig. 5.24. All the patterns shown are spaced one second apart excluding the last one which is five seconds from the rest. The first eight isopemps represent the intercept of the ray cone during the 10° climb. The focal zones that exist are produced when the aircraft becomes more parallel with the ground. The isopemps intersect at the edges during this time causing a buildup

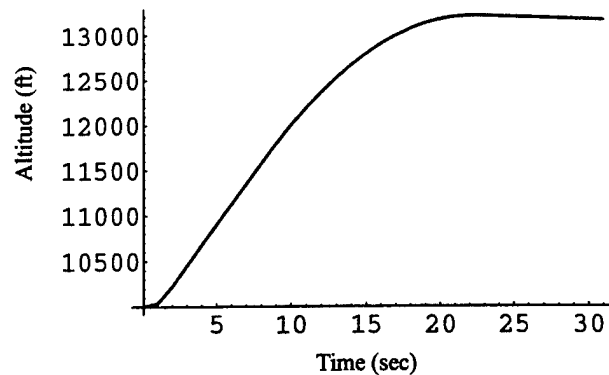


Figure 5.22: Trajectory for a pushover. The horizontal axis is time in seconds. The vertical axis is altitude in feet, 1 ft = 0.3 m.

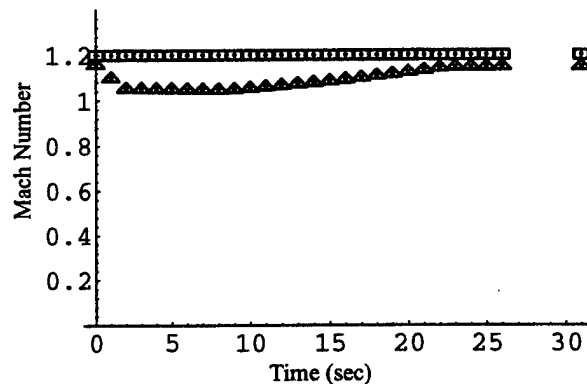


Figure 5.23: Plot of aircraft Mach number and local Mach number vs. time for a pushover. The horizontal axis is time in seconds, the vertical axis is Mach number. The aircraft Mach number is represented by squares and the local Mach number by triangles. A symbol at $M=0$ means there is no sonic boom at the ground for that time.

of acoustic pressure. The isopemps on the left represent almost level flight and show a lack of focus conditions.

Again to determine the effect of the pushover on sonic boom noise penetration into a flat water surface, the initial parameters of the maneuver were used to create a straight flight case. Here, the F-15 did not perform the pushover, but continued to fly straight at 3,048 m (10,000 ft), at Mach 1.2, through a U.S. standard atmosphere with no winds. The

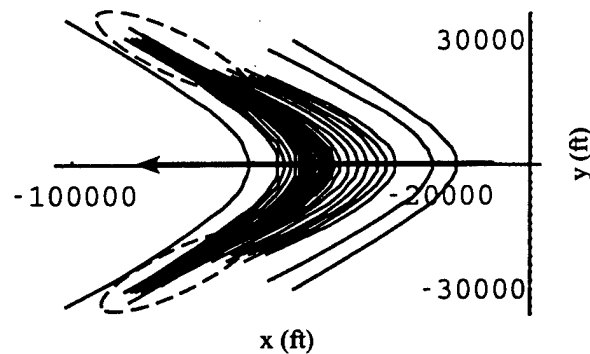


Figure 5.24: Isopemps created during a pushover. The horizontal and vertical axes are x and y ground positions in ft, $1 \text{ ft} = 0.3 \text{ m}$. The figure is shown as if looking down on the flight path which is shown with an arrow. The plane is flying from right to left.

sonic booms that were created during this flight path were all carpet booms. For each waveform chosen to examine, the corresponding straight flight signature will be shown to illustrate the difference the maneuver makes on the penetration into water.

The underwater sound field was first calculated from a trajectory point that fell during the climb, or at $t = 6$ seconds. At this time, the F-15 was flying at Mach 1.2, but because of the 10° climb angle, the local Mach number was 1.0. At an altitude of 3,390 m (11,123 ft), PCBoom3 predicted an N-wave shaped sonic boom directly under the flight path with a peak pressure of 356.1 Pa (7.4 psf) and a duration of 0.1202 seconds. The incident wave was sampled every 1 ms which is a sampling frequency of 1,000 Hz. The corresponding straight flight carpet boom was projected to have a peak pressure of 506.4 Pa (10.6 psf) and a duration of 0.105 seconds. Since the aircraft is in straight flight, the aircraft Mach number and the local Mach number are 1.2. From comparing the pushover underwater waveforms to the straight flight ones in Fig. 5.25 and Tbl. 5.8, it is noticeable that the signatures for straight flight are larger. More specifically, the peak dB values for the straight flight waves are approximately 3 dB greater than the pushover ones at all depths examined. This demonstrates that if an aircraft climbs rather than flying straight, the sonic booms that are produced can be smaller in amplitude and Mach number and penetrate less far into the ocean.

The next point that the underwater waveforms and sound exposure levels were calculated was directly under the flight path at $t = 10$ seconds. During this time, the aircraft

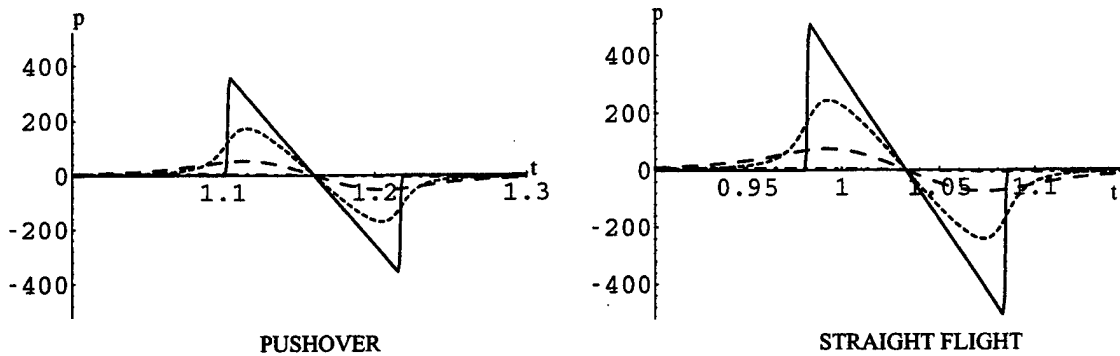


Figure 5.25: Underwater waveforms for a sonic boom predicted directly under the flight path at trajectory time 6 seconds. The picture on the left is created during a pushover and the one on the right during straight flight. Waveforms are shown at depths of 0 (solid), 4 (short dashes), 16 (long dashes), and 64 (dash/dot) meters. The horizontal axis is time in seconds, the vertical axis is pressure in pascals.

Table 5.8: Metrics for trajectory time 6 seconds, $\phi = 0^\circ$ for a pushover and the corresponding straight flight boom.

	Pushover		Straight Flight	
Depth(m)	peak dB	L_{UE} (dB)	peak dB	L_{UE} (dB)
0	142.0	125.0	145.1	127.6
4	135.7	120.9	138.7	123.4
16	125.5	112.9	128.4	115.4
64	105.4	97.6	108.3	100.1

was engaged in a 8.9° climb angle at an altitude of 3,657 m (11,998 ft). PCBoom3 predicted an N-wave shaped sonic boom that was sampled at 833 Hz or every 1.2 ms. The incident wave had a duration of 0.1246 seconds and a peak pressure of 584.7 Pa (12.2 psf). The corresponding straight flight wave was the same signature that was generated at six seconds. Therefore from examining Fig. 5.26 and Tbl. 5.9, it is observed that the wave shapes created during the pushover have a greater amplitude being approximately 1.2 times the straight flight signatures at the surface. Although the aircraft is at a higher altitude and a lower Mach number, even at a depth of 64 meters, the peak dB values differ by 2.4 dB. Therefore, the process of leveling can create sonic booms that will penetrate farther into the ocean than ones produced during straight flight.

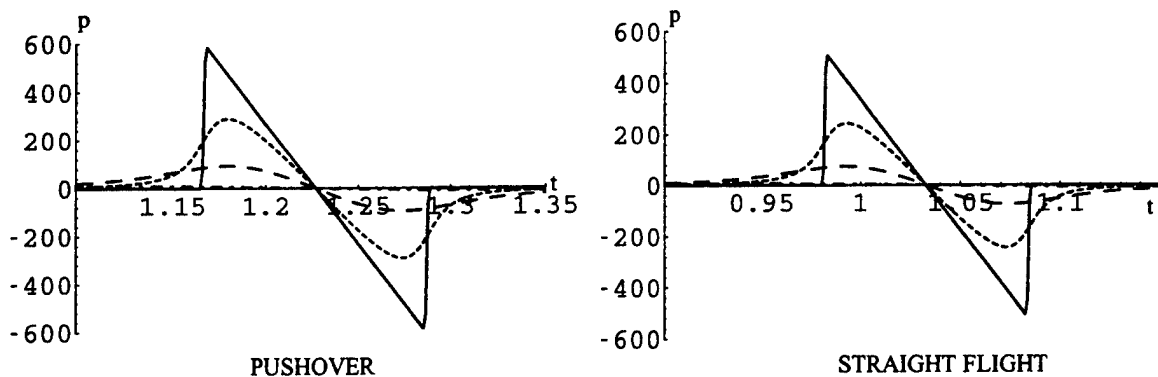


Figure 5.26: Signatures calculated underwater for a sonic boom predicted directly under the flight path at trajectory time 10 seconds. The picture on the left is created during a pushover and the one on the right during straight flight. Waveforms are shown at depths of 0 (solid), 4 (short dashes), 16 (long dashes), and 64 (dash/dot) meters. The horizontal axis is time in seconds, the vertical axis is pressure in pascals.

Table 5.9: Metrics for trajectory time 10 seconds, $\phi = 0^\circ$ for a pushover and the corresponding straight flight boom.

Depth(m)	Pushover		Straight Flight	
	peak dB	L_{UE} (dB)	peak dB	L_{UE} (dB)
0	146.3	129.6	145.1	127.6
4	140.2	125.6	138.7	123.4
16	130.4	118.0	128.4	115.4
64	110.7	102.9	108.3	100.1

The greatest difference between the pushover and straight flight is viewed again at $t = 10$ seconds, but 35 degrees off the flight path. This point was located in a focal zone that was created during the leveling. At this point, the aircraft was again at an altitude of 3,657 m (11,998 ft) flying at Mach 1.2. Since the sonic boom was located off the flight path, the local ground Mach number was only 1.0. The incident waveform predicted by PCBoom3 was a maximum focused U wave that was sampled every 1.5 ms or at 667 Hz. This wave had a signal length of 0.2464 seconds and a very substantial amplitude being 1,554.8 Pa (32.5 psf) after pressure doubling. The corresponding straight flight case also had the aircraft flying at Mach 1.2 with a local Mach number of 1.0. However, the projected

incident wave was a carpet boom that was almost a fourth of the amplitude of the U wave. This sonic boom had a duration of 0.1104 seconds and a peak pressure of only 423.0 Pa (8.8 psf). The difference in amplitude is clearly seen in Fig. 5.27 and Tbl. 5.10, where the initial peak dB values differ by 11.3 dB. As compared with focused booms produced in other maneuvers, the high frequency components of the wave again diminish rapidly with depth, but the spikes in this signature are barely noticeable at four meters below the surface, and disappear by sixteen. Even though the peaks are not noticeable, there still is a significant acoustic pressure at a depth of 64 meters.

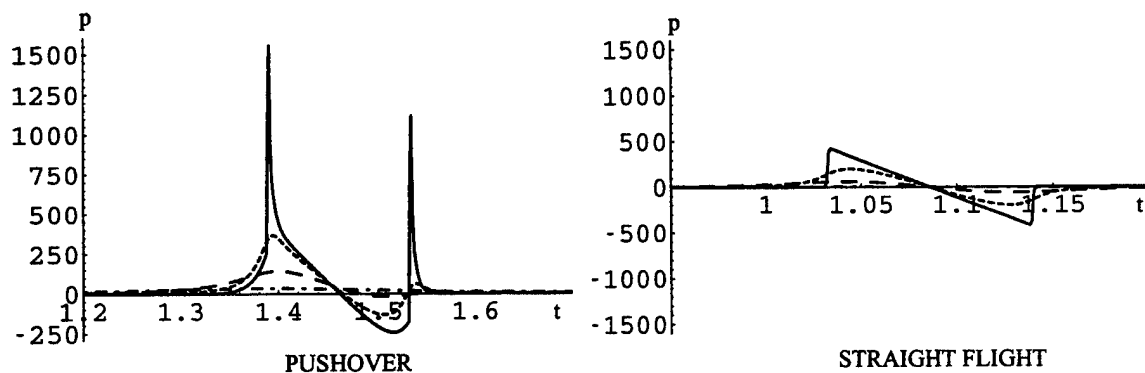


Figure 5.27: Underwater wave shapes for a sonic boom predicted 35° off the flight path at trajectory time 10 seconds. The picture on the left is created during a pushover and the one on the right during straight flight. Waveforms are shown at depths of 0 (solid), 4 (short dashes), 16 (long dashes), and 64 (dash/dot) meters. The horizontal axis is time in seconds, the vertical axis is pressure in pascals.

Table 5.10: Metrics for trajectory time 10 seconds, $\phi = 35^\circ$ for a pushover and the corresponding straight flight boom.

Depth(m)	Pushover		Straight Flight	
	peak dB	L_{UE} (dB)	peak dB	L_{UE} (dB)
0	154.8	130.4	143.5	126.2
4	142.3	125.5	137.0	122.0
16	134.0	120.1	126.6	113.8
64	121.6	114.2	106.4	98.4

Therefore, from this example it was determined that a pushover at a constant Mach number will have an effect on sonic boom noise penetration into the ocean. While the aircraft is climbing, the signatures that are produced are smaller in amplitude and Mach number than those created if the maneuver was never executed. This causes a decreased penetration of sonic boom noise into the ocean. However, when the airplane turns to level flight, focus conditions exist on the edges of the isopemps. The focal zones will persist until true level flight is achieved. The focused U waves generated tend to be much larger in amplitude, but not in Mach number. Still, focusing effects and the sonic boom amplitude cause a high penetration depth into the water. One way to counter the focusing effects again would be to fly at a higher altitude.

5.3.5. Constant g turn

The last maneuver that was explored was a constant $4g$ turn, where g is the acceleration due to gravity. The input parameters included an F-15 Eagle which was flying through a U.S. Standard atmosphere with no winds. It was initially flying Mach 1.2 at an altitude of 3,048 m (10,000 ft). The flight path created by the trajectory file is depicted in Fig. 5.28. From this figure, it is noticed that the aircraft is flying straight until six seconds into the trajectory. At that point, a turn is performed until twelve seconds when straight flight resumes. Because this maneuver is performed at a constant Mach number and a constant altitude, the aircraft Mach number and calculated local ground Mach number directly under the flight path remains at 1.2 throughout.

The isopemps projected as a result of the turn are shown in Fig. 5.29. All the patterns are spaced one second apart. The only focal zone that exists in the flight path is located on the inside of the turn. In this circled area, the isopemps clearly intersect thus again causing a buildup of acoustic pressure. On the outside of the turn, the isopemps tend to diverge, discouraging focus conditions.

To evaluate the effect a constant $4g$ turn has on sonic boom noise penetration into the ocean, a straight flight case was created. This situation used the same initial parameters, but instead of turning, the aircraft flew straight. Therefore, a Mach 1.2 F-15 was flying straight at 3,048 m (10,000 ft) through a U.S. atmosphere with no winds. The sonic booms that were created during this flight path were all carpet booms. For each waveform chosen

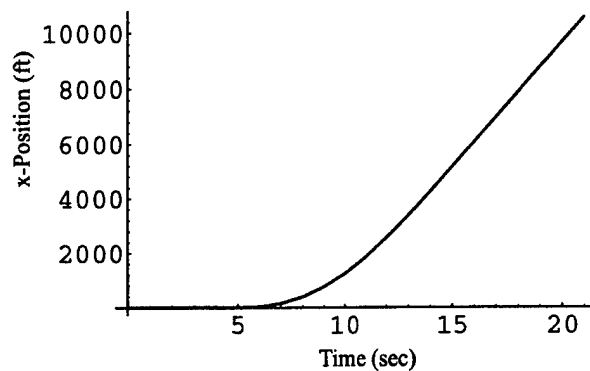


Figure 5.28: Trajectory for a constant g turn. The horizontal axis is time in seconds. The vertical axis is x-position in feet, 1 ft = 0.3 m.

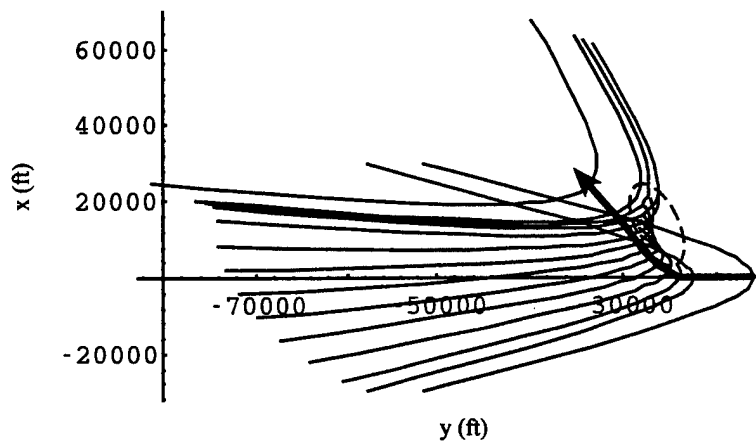


Figure 5.29: Plot of isopemps for a constant g turn. The superimposed flight path is shown with an arrow. The horizontal and vertical axes are x and y ground position in ft, 1 ft = 0.3 m. The plane is flying from right to left.

to examine during the turn, the corresponding straight flight signature will be shown to illustrate the difference the maneuver makes on the penetration into water.

The first trajectory point chosen was during the turn, directly under the flight path at $t = 11$ seconds. At this position, PCBoom3 predicted a carpet boom with a peak pressure of 503.8 Pa (10.5 psf) and a duration of 0.1059 seconds. This wave was sampled every 1 ms, a sampling frequency of 1,000 Hz. If one compares this N wave in Fig. 5.30 to the straight

flight case, it is seen that there is no noticeable difference in the two sets of signatures. The peak dB values in Tbl. 5.11 show a maximum difference of 0.1 dB. Therefore, at this time, the constant $4g$ turn has no effect on sonic boom noise penetration into water.

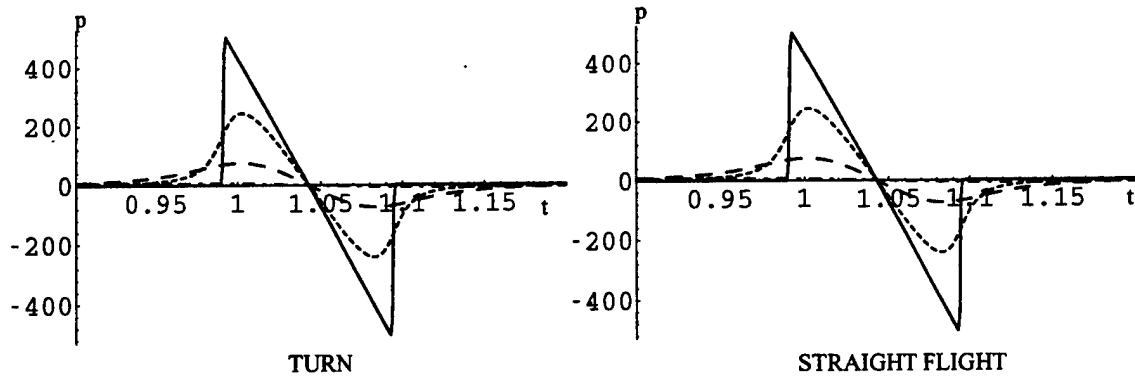


Figure 5.30: Underwater waveforms for a sonic boom predicted directly under the flight path at trajectory time 11 seconds. The picture on the left is created during a constant g turn and the one on the right during straight flight. Waveforms are shown at depths of 0 (solid), 4 (short dashes), 16 (long dashes), and 64 (dash/dot) meters. The horizontal axis is time in seconds, the vertical axis is pressure in pascals.

Table 5.11: Metrics for trajectory time 11 seconds, $\phi = 0^\circ$ for a constant $4g$ turn and the corresponding straight flight boom.

	4g Turn		Straight Flight	
Depth(m)	peak dB	L_{UE} (dB)	peak dB	L_{UE} (dB)
0	145.0	127.6	145.1	127.6
4	138.7	123.4	138.7	123.4
16	128.5	115.5	128.4	115.4
64	108.4	100.2	108.3	100.1

The next position examined was -20° off the flight path at $t = 11$ seconds. As noticed in Fig. 5.29, the time is located within the focal zone. Since the point examined is not directly under the aircraft, the calculated local Mach number was 1.1. At this time, PCBoom3 predicted a focused U wave that was sampled at 833 Hz or every 1.2 ms. The signal length was 0.2395 seconds with a peak amplitude of 1,397.5 Pa (29.2 psf) after pressure doubling.

For the straight flight case, an N wave was projected -20° off the flight path with a local Mach number also of 1.1. The duration of this boom was 0.1063 seconds with a peak pressure of only 479.3 Pa (10.0 psf). The U wave in Fig. 5.31 is much like the one created during the pushover. When compared with the straight flight signature it is immediately noticed that the U wave is almost three times the size of the corresponding N wave at all depths examined. Therefore, we again see that focus conditions create sonic booms that have a greater penetration depth into water.

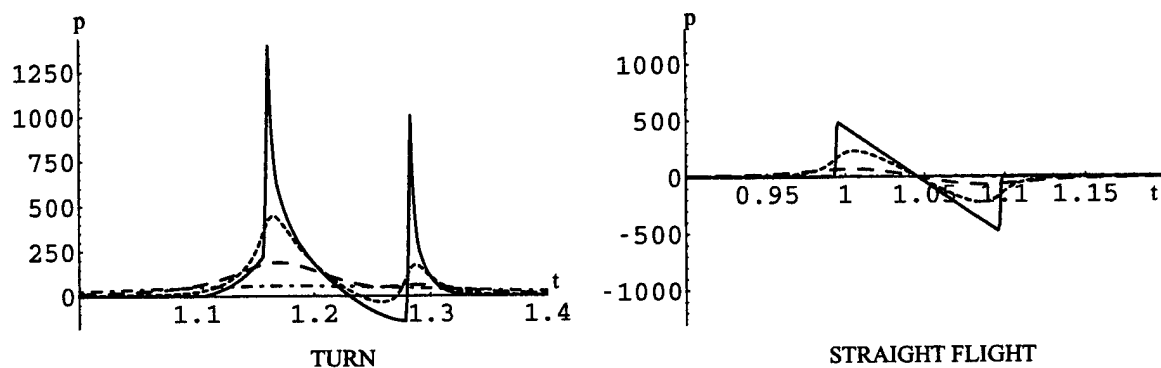


Figure 5.31: Signatures calculated underwater for a sonic boom predicted -20° off the flight path at trajectory time 11 seconds. The picture on the left is created during a constant g turn and the one on the right during straight flight. Waveforms are shown at depths of 0 (solid), 4 (short dashes), 16 (long dashes), and 64 (dash/dot) meters. The horizontal axis is time in seconds, the vertical axis is pressure in pascals.

Table 5.12: Metrics for trajectory time 11 seconds, $\phi = -20^\circ$ for a constant $4g$ turn and the corresponding straight flight boom.

	4g Turn		Straight Flight	
Depth(m)	peak dB	L_{UE} (dB)	peak dB	L_{UE} (dB)
0	153.9	130.7	144.6	127.2
4	144.0	126.9	138.1	122.9
16	136.5	123.3	127.8	114.8
64	126.4	119.4	107.6	99.4

Finally, it was determined from this example that a constant $4g$ turn has an effect on sonic boom noise penetration into water. The focal zones created will exist on the inside of the turn. The focused U waves that are created have the same local Mach number, but a large amplitude. Because of the focusing effects, the U waves decay slower with increased depth as compared with the straight flight case thus causing a greater penetration of sonic boom noise into the ocean. To counter the focusing effects, again altitude and atmospheric dissipation should be considered.

Chapter 6.

Effect of Waveform Distortion on Underwater Sound Levels

6.1. Introduction

After determining the impact of select maneuvers on sonic boom noise penetration into the ocean, the effects of waveform distortion were examined. Recalling Chapter 3, in realistic situations, the sonic booms that hit the surface of the water are of arbitrary shape. They will be distorted either by aircraft maneuvers or atmospheric processes such as dissipation or turbulence. However, from each arbitrarily shaped sonic boom, a corresponding N wave can be constructed that has the same energy content. Comparing the signatures from each case at fixed depths, the influence of waveform distortion can be determined. If at greater depths, the waveforms are seen to be equal or similar, the distortions are only of great concern near the surface of the water. If the wave shapes are different, the distortion will have a greater bearing on sonic boom noise penetration into water.

6.2. Methods

In order to discover the impact of distortions, equal energy N waves were calculated for the experimentally measured F-15 and F-16 data in Chapter 3. This was accomplished through many steps which followed the method for finding corresponding N waves of equal energy found in Reference 1. The *Mathematica* codes used to calculate the equal energy N wave and predict the underwater sound field from this incident waveform are listed in Appendix B.

First, a list of pressure values in pascals representing the incident experimental waveform was read into *Mathematica*. Next, the incident signature was doubled to account for the boundary conditions at the air/water interface. From the list of doubled pressure values, the sampling frequency was found by dividing the number of samples in the signal by the signal duration.

Second, the *leading energy ratio*, LER, and *trailing energy ratio*, TER, were determined for each experimentally measured waveform. The LER and TER were used to find the correct start and stop times for the N wave. The leading energy ratio is defined as the ratio of the energy accumulated from the start of the recorded sonic boom to the maximum overpressure (leading energy) to the total energy contained in the signal;

$$\text{LER} = \frac{\sum_{n=1}^{n(p_{\max})} p_{\text{recorded}}^2 [n]}{\sum_{n=1}^{\text{samples}} p_{\text{recorded}}^2 [n]}. \quad (6.1)$$

The trailing energy ratio is the ratio of the energy stored from the minimum overpressure to the end of the signal (trailing energy) to the total energy in the signature;

$$\text{TER} = \frac{\sum_{n=n(p_{\max})}^{\text{samples}} p_{\text{recorded}}^2 [n]}{\sum_{n=1}^{\text{samples}} p_{\text{recorded}}^2 [n]}. \quad (6.2)$$

Figure 6.1 shows an example of the leading and trailing energy sections of a sonic boom signature. Because these values are believed to be dependent on the physical properties of an aircraft, average values for the LER and TER were determined for several aircraft. This was accomplished by using recorded N-wave shaped sonic booms, Eq. (6.1), and Eq. (6.2).¹ For this analysis, the average LER for an F-15 was 0.0503 and the average TER was 0.0416. For an F-16, the average LER and TER were 0.108 and 0.052, respectively.

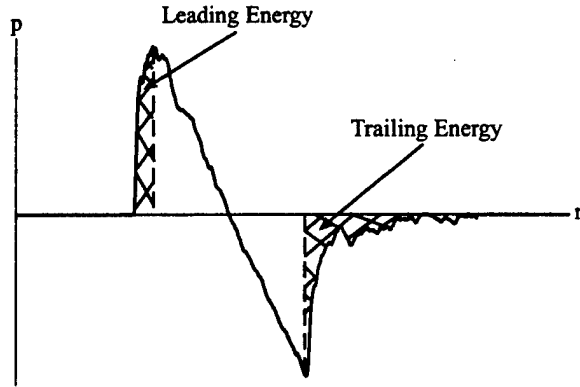


Figure 6.1: Leading and trailing energy sections of an experimental signature. The horizontal axis is sample number and the vertical axis is pressure in pascals.

Third, the total energy contained in the experimental waves was computed. The constant $1/\rho_0 c^2$ has been suppressed throughout these energy calculations. All waves are assumed to be plane waves. Hence, the expression for the total energy in a signature takes

the form

$$\text{Total Energy} = \frac{1}{f_s} \sum_{n=1}^{\text{samples}} p[n]^2, \quad (6.3)$$

where f_s is again the sampling frequency. First, the incident, doubled pressure values were squared. Then, the elements of the list were simply added together. After adding the elements together, this value was divided by the sampling frequency to obtain the total energy contained in the experimental wave. To find the total energy in *Mathematica*, Eq. (6.3) is rewritten as

$$\text{totalenergy} = 1/f_s \text{ Apply [Plus, datalist]}. \quad (6.4)$$

Next, the duration of the equal energy N wave was determined. First, the energy values at which the N wave should begin and end were calculated. The N wave should reach peak overpressure at the time when the accumulated energy in the experimental wave is equal to the total energy multiplied by the LER;

$$\text{N wavestart} = \text{totalenergy} \times \text{LER}. \quad (6.5)$$

The N wave should return to ambient pressure at the time when the stored energy in the measured wave is equal to the total energy multiplied by 1 minus the TER;

$$\text{N waveend} = \text{totalenergy} \times (1 - \text{TER}). \quad (6.6)$$

To find the beginning and ending time of the N wave in seconds, a trial and error method was used. Equation 6.5 and 6.6 were calculated repeatedly with different sample numbers until values close to the N wave start and end were achieved. Once starting and ending sample numbers were determined, they were multiplied by Δt to obtain time in seconds. Finally, the beginning time was subtracted from the ending time to get the N wave duration in seconds.

The last parameter that was computed for the equal energy N wave was the peak overpressure. This was simply obtained by using the total energy of the measured signature and the duration of the N wave,

$$p_{\max} = \sqrt{\frac{3 \text{ total energy}}{\text{duration}}}. \quad (6.7)$$

The equal energy N wave was created by substituting the peak overpressure and duration into Cook's equation for I_1 , Eq. (2.21). It was then discretized with the same number

of samples as the corresponding arbitrary wave. The initial pressure values of the N wave were copied and saved to a file in BBEdit, making it possible to find the underwater sound field and determine the impact of distortion.

6.3. Results

As stated above, the waveforms chosen to analyze were the experimentally obtained F-15 and F-16 data introduced in Chapter 4. A corresponding N wave of equal Mach number was created for each data set using the total energy in the measured signature. For the F-15 rounded wave, an N wave was produced that had a peak pressure of 96.6 Pa (2.0 psf) and a duration of 0.1218 seconds. The N wave created from the energy contained in the F-15 double peaked wave had a duration of 0.1234 seconds and a peak pressure of 94.9 Pa (1.9 psf). Using the equal energy *Mathematica* notebook in Appendix B, wave shapes were found for both the experimental wave and equal energy N wave at depths of 0, 4, 16, and 64 meters below the water surface. The signatures were plotted on top of one another to clearly see the difference in the patterns. The sound metrics were computed for the equal energy N waves and compared with the levels for the experimental ones.

From examining the sets of signatures for the F-15 data in Fig. 6.2 and Fig. 6.3 and the peak dB values in Tbl. 6.1 and Tbl. 6.2, it is noticed that the results are similar. The peak dB values of the sonic booms are the same at the surface, but with increasing depth, they diverge from each other. More specifically, the signatures differ by 3 or more dB. The unweighted sound exposure levels also separate with increasing depth. In each case, the L_{UE} for the distorted waveform is 4 or more dB greater than the equal energy N wave. The actual profile of the sonic booms also becomes increasingly different at greater depths thus displaying the difference in the frequency content of the two waves.

A slightly different outcome is observed from the F-16 U wave. The total energy in this sonic boom constructed an N wave with a peak pressure of 195.6 Pa (4.1 psf) and a duration of 0.1058 seconds. Some opposing trends from the F-15 data are seen in Fig. 6.4 and Tbl. 6.3. The peak dB values from the N wave and the U wave begin 3.9 dB apart. However, by 64 meters below the surface, the signatures are only separated by 0.1 dB. Similar to the F-15 data, the unweighted sound exposure levels are equal at the surface and diverge with depth. The distorted wave is 5.6 dB greater than the N wave at a depth of 64

meters. Again, the difference in frequency content of the waves is seen from the fact that the actual profile of the sonic booms becomes increasingly different at greater depths.

An important point to notice concerning all signatures examined is the decay rate with respect to depth. As seen from the tables of calculated peak dB and unweighted sound exposure levels, the equal energy N wave is at a lower value than the experimental wave at 64 meters below the surface. This result suggests that the waveform distortions could cause a slightly higher penetration depth of sonic boom noise into the ocean. From examining plots of peak pressure with respect to depth, it is determined that the magnitude of the effect of waveform distortion on sonic boom noise penetration into the ocean is dependent on the incident signature. For the F-15 cases in Fig. 6.5 and Fig. 6.6, the distortion has a significant influence on the decay rate of the peak pressure values. At a depth of 64 meters, the F-15 rounded sonic boom has a peak pressure that is 23 percent larger than the equal energy N wave and the F-15 double peaked sonic boom is 37 percent greater. In contrast, the waveform distortion in the incident F-16 U wave, Fig. 6.7, has a lesser impact. At 64 meters below the surface, the peak pressure of the experimental U wave is only 4 percent larger than the corresponding equal energy N wave.

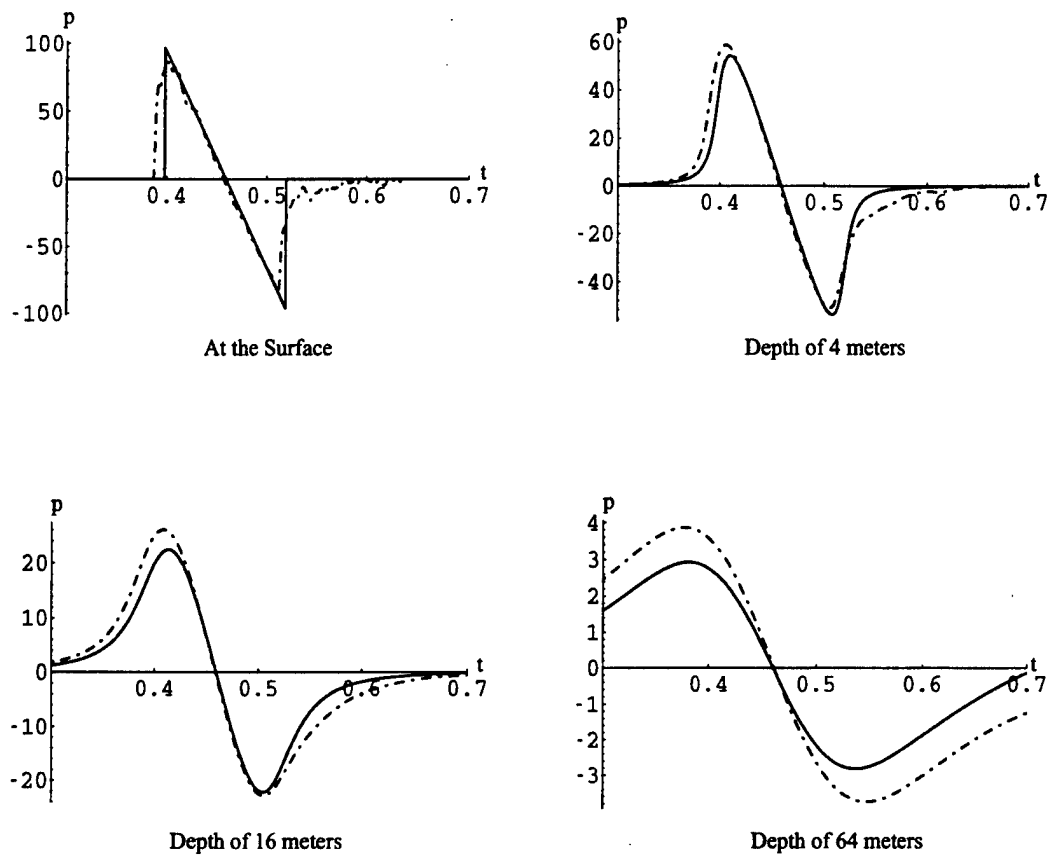


Figure 6.2: Comparison of the F-15 rounded sonic boom and a corresponding N wave having the same energy content. The rounded sonic boom signatures are shown with a dash-dot line. The N wave signatures are represented with a solid line. All horizontal axes are time in seconds; all vertical axes are pressure in pascals. Sets are shown at depths of 0, 4, 16, and 64 meters below the surface of the water.

Table 6.1: Metrics for an F-15 rounded sonic boom and the corresponding equal energy N wave.

Depth(m)	Actual Data		N wave	
	peak dB	L_{UE} (dB)	peak dB	L_{UE} (dB)
0	129.7	113.8	129.7	113.8
4	126.3	111.4	125.7	110.6
16	119.3	106.1	117.8	104.4
64	102.7	93.6	99.7	89.6

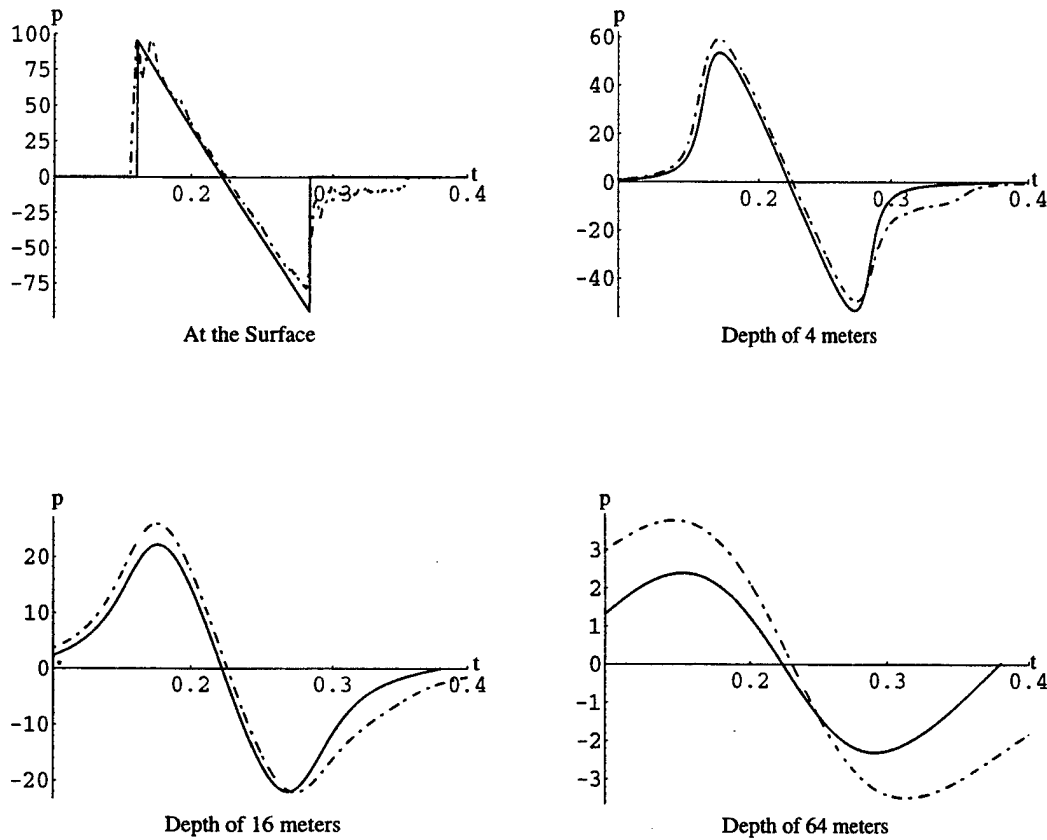


Figure 6.3: Comparison of the F-15 double peaked sonic boom and a corresponding N wave having the same energy content. The double peaked sonic boom signatures are shown with a dash-dot line. The N wave signatures are represented with a solid line. All horizontal axes are time in seconds; all vertical axes are pressure in pascals. Sets are shown at depths of 0, 4, 16, and 64 meters below the surface of the water.

Table 6.2: Metrics for an F-15 double peaked sonic boom and the corresponding equal energy N wave.

Depth(m)	Actual Data		N wave	
	peak dB	L_{UE} (dB)	peak dB	L_{UE} (dB)
0	130.6	113.7	130.5	113.7
4	126.4	111.2	125.5	110.6
16	119.2	105.9	117.9	104.6
64	102.5	92.5	98.6	87.3

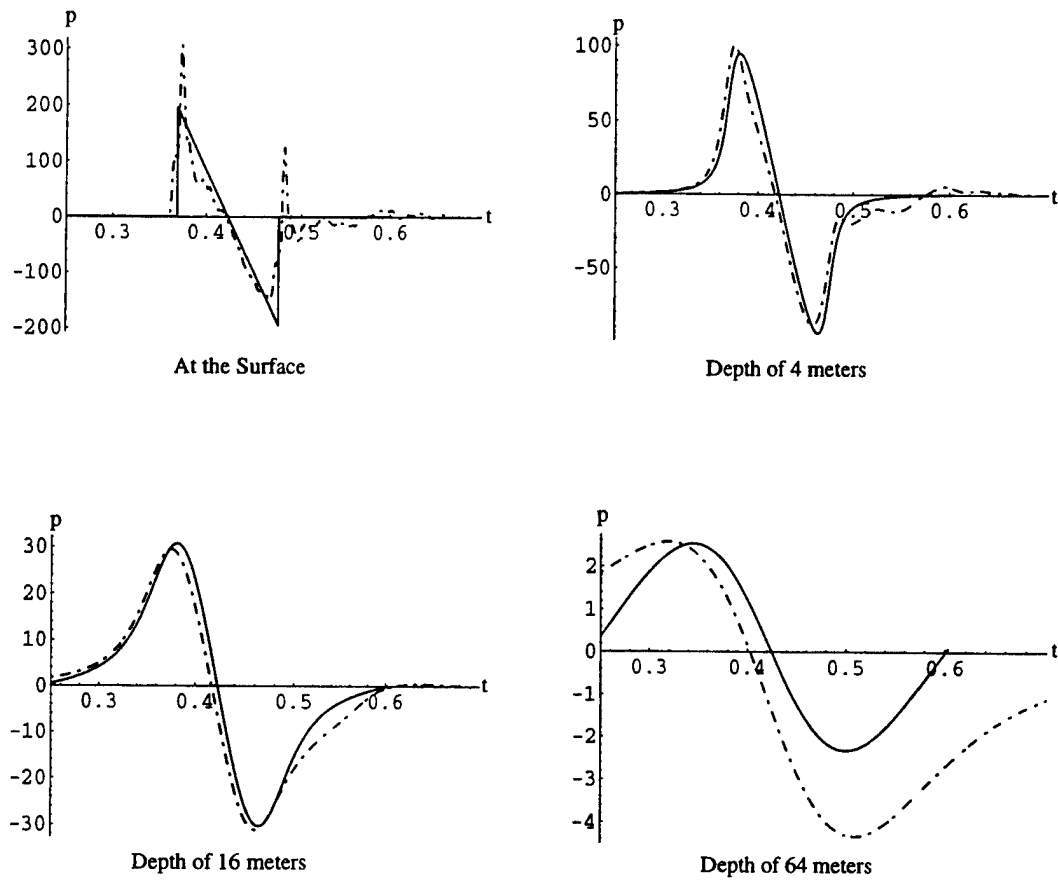


Figure 6.4: Comparison of the F-16 U wave and a corresponding N wave having the same energy content. The U wave signatures are shown with a dash-dot line. The N wave signatures are represented with a solid line. All horizontal axes are time in seconds; all vertical axes are pressure in pascals. Sets are shown at depths of 0, 4, 16, and 64 meters below the surface of the water.

Table 6.3: Metrics for an F-16 U wave and the corresponding equal energy N wave.

	Actual Data		N wave	
Depth(m)	peak dB	L_{UE} (dB)	peak dB	L_{UE} (dB)
0	140.7	119.3	136.8	119.3
4	131.0	115.1	130.5	115.3
16	120.4	107.9	120.7	107.6
64	99.1	93.7	99.0	88.1

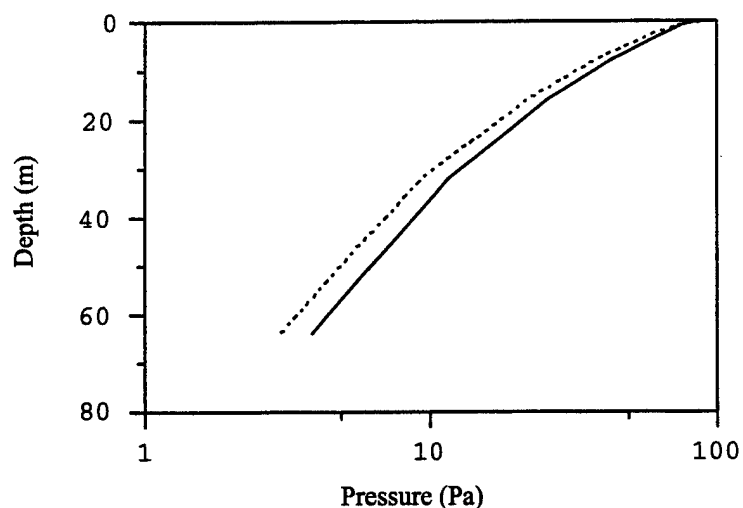


Figure 6.5: Semilog plot of peak pressure with respect to depth for an F-15 rounded sonic boom and a corresponding equal energy N wave. The rounded sonic boom peak pressure is shown with a solid line. The N wave peak pressure is represented with a dashed line. The horizontal axis is pressure in pascals and the vertical axis is depth in meters.

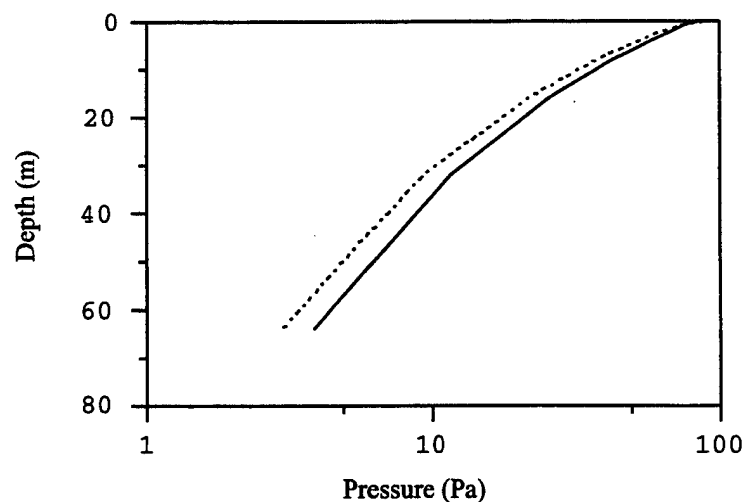


Figure 6.6: Semilog plot of peak pressure with respect to depth for an F-15 double peaked sonic boom and a corresponding equal energy N wave. The double peaked sonic boom peak pressure is shown with a solid line. The N wave peak pressure is represented with a dashed line. The horizontal axis is pressure in pascals and the vertical axis is depth in meters.

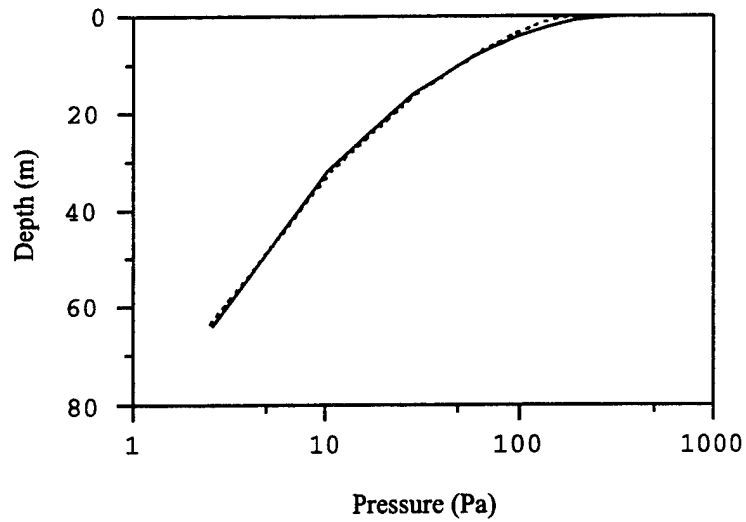


Figure 6.7: Semilog plot of peak pressure with respect to depth for an F-16 U wave and a corresponding equal energy N wave. The U wave peak pressure is shown with a solid line. The N wave peak pressure is represented with a dashed line. The horizontal axis is pressure in pascals and the vertical axis is depth in meters.

Chapter 7.

Conclusions

7.1. Summary of Results

As described in Chapter 2, steady and level supersonic flights under Mach 4.4 will produce sonic booms that impinge on the surface of the water at an angle that is greater than the critical angle. The incident wave is completely reflected off the surface of the water, but a penetrating evanescent wave will exist in the water that decays exponentially with depth. Assuming a flat, homogeneous ocean, Sawyers⁸ and Cook⁵ developed analytical expressions for the underwater signatures from an incident N wave. It was shown that with increasing depth, the N wave becomes more rounded with shape and diminishes in amplitude. Their analyses also stated that the higher frequency components of the incident sonic boom noise penetrate less far into the ocean. The work of Sawyers and Cook has been experimentally verified with sonic booms created from small projectiles, dynamite caps, and more recently an Air France Concorde flyover. All these experiments proved that sonic boom noise penetration into a flat ocean is well defined by existing theory for N waves incident on a flat ocean.

In realistic situations most of the waves that hit the surface of the water are not perfect N waves, but are spiked or rounded. Thus, an algorithm was introduced in Chapter 3 which predicted the signatures for any arbitrary waveform at any specified depth. The algorithm also calculated peak dB values, unweighted sound exposure levels, and C- and A- weighted sound exposure levels for each wave. The method implemented a discretized version of the results of Cook and assumed the signature was incident on a flat ocean surface and the aircraft was at a speed less than Mach 4.5. The results of the algorithm were verified with known analytical solutions for an incident N wave. The wave shapes were compared with the theory of Sawyers and were found to agree very well. Next, the sound descriptor results were validated by comparing them to the findings of Rochat and Sparrow.¹⁴ The peak dB values and unweighted sound exposure levels agreed very well, while the C- and A-weighted levels did not match. This was because the process to find these sound exposure

levels is extremely frequency sensitive, and the N waves were generated in slightly different manners. The unweighted sound exposure level was compared with a result of analytical theory and was found to match exactly. Finally, the algorithm was tested with a Mach 4.5 aircraft. The incident N wave did not decay with depth, but propagated through the water, as predicted.

In Chapter 4, the algorithm was used to find the underwater sound field from many incident waveforms. Underwater waveforms and sound exposure levels were found at depths of 0, 4, 16, and 64 meters for non N-wave shaped sonic booms using published spectra, experimental data, and PCBoom3, a sonic boom prediction model. From all examples, it was clearly observed that sonic boom noise does penetrate the ocean surface and can be prevalent even at depths of 64 meters. Higher Mach numbers were seen to produce sonic booms with a greater sound penetration into the ocean at a fixed depth, thus agreeing with the work of Sparrow.⁷ The distortions in the experimental waveforms which could have been caused by atmospheric turbulence, were evident at the water surface, but disappeared from the wave contour below 16 meters. This is because the high frequency components that were contained in the wave diminished rapidly with depth, thus causing the wave shape to become smooth. For all cases, the decay order of the sound metrics calculated from slowest rate to quickest was unweighted sound exposure level, peak dB value, C-weighted sound exposure level, then A-weighted sound exposure level.

In Chapter 5, the effect of aircraft maneuvers on sonic boom noise penetration into a flat ocean was investigated. PCBoom3 was used exclusively to create sonic boom footprints and isopemps from existing trajectory files for a linear acceleration, a 10° dive, a 30° dive, a pushover, and a constant g turn. From the isopemps, focal zones were determined for each maneuver. In these areas, focused U waves were produced that had an amplitude which was two to five times greater than the amplitude of a comparable N wave. The underwater signatures and sound exposure levels were computed from key trajectory points in each maneuver. Finally, the underwater sound fields from the selected points were compared with a straight flight case which was created from the initial parameters of the maneuver. From this comparison, the effect of the maneuver on the noise penetration was determined.

For a constant altitude linear acceleration, it was shown that a subsonic aircraft, will cause sonic booms upon going supersonic. Early in the supersonic acceleration, focal zones

will be produced, causing U waves which have a greater penetration depth into the ocean. The focusing will persist until the plane has accelerated to a point where the ray cone has flattened enough to only produce carpet booms. Comparing the example to the straight flight case created from the linear acceleration initial parameters, it was determined that the booms created were a direct result of the maneuver. This is because in the straight flight case, the aircraft remained subsonic.

For a 10° dive, it was seen that a subsonic airplane will accelerate and eventually will go supersonic. Because the plane is accelerating while diving, focused sonic booms will be produced that have a higher local Mach number than the aircraft Mach number. The focusing again causes the wave to decay less quickly, and thus causes a greater penetration of sonic boom noise into the ocean. The climb portion of this trajectory, however, created waves that were considerably less in amplitude than those in the dive. Climbing also caused the local Mach number to be lower than the aircraft speed, thus causing the sonic boom noise to penetrate less far.

As compared with the 10° dive, a 30° dive created sonic booms with amplitudes which were 20 percent larger and local Mach numbers which were 50 percent greater, therefore having an increased influence on the underwater sound field. However, as compared with a 5 degree climb, a 15 degree climb had the same or a decreased noise impact. This section of the flight path produced sonic booms with a slightly higher amplitude than the climb portion of the 10° dive trajectory, but because of the climb angle, they penetrated less far into the water. The straight flight case created from the initial parameters of the 10° and 30° dives also kept the aircraft subsonic. Therefore, the sonic booms that were present were a direct result of the maneuvers.

It was then shown that a pushover at a constant Mach number will have an effect on sonic boom noise penetration into the ocean. While the aircraft was climbing, the signatures that were produced were smaller in amplitude and Mach number than those created if the maneuver was never executed. This caused a decreased penetration of sonic boom noise into the ocean. When the airplane returned to level flight, focus conditions existed on the edges of the isopemps. The focal zones persisted until true level flight was achieved. The focused U waves generated tended to be much larger in amplitude, but not in Mach number.

However, the focusing effects and the sonic boom amplitude caused a high penetration depth into the water.

Lastly, a constant $4g$ turn was also determined to have an effect on sonic boom noise penetration into water. The focal zones created existed on the inside of the turn. The focused U waves that were created had the same local Mach number, but a large amplitude. Because of the focusing effects, again the U waves decayed slower with increased depth as compared with the straight flight case, thus causing a greater penetration of sonic boom noise into the ocean. At all other points in the turn trajectory, the sonic booms that were created equaled the ones created in the straight flight trajectory.

Finally, the effects of waveform distortions on sonic boom noise penetration into a flat ocean were examined. Using the F-15 and F-16 experimental data and the method described in Reference 1, N waves containing the same energy as the corresponding experimental waves were constructed. The underwater sound field was found for both the experimental wave and the equal energy N wave, and the two signatures were plotted on top of one another. From this comparison it was noticed that the wave shapes for the equal energy N waves did not look the same as the experimental waves with greater depths. For non focused conditions, the peak dB and L_{UE} decay rates began similarly then diverged with increased depth. For the U wave, the unweighted sound exposure levels followed the same trend, but the peak dB levels started differently and converged with greater depth. An important point noticed concerning all the sonic booms examined was the decay rate with depth. From all the peak dB and unweighted sound exposure levels calculated, the equal energy N wave was at a lower value than the experimental wave at 64 meters below the surface. This result suggests that the waveform distortions can cause a slightly greater penetration depth of sonic boom noise into the ocean. However, from examining plots of peak pressure with respect to depth, it was determined that the magnitude of the effect of waveform distortion on sonic boom noise penetration into the ocean is dependent on the incident signature.

7.2. Recommendations

Future research involving the present algorithm might first include experimental verification of underwater signatures from military aircraft. This would be accomplished by

running the initial waveform through the algorithm and comparing the waveforms at specified depths to the measured ones. Second, the experimental data used in this thesis is only from an F-15 and F-16, therefore underwater sound fields could be calculated from other aircraft and rockets deployed by the United States Air Force. Cases involving PCBoom3 might entail more complex maneuvers. It could be observed that extreme conditions such as greater dive angles could produce local Mach numbers which are over 4.4, thus causing sonic booms that propagate into the ocean. More realistic and intricate atmospheric profiles involving high winds or increased temperature effects could be examined. This would produce more distortions in the wave shapes and perhaps more complicated signatures with increased depth. The relationship concerning waveform distortion and penetration depth also could be examined to determine if distortion truly causes a greater penetration depth of sonic boom energy. Finally, since this thesis assumes that the ocean is infinitely deep, future work with shallow water should be investigated. Shallow water will cause bottom reflections, thus resulting in an increase of the underwater sonic boom energy.

7.3. Conclusions

In conclusion, a well known theory exists that analytically calculates the underwater waveshapes and sound exposure levels from an ideal N wave. To incorporate realistically shaped sonic booms, this thesis introduced an algorithm that successfully determines the underwater sound field from any arbitrarily shaped incident waveform given a flat, homogeneous ocean and a local Mach number under 4.5. Also, by using the output of PCBoom3 with the present algorithm, the underwater sound field created by military aircraft during overwater supersonic training exercises was characterized. Since sonic boom noise does penetrate the water to significant depths, it is thought that US Air Force overwater operations at supersonic speeds may have an environmental noise impact on marine mammals close to the surface. Even though more work needs to be done, it is hoped that the results in this thesis may aid in the determination of the extent of this noise impact on ocean wildlife.

References

1. Gionfriddo, T.A., "Quantification of Sonic Boom Signature Distortions From Propagation Through Atmospheric Turbulence," MS Thesis, Pennsylvania State University, University Park, PA (1992).
2. Maglieri, D.J., and Plotkin, K.J., "Sonic Boom," *Aeroacoustics of Flight Vehicles: Theory and Practice*, edited by H. Hubbard, NASA Reference Publication 1258, Vol. 1 WRDC Technical Report 90-3052, pp. 519-561, (1991).
3. Sparrow, V.W., and Ferguson, T.J., "Penetration of Shaped Sonic Boom Noise Into a Flat Ocean," AIAA Paper 97-0486, 35th Aerospace Sciences Meeting and Exhibit, Reno, NV, 1997.
4. PCBOOM3 Sonic Boom Prediction Model, Ver. 1.0c, Wyle Research Rept. WR 95-22C, Wyle Laboratories, Arlington, VA, May 1996.
5. Cook, R.K., "Penetration of a Sonic Boom Into Water," J. Acoust. Soc. Am., **47**(5, pt.2), 1430-1436, (1970).
6. Kinsler, L.E., Frey, A.R., Coppens, A.B., and Sanders, J.V., *Fundamentals of Acoustics* (John Wiley and Sons, New York, 1982), pp. 124-133.
7. Sparrow, V.W., "The effect of supersonic aircraft speed on the penetration of sonic boom noise into the ocean," J. Acoust. Soc. Am., **97**(1), 159-162, (1995).
8. Sawyers, K., "Underwater sound pressure from sonic booms," J. Acoust. Soc. Am., **44**, 523-524, (1968).
9. Gradshteyn, I.S., and Ryzhik, I.M., *Table of Integrals, Series, and Products*, (Academic Press, San Diego, 1980), pp. 491-492, Eqs. 3.947.2 and 3.947.3.
10. Waters, J., and Glass, R.E., "Penetration of sonic boom energy into the ocean: an experimental simulation," Hydrospace Research Corp. Final Report on Contract FA70-WAI-185, HRC TR 288, June (1970), available from NTIS/DTIC as AD 711 963.
11. Malcolm, G., and Intrieri, P., "Ballistic range investigation of sonic-boom overpressures in water," AIAA **11**, 520-516 (1973).
12. Desharnais, F., and Chapman, D.M.F., "Underwater measurements of a sonic boom," To be published in the proceedings of Oceans '97, Halifax, Canada, October 1997.
13. Rochat, J.L., and Sparrow, V.W., "Sound levels under the ocean surface due to sonic boom penetration," Proceedings of Inter-noise 95, Noise Control Foundation, NY, pp. 967-970 (1995).
14. Rochat, J.L., and Sparrow, V.W., "Two-dimensional focusing of sonic boom noise penetrating an air-water interface," AIAA **35**(No. 1), 35-39 (1997).
15. Pierce, A.D., *Acoustics: An Introduction to its Physical Principles and Applications* (Acoustical Society of America, Woodbury, NY, 1989), p. 613.
16. Wolfram Research Inc., MATHEMATICA, Version 2.2 (Wolfram Research, Champaign, IL, 1993).
17. Seebass, R., "Sonic Boom Theory," J. of Aircraft, **6**(No. 3), 177-183, (1969).
18. Pierce, A.D., "Spikes on sonic-boom pressure waveforms," J. Acoust. Soc. Am., **44**(4), 1052-1061, (1968).

19. Oppenheim, A.V., and Schafer, R.W., *Discrete-Time Signal Processing* (Prentice-Hall, Inc., Englewood Cliffs, NJ, 1989).
20. Crandall, R.E., *Mathematica for the Sciences* (Addison-Wesley Publishing Company, Inc., Redwood City, CA, 1991).
21. Brown, D., and Sutherland, L.C., "Evaluation of outdoor-to indoor response to minimized sonic booms," NASA CR-189643 (1992).
22. American National Standard Specification for Sound Level Meters, S1.4-1983, American Nat. Stand. Inst., Inc., Feb., 1983.
23. Schultz, T.J., *Community Noise Rating*, 2nd ed. (Applied Science Publishers, New York, NY, 1982), pp. 110-111.
24. Shepherd, K.P., and Sullivan, B.M., "A Loudness Calculation Procedure Applied to Shaped Sonic Booms," NASA Technical Paper 3134 (1991).
25. Lee, R.A., and Downing, J.M., "Comparison of measured and predicted lateral distribution of sonic boom overpressures from the United States Air Force sonic boom database," *J. Acoust. Soc. Am.*, **99**(2), 768-776, (1996).
26. Bare Bones Software, BBEdit, Version 4.0.1 (Bare Bones Software, Bedford, MA, 1996).
27. Spiegel, M.R., *Mathematical Handbook of Formulas and Tables*, 27th printing (McGraw Hill, Inc., New York, NY, 1991), pp. 50.

Appendix A.

Tables of Sound Exposure Levels

This appendix is presented as a quick reference point to compare various metrics from the sonic booms analyzed in this thesis.

The tables that follow list the dB peak, unweighted sound exposure levels, L_{UE} , C-weighted sound exposure levels, L_{CE} , and A-weighted sound exposure levels, L_{AE} , for each signature. Tables normalized relative to the values at the water surface are also shown. This is again because even though the reference pressure was $20 \mu\text{Pa}$ and the reference time was 1 second, this algorithm can be used with any other reference values. Plus, in this form it is easy to notice the amount of decay of the dB values relative to depth. For all ideal N wave cases, the analytical calculation for the unweighted sound exposure level is also given.

HSCT N Wave Metrics

Peak Pressure - 100 Pa (2.1 psf)

Duration - 0.3 sec

Mach number - 2.4

Depth(m)	peak dB	L_{UE} (dB)	L_{CE} (dB)	L_{AE} (dB)
0	131.0	118.0*	104.2	91.2
4	129.0	117.1	97.0	61.0
16	126.3	115.2	88.6	38.4
64	119.4	109.8	76.7	8.0

HSCT Metrics Relative To Those At The Surface

Depth(m)	peak dB	L_{UE} (dB)	L_{CE} (dB)	L_{AE} (dB)
0	0.0	0.0	0.0	0.0
4	-2.0	-0.9	-7.2	-30.2
16	-4.7	-2.8	-15.6	-52.8
64	-11.6	-8.2	-27.5	-83.2

$$* \text{Analytical } L_{UE} = 10 \log \left(\frac{Tp_o^2}{6p_{ref}^2} \right) - 3 = 118.0$$

HSCT Expanded Rise Time Sonic Boom Metrics

Peak Pressure - 100 Pa (2.1 psf)

Duration - 0.3 sec

Mach number - 2.4

Depth(m)	peak dB	L_{UE} (dB)	L_{CE} (dB)	L_{AE} (dB)
0	131.0	118.0	94.6	56.3
4	129.6	117.3	92.5	43.9
16	127.0	115.4	88.1	29.9
64	119.2	109.3	77.5	8.5

HSCT Expanded Rise Time Metrics Relative To Those At The Surface

Depth(m)	peak dB	L_{UE} (dB)	L_{CE} (dB)	L_{AE} (dB)
0	0.0	0.0	0.0	0.0
4	-1.4	-0.7	-2.1	-12.4
16	-4.1	-2.6	-6.5	-26.4
64	-11.8	-8.7	-17.1	-47.8

HSCT Flat Top Sonic Boom Metrics

Peak Pressure - 100 Pa (2.1 psf)

Duration - 0.3 sec

Mach number - 2.4

Depth(m)	peak dB	L_{UE} (dB)	L_{CE} (dB)	L_{AE} (dB)
0	131.0	119.8	101.2	70.5
4	130.3	119.1	96.7	56.6
16	128.3	117.3	89.9	37.5
64	121.3	111.7	79.0	9.8

HSCT Flat Top Metrics Relative To Those At The Surface

Depth(m)	peak dB	L_{UE} (dB)	L_{CE} (dB)	L_{AE} (dB)
0	0.0	0.0	0.0	0.0
4	-0.7	-0.7	-4.5	-13.9
16	-2.7	-2.5	-11.3	-33.0
64	-9.7	-8.1	-22.2	-60.7

Experimental F-15 Rounded Sonic Boom Metrics

Peak Pressure - 86.2 Pa (1.8 psf)

Signal Length - 0.1497 sec

Mach number - 1.45

Depth(m)	peak dB	L_{UE} (dB)	L_{CE} (dB)	L_{AE} (dB)
0	129.7	113.8	100.1	76.4
4	126.3	111.4	92.7	48.2
16	119.3	106.1	82.6	24.6
64	102.7	93.6	61.1	-7.9

F-15 Rounded Sonic Boom Metrics Relative To Those At The Surface

Depth(m)	peak dB	L_{UE} (dB)	L_{CE} (dB)	L_{AE} (dB)
0	0.0	0.0	0.0	0.0
4	-3.4	-2.4	-7.4	-28.2
16	-10.4	-7.7	-17.5	-51.8
64	-27.0	-20.2	-39.0	-84.3

Experimental F-15 Double Peaked Sonic Boom Metrics

Peak Pressure - 95.3 Pa (2.0 psf)

Signal Length - 0.1325 sec

Mach number - 1.45

Depth(m)	peak dB	L_{UE} (dB)	L_{CE} (dB)	L_{AE} (dB)
0	130.6	113.7	101.7	79.7
4	126.4	111.2	94.1	49.8
16	119.2	105.9	84.6	27.4
64	102.5	92.5	65.0	-2.2

F-15 Double Peaked Sonic Boom Metrics Relative To Those At The Surface

Depth(m)	peak dB	L_{UE} (dB)	L_{CE} (dB)	L_{AE} (dB)
0	0.0	0.0	0.0	0.0
4	-4.2	-2.5	-7.6	-29.9
16	-11.4	-7.8	-17.1	-52.3
64	-28.1	-21.2	-36.7	-81.9

F-16 U Wave Metrics

Peak Pressure - 305.8 Pa (6.4 psf)

Signal Length - 0.1263 sec

Mach number - 1.2

Depth(m)	peak dB	L_{UE} (dB)	L_{CE} (dB)	L_{AE} (dB)
0	140.7	119.3	110.8	89.7
4	131.0	115.1	98.9	56.5
16	120.3	107.9	85.1	27.3
64	99.1	93.7	59.5	-11.2

F-16 U Wave Metrics Relative To Those At The Surface

Depth(m)	peak dB	L_{UE} (dB)	L_{CE} (dB)	L_{AE} (dB)
0	0.0	0.0	0.0	0.0
4	-9.7	-4.2	-11.9	-33.2
16	-20.3	-11.4	-25.7	-62.4
64	-41.6	-25.6	-51.3	-100.9

PCBoom3 Predicted, F-22 N-Shaped Sonic Boom Metrics

Peak Pressure - 274.8 Pa (5.7 psf)

Signal Length - 0.134 sec

Mach number - 1.2

Depth(m)	peak dB	L_{UE} (dB)	L_{CE} (dB)	L_{AE} (dB)
0	139.8	123.3	112.6	93.4
4	134.5	120.0	100.9	57.2
16	126.1	113.5	88.1	28.4
64	107.7	99.4	61.9	-10.0

F-22 N-Shaped Sonic Boom Metrics Relative To Those At The Surface

Depth(m)	peak dB	L_{UE} (dB)	L_{CE} (dB)	L_{AE} (dB)
0	0.0	0.0	0.0	0.0
4	-5.3	-3.3	-11.7	-36.2
16	-13.7	-9.8	-24.5	-65.0
64	-32.1	-23.9	-50.7	-103.4

Linear Acceleration
Trajectory Time = 19 sec, $\Phi = 0^\circ$

Peak Pressure - 420.2 Pa (8.8 psf)

Signal Length - 0.2558 sec

Aircraft Mach Number - 1.1

Local Mach Number - 1.0

Depth(m)	peak dB	L_{UE} (dB)	L_{CE} (dB)	L_{AE} (dB)
0	143.4	120.4	113.2	92.1
4	132.8	116.7	97.1	54.7
16	125.4	113.7	79.9	21.8
64	116.6	110.3	57.9	-17.7

Linear Acceleration Metrics Relative To Those At The Surface

Depth(m)	peak dB	L_{UE} (dB)	L_{CE} (dB)	L_{AE} (dB)
0	0.0	0.0	0.0	0.0
4	-10.6	-3.7	-16.1	-37.4
16	-18.0	-6.7	-33.3	-70.3
64	-26.8	-10.1	-55.3	-109.8

Linear Acceleration
Trajectory Time = 90 sec, $\Phi = 0^\circ$

Peak Pressure - 638.9 Pa (13.4 psf)

Signal Length - 0.0843 sec

Aircraft Mach Number - 1.7

Local Mach Number - 1.6

Depth(m)	peak dB	L_{UE} (dB)	L_{CE} (dB)	L_{AE} (dB)
0	147.1	128.6	120.3	103.3
4	141.4	125.0	111.0	70.3
16	132.2	117.8	98.9	44.8
64	113.1	103.2	72.1	6.3

Linear Acceleration Metrics Relative To Those At The Surface

Depth(m)	peak dB	L_{UE} (dB)	L_{CE} (dB)	L_{AE} (dB)
0	0.0	0.0	0.0	0.0
4	-5.6	-3.6	-9.3	-33.0
16	-14.9	-10.8	-21.4	-58.5
64	-34.0	-25.4	-48.2	-97.0

10 Degree Dive
Trajectory Time = 19 sec, $\Phi = 0^\circ$

Peak Pressure - 518.3 Pa (10.8 psf)

Signal Length - 0.2485 sec

Aircraft Mach Number - 1.1

Local Mach Number - 1.2

Depth(m)	peak dB	L_{UE} (dB)	L_{CE} (dB)	L_{AE} (dB)
0	145.3	121.4	115.1	95.5
4	134.4	117.5	99.5	58.8
16	126.8	114.3	83.0	26.5
64	117.7	110.8	60.1	-17.0

10 Degree Dive Metrics Relative To Those At The Surface

Depth(m)	peak dB	L_{UE} (dB)	L_{CE} (dB)	L_{AE} (dB)
0	0.0	0.0	0.0	0.0
4	-10.9	-3.9	-15.6	-36.7
16	-18.5	-7.1	-32.1	-69.0
64	-27.6	-10.6	-55.0	-112.5

10 Degree Dive
Trajectory Time = 23 sec, $\Phi = 0^\circ$

Peak Pressure - 167.1 Pa (3.5 psf)

Signal Length - 0.1816 sec

Aircraft Mach Number - 1.2

Local Mach Number - 1.0

Depth(m)	peak dB	L_{UE} (dB)	L_{CE} (dB)	L_{AE} (dB)
0	135.4	120.2	108.0	87.3
4	130.6	117.3	95.3	50.1
16	122.9	111.3	82.2	20.0
64	105.5	97.9	57.3	-17.6

10 Degree Dive Metrics Relative To Those At The Surface

Depth(m)	peak dB	L_{UE} (dB)	L_{CE} (dB)	L_{AE} (dB)
0	0.0	0.0	0.0	0.0
4	-4.8	-2.9	-12.7	-37.2
16	-12.5	-8.9	-25.8	-67.3
64	-29.9	-22.3	-50.7	-104.9

30 Degree Dive
Trajectory Time = 11 sec, $\Phi = 0^\circ$

Peak Pressure - 675.4 Pa (14.1 psf)

Signal Length - 0.2197 sec

Aircraft Mach Number - 1.1

Local Mach Number - 1.6

Depth(m)	peak dB	L_{UE} (dB)	L_{CE} (dB)	L_{AE} (dB)
0	147.6	123.7	117.2	97.8
4	138.2	120.5	104.9	67.5
16	131.2	117.6	90.4	38.2
64	122.6	114.3	68.2	-3.1

30 Degree Dive Metrics Relative To Those At The Surface

Depth(m)	peak dB	L_{UE} (dB)	L_{CE} (dB)	L_{AE} (dB)
0	0.0	0.0	0.0	0.0
4	-9.4	-3.2	-12.3	-30.3
16	-16.4	-6.1	-26.8	-59.6
64	-25.0	-9.4	-49.0	-100.9

30 Degree Dive
Trajectory Time = 16 sec, $\Phi = 0^\circ$

Peak Pressure - 885.6 Pa (18.5 psf)

Signal Length - 0.0988 sec

Aircraft Mach Number - 1.2

Local Mach Number - 2.1

Depth(m)	peak dB	L_{UE} (dB)	L_{CE} (dB)	L_{AE} (dB)
0	149.9	132.2	123.0	105.3
4	145.8	129.7	115.4	77.8
16	139.3	124.7	105.6	53.9
64	123.5	112.5	84.2	21.0

30 Degree Dive Metrics Relative To Those At The Surface

Depth(m)	peak dB	L_{UE} (dB)	L_{CE} (dB)	L_{AE} (dB)
0	0.0	0.0	0.0	0.0
4	-4.1	-2.5	-7.6	-27.5
16	-10.6	-7.5	-17.4	-51.4
64	-26.4	-19.7	-38.8	-84.3

30 Degree Dive
Trajectory Time = 22 sec, $\Phi = 0^\circ$

Peak Pressure - 193.9 Pa (4.1 psf)

Signal Length - 0.1381 sec

Aircraft Mach Number - 1.2

Local Mach Number - 1.0

Depth(m)	peak dB	L_{UE} (dB)	L_{CE} (dB)	L_{AE} (dB)
0	136.7	120.3	109.5	90.4
4	130.8	116.5	96.6	50.8
16	121.2	109.0	82.6	20.9
64	101.7	94.1	54.3	-19.8

30 Degree Dive Metrics Relative To Those At The Surface

Depth(m)	peak dB	L_{UE} (dB)	L_{CE} (dB)	L_{AE} (dB)
0	0.0	0.0	0.0	0.0
4	-5.9	-3.8	-12.9	-39.6
16	-15.5	-11.3	-26.9	-69.5
64	-35.0	-26.2	-55.2	-110.2

Pushover
Trajectory Time = 6 sec, $\Phi = 0^\circ$

Peak Pressure - 356.1 Pa (7.4 psf)

Signal Length - 0.1202 sec

Aircraft Mach Number - 1.2

Local Mach Number - 1.0

Depth(m)	peak dB	L_{UE} (dB)	L_{CE} (dB)	L_{AE} (dB)
0	142.0	125.0	114.9	96.5
4	135.7	120.9	102.3	56.9
16	125.5	112.9	88.1	27.8
64	105.4	97.6	59.0	-14.2

Pushover Metrics Relative To Those At The Surface

Depth(m)	peak dB	L_{UE} (dB)	L_{CE} (dB)	L_{AE} (dB)
0	0.0	0.0	0.0	0.0
4	-6.3	-4.1	-12.6	-39.6
16	-16.5	-12.1	-26.8	-68.7
64	-36.6	-27.4	-55.9	-110.7

Pushover
Trajectory Time = 10 sec, $\Phi = 0^\circ$

Peak Pressure - 584.7 Pa (12.2 psf)

Signal Length - 0.1246 sec

Aircraft Mach Number - 1.2

Local Mach Number - 1.1

Depth(m)	peak dB	L_{UE} (dB)	L_{CE} (dB)	L_{AE} (dB)
0	146.3	129.6	119.2	100.5
4	140.2	125.6	106.6	61.3
16	130.4	118.0	92.6	32.0
64	110.7	102.9	64.1	-9.4

Pushover Metrics Relative To Those At The Surface

Depth(m)	peak dB	L_{UE} (dB)	L_{CE} (dB)	L_{AE} (dB)
0	0.0	0.0	0.0	0.0
4	-6.1	-4.0	-12.6	-39.2
16	-15.9	-11.6	-26.6	-68.5
64	-35.6	-26.7	-55.1	-109.9

Straight Flight Case For Pushover And Constant g Turn

Pushover Trajectory Time = 6 sec, $\Phi = 0^\circ$

Pushover Trajectory Time = 10 sec, $\Phi = 0^\circ$

Constant g Turn Trajectory Time = 11 sec, $\Phi = 0^\circ$

Peak Pressure - 506.4 Pa (10.6 psf)

Signal Length - 0.105 sec

Aircraft Mach Number - 1.2

Local Mach Number - 1.2

Depth(m)	peak dB	L_{UE} (dB)	L_{CE} (dB)	L_{AE} (dB)
0	145.1	127.6	118.1	100.2
4	138.7	123.4	106.3	61.9
16	128.4	115.4	92.2	33.6
64	108.3	100.1	63.2	-8.3

Metrics Relative To Those At The Surface

Depth(m)	peak dB	L_{UE} (dB)	L_{CE} (dB)	L_{AE} (dB)
0	0.0	0.0	0.0	0.0
4	-6.4	-4.2	-11.8	-38.3
16	-16.7	-12.2	-25.9	-66.6
64	-36.8	-27.5	-54.9	-108.5

Pushover
Trajectory Time = 10 sec, $\Phi = 35^\circ$

Peak Pressure - 1554.8 Pa (32.5 psf)

Signal Length - 0.2464 sec

Aircraft Mach Number - 1.2

Local Mach Number - 1.0

Depth(m)	peak dB	L_{UE} (dB)	L_{CE} (dB)	L_{AE} (dB)
0	154.8	130.4	124.7	108.0
4	142.3	125.5	106.4	64.0
16	134.0	120.1	90.5	30.0
64	121.6	114.2	64.5	-11.8

Pushover Metrics Relative To Those At The Surface

Depth(m)	peak dB	L_{UE} (dB)	L_{CE} (dB)	L_{AE} (dB)
0	0.0	0.0	0.0	0.0
4	-12.5	-4.9	-18.3	-44.0
16	-20.8	-10.3	-34.2	-78.0
64	-33.2	-16.2	-60.2	-119.8

Straight Flight Case For Pushover
Trajectory Time = 10 sec, $\Phi = 35^\circ$

Peak Pressure - 423.0 Pa (8.8 psf)

Signal Length - 0.1104 sec

Aircraft Mach Number - 1.2

Local Mach Number - 1.1

Depth(m)	peak dB	L_{UE} (dB)	L_{CE} (dB)	L_{AE} (dB)
0	143.5	126.2	116.5	98.3
4	137.0	122.0	104.1	59.1
16	126.6	113.8	89.8	30.3
64	106.4	98.4	60.5	-12.1

Metrics Relative To Those At The Surface

Depth(m)	peak dB	L_{UE} (dB)	L_{CE} (dB)	L_{AE} (dB)
0	0.0	0.0	0.0	0.0
4	-6.5	-4.2	-12.4	-39.2
16	-16.9	-12.4	-26.7	-68.0
64	-37.1	-27.8	-56.0	-110.4

Constant g Turn
Trajectory Time = 11 sec, $\Phi = 0^\circ$

Peak Pressure - 503.8 Pa (10.5 psf)

Signal Length - 0.1059 sec

Aircraft Mach Number - 1.2

Local Mach Number - 1.2

Depth(m)	peak dB	L_{UE} (dB)	L_{CE} (dB)	L_{AE} (dB)
0	145.0	127.6	118.0	100.1
4	138.7	123.4	106.2	61.9
16	128.5	115.5	92.2	33.6
64	108.4	100.2	63.3	-8.3

Constant g Turn Metrics Relative To Those At The Surface

Depth(m)	peak dB	L_{UE} (dB)	L_{CE} (dB)	L_{AE} (dB)
0	0.0	0.0	0.0	0.0
4	-6.3	-4.2	-11.8	-38.2
16	-16.5	-12.1	-25.8	-66.5
64	-36.6	-27.4	-54.7	-108.4

Constant g Turn
Trajectory Time = 11 sec, $\Phi = -20^\circ$

Peak Pressure - 1397.5 Pa (29.2 psf)

Signal Length - 0.2395 sec

Aircraft Mach Number - 1.2

Local Mach Number - 1.2

Depth(m)	peak dB	L_{UE} (dB)	L_{CE} (dB)	L_{AE} (dB)
0	153.9	130.7	123.4	103.5
4	144.0	126.9	108.4	66.7
16	136.5	123.3	92.5	34.6
64	126.4	119.4	69.1	-7.9

Constant g Turn Metrics Relative To Those At The Surface

Depth(m)	peak dB	L_{UE} (dB)	L_{CE} (dB)	L_{AE} (dB)
0	0.0	0.0	0.0	0.0
4	-9.9	-3.8	-15.0	-36.8
16	-17.4	-7.4	-30.9	-68.9
64	-27.5	-11.3	-54.3	-111.4

Straight Flight Case For Constant g Turn
Trajectory Time = 11 sec, $\Phi = -20^\circ$

Peak Pressure - 479.3 Pa (10.0 psf)

Signal Length - 0.1063 sec

Aircraft Mach Number - 1.2

Local Mach Number - 1.1

Depth(m)	peak dB	L_{UE} (dB)	L_{CE} (dB)	L_{AE} (dB)
0	144.6	127.2	117.6	99.6
4	138.1	122.9	105.6	61.0
16	127.8	114.8	91.4	32.5
64	107.6	99.4	62.2	-9.7

Metrics Relative To Those At The Surface

Depth(m)	peak dB	L_{UE} (dB)	L_{CE} (dB)	L_{AE} (dB)
0	0.0	0.0	0.0	0.0
4	-6.5	-4.3	-12.0	-38.6
16	-16.8	-12.4	-26.2	-67.1
64	-37.0	-27.8	-55.4	-109.3

Equal Energy N Wave For F-15 Rounded Sonic Boom

Peak Pressure - 98.9 Pa (2.1 psf)

Signal Length - 0.1163 sec

Mach Number - 1.45

Depth(m)	peak dB	L_{UE} (dB)	L_{CE} (dB)	L_{AE} (dB)
0	129.7	113.8*	104.5	92.2
4	125.7	110.6	95.2	52.7
16	117.8	104.4	84.8	28.6
64	99.7	89.6	63.2	-3.0

Metrics Relative To Those At The Surface

Depth(m)	peak dB	L_{UE} (dB)	L_{CE} (dB)	L_{AE} (dB)
0	0.0	0.0	0.0	0.0
4	-4.0	-3.2	-9.3	-39.5
16	-11.9	-9.4	-19.7	-63.6
64	-30.0	-24.2	-41.3	-95.2

$$* \text{Analytical } L_{UE} = 10 \log \left(\frac{Tp_o^2}{6p_{ref}^2} \right) - 3 = 113.8$$

Equal Energy N Wave For F-15 Double Peaked Sonic Boom

Peak Pressure - 94.9 Pa (2.0 psf)

Signal Length - 0.1234 sec

Mach Number - 1.45

Depth(m)	peak dB	L_{UE} (dB)	L_{CE} (dB)	L_{AE} (dB)
0	130.5	113.7*	104.6	92.0
4	125.5	110.6	96.2	53.1
16	117.9	104.6	86.8	31.1
64	98.6	87.3	66.3	3.2

Metrics Relative To Those At The Surface

Depth(m)	peak dB	L_{UE} (dB)	L_{CE} (dB)	L_{AE} (dB)
0	0.0	0.0	0.0	0.0
4	-5.0	-3.1	-8.4	-38.9
16	-12.6	-9.1	-17.8	-60.9
64	-31.9	-26.4	-38.3	-88.8

$$* \text{Analytical } L_{UE} = 10 \log \left(\frac{Tp_o^2}{6p_{ref}^2} \right) - 3 = 113.7$$

Equal Energy N Wave For F-16 U Wave

Peak Pressure - 195.6 Pa (4.1 psf)

Signal Length - 0.1058 sec

Mach Number - 1.2

Depth(m)	peak dB	L_{UE} (dB)	L_{CE} (dB)	L_{AE} (dB)
0	136.8	119.3*	110.7	98.2
4	130.5	115.3	100.8	56.0
16	120.7	107.6	89.1	32.7
64	99.0	88.1	65.0	-0.2

Metrics Relative To Those At The Surface

Depth(m)	peak dB	L_{UE} (dB)	L_{CE} (dB)	L_{AE} (dB)
0	0.0	0.0	0.0	0.0
4	-6.3	-4.0	-9.9	-42.2
16	-16.1	-11.7	-21.6	-65.5
64	-37.8	-31.2	-45.7	-98.4

$$*Analytical L_{UE} = 10 \log \left(\frac{Tp_o^2}{6p_{ref}^2} \right) - 3 = 119.3$$

Appendix B.

Mathematica Code

The following pages contain the *Mathematica* Notebook code used for analyses in this thesis. First presented is the algorithm described in Chapter 3 that computed the underwater signatures and sound exposure levels for all waves in Chapters 3, 4, and 5. Next, the notebooks used to generate the parameters and predict the underwater sound field for the equal energy N waves in Chapter 6 is listed. These *Mathematica* Notebooks were created and run on a Power Macintosh 7100/80 and a Macintosh Quadra 700. The code has some comments describing the purpose of certain sections, but the reader is expected to have some familiarity with *Mathematica* syntax.

Algorithm to Find Underwater Sound Fields

This *Mathematica* notebook presents the algorithm described in Chapter 3. It was used to calculate the underwater sound field from all the signatures presented in Chapters 3, 4, and 5.

■ Reading in the incident waveform and predicting the underwater signature at a specified depth

Wave2 inputs signal length, depth, Mach number, and the data file, then calculates the signature at the specified depth using the method described in Chapter 3. The last line of Wave2 computes the peak dB of the wave.

```
$DefaultFont={"Courier",14};

Wave2[siglength_,depth_,Machno_,datafile_] := {
  datalist=ReadList[datafile,Number];
  signalsamples=Length[datalist];
  duration=siglength;
  samples=2048;
  M=Machno;
  c=343;
  W=4.5;
  mu=Sqrt[1-(M^2/W^2)];
  z=depth;
  h=mu z;
  pref=20 10^(-6);
  fs=signalsamples/duration;
  zerosamples=Round[samples-signalsamples];
  totalduration=(duration/signalsamples)*samples;
  deltat=duration/signalsamples;
  T=totalduration/samples;
  fs1=1/T;
  deltaf=fs1/samples;
  timeaxis=Table[y,{y,0,totalduration-totalduration
/samples,totalduration/samples}];
  zeros=Table[0 i,{i,1,zerosamples/2}];
  zeropad=Join[zeros,datalist,zeros];
  maxdata=Max[zeropad];
  normlist=zeropad/maxdata;
  transform=N[Sqrt[samples]*InverseFourier
[normlist]];
  listswitch=N[RotateRight[transform,samples/2]];
```

```

explist=N[Table[Exp[-h*Abs[(om)/(c*M)]],
{om,-Pi fs,Pi fs-(2 Pi fs)/samples,(2 Pi fs)
/samples}]];
integrand=N[explist listswitch];
switchback=N[RotateLeft[integrand,samples/2]];
invtrans=N[(2/Sqrt[samples])*Fourier
[switchback]];
finalform=maxdata*N[Chop[invtrans]];
pressmax=Max[finalform];
dBpeak=20 Log[10,pressmax/(pref Sqrt[2])];
}

```

■ Calculating the various metrics

This section calculates unweighted, C-weighted, and A-weighted sound exposure levels of the signature at the specified depth. This code is taken from Reference 13.

fftcomplex inputs a list of peak pressure values and takes the Fourier Transform.

```

fftcomplex[list_] := {
  fftpressz=20 N[Log[10,((Sqrt[samples]
  *InverseFourier[list])/
  (Sqrt[2] pref))]];
  fftpos= Table[{fftpressz[[i+1]]},
  {i,0,(Quotient[samples,2]-1)}];
}

```

■ C weighting, A weighting

Weighting Constants

```

f1=20.598997;
f2=107.65265;
f3 = 737.86223;
f4 = 12194.22;
f5 = 158.48932;
K1 = 2.242881 10^16;
K2 = 1.025119;
K3 = 1.562339;

```

C weighting for frequency:

```
WC[f_] := {
  10 Log[10,
    (K1 f^4) / ((f^2+f1^2)^2 (f^2+f4^2)^2)]};
```

A weighting for frequency:

```
WA[f_] :=
  10 Log[10,
    ((K3 f^4) / ((f^2 + f2^2) (f^2 +
    f3^2)))] + WC[f];
```

dBAPolar and dBCPolar attenuate the magnitude of the complex numbers and create a list of polar complex numbers A or C-weighted.

```
dBcpolar[list_] :={
  dBcList =
  Table[
    (Abs[list[[i]]] +
    WC[(i deltaf)]) Exp[I Arg[list[[i]]]],
    {i,1,(Length[list])}];}
```

```
dBApolar[list_] :={
  dBaList =
  Table[
    (Abs[list[[i]]] +
    WA[(i deltaf)]) Exp[I Arg[list[[i]]]],
    {i,1,(Length[list])}];
}
```

Changing dB into pressure

```
pressfromdB[list_] :=
  p=N[10^(list/20) Sqrt[2] pref];
```

Changing peak pressure into dB

```
dBvalue[list_] :=
  dB=20 N[Log[10,(Abs[list]/(Sqrt[2] pref))]];
```

Changing rms pressure into dB

```
dBvaluerms[list_] :=  
  dB=20 N[Log[10, (Abs[list]/pref)]];  
  
Pos2Full[list_] := {  
  presslist=pressfromdB[list];  
  revlist=Reverse[presslist];  
  addlist=Conjugate[revlist];  
  list2xform=Join[presslist,addlist];  
}
```

invfft takes the list of discrete values and takes the inverse fourier transform.

```
invfft[list_] := {  
  templist=N[Abs[(Fourier[list])/Sqrt[samples]]];  
  invfftlist=Flatten[templist];  
}
```

SELtheorhalf uses rms pressures, and also subtracts 3 dB since we should be using only half the energy.

```
SELtheorhalf[list_] := N[10 Log[10,  
  deltat Sum[(list[[j]] / Sqrt[2])^2 / pref^2,  
  {j,1,Length[list]}]] - 3]
```

■ Calculations

These calculations are in the form of dB peak, unweighted SEL, C-Weighted SEL, then A-Weighted SEL. In order to use this, values must be substituted for the signal length, depth, local Mach number and data file. The data file name must also be placed in quotations. The For loop places the x axis in time in seconds.

```
Wave2[siglength,depth,Machno,datafile];  
plot1table=Table[Null,{i,1,2*samples}];  
plot1table2=Partition[plot1table,2];  
plot1plot=For[i=1, i<=samples, i++,  
  plot1table2[[i]]={timeaxis[[i]],finalform[[i]]}  
];  
plot1=ListPlot[plot1table2,PlotJoined->True];
```

N[dBpeak] displays the peak dB value calculated in Wave2.

N[dBpeak]

This routine calculates the unweighted sound exposure level.

```
fftcomplex[finalform];  
Pos2Full[fftpos];  
invfft[list2xform];  
SELtheorhalf[invfftlist]
```

This routine calculates the C-weighted sound exposure level.

```
dBcpolar[fftpos];  
Pos2Full[dBClist];  
invfft[list2xform];  
SELtheorhalf[invfftlist]
```

This routine calculates the A-weighted sound exposure level.

```
dBApolar[fftpos];  
Pos2Full[dBAlist];  
invfft[list2xform];  
SELtheorhalf[invfftlist]
```

Generating Parameters For Equal Energy N Waves

This notebook finds the total energy of a given experimental wave shape and then calculates the maximum overpressure and duration of an N Wave that has the same energy. The N Wave is then plotted and a column of data is created to copy and paste into a BBEdit file. The method to find the equal energy N Wave is from Reference 1.

Note: Pressure doubling is taken into account here.

■ Reading in the experimental waveform

This section reads in the experimental waveform and doubles and squares the pressure values and calculates the number of samples in the signal and the sampling frequency. The user must substitute values for the datafile, signal duration, the LER and the TER.

```
Clear[datalist,sqdatalist,signalsamples,fs];
datalist=ReadList["datafile",Number];
datalist2=2 datalist;
sqdatalist=datalist2^2;
signalsamples=Length[datalist]
signalduration=duration of signal;
fs=signalsamples/signalduration
LER=LER for aircraft;
TER=TER for aircraft;
```

■ Finding the energy in the experimental wave

```
energy=1/fs Apply[Plus,sqdatalist]
```

■ Finding the energy amounts at which the N Wave should start and stop.

```
LDE=energy*LER
TDE=energy*(1-TER)
```

■ Finding the starting and ending sample numbers and times

This section uses a trial and error method. The user should repeatedly run this section with different sample numbers, i and j, until values closest to the LDE and TDE are found. After the appropriate sample numbers are found, the starting and ending times in seconds are calculated.

```
Clear[EA,j,startenergy];
j=12;
EA=Take[sqdatalist,j];
startenergy=1/fs Apply[Plus,EA]
```

```

starttime=j/fs
Clear[EB,i,endenergy];
i=256;
EB=Take[sqdatalist,i];
endenergy=1/fs Apply[Plus,EB]
endtime=i/fs

```

■ Finding the duration of the N wave

```

Clear[duration];
duration=endtime-starttime

```

■ Finding the Maximum Overpressure of the equivalent N Wave

```

pkpressure=Sqrt[(3 energy)/duration]

```

■ Plotting the N-Wave and creating a column to place into BBEEdit.

This section uses the equations of Cook to generate the N wave from the above parameters. After generating the N wave, the initial pressure values in pascals are listed in a column to be copied and pasted into BBEEdit. The user must enter the appropriate Mach number.

```

Clear[testfunction, trialfcn, h, cookilterm2,
      testfunction,t];
c=343;
M=1.45;
time=duration/2;
L=M c time;
scale=1/L;
W=4.5;
mu=Sqrt[1-(M^2/W^2)];
h=(mu z scale);
z=0;

cookilterm1= ((h/2) Log[(h^2 +((t*c*M*scale)+1)^2)/
      (h^2+((t*c*M*(scale))-1)^2)]/Pi;
cookilterm2= (
      (-t*c*M*(scale)) ArcTan[ (2*h) / (h^2 + (t*c*M*
      (scale))^2 -1)]/Pi;

testfunction=((-c*t*M*(scale))/Pi)* (ArcTan[ (2*h) /
      (h^2 + (c*M*t*(scale))^2 -1)]+Pi);

trialfcn=Which[t <-Sqrt[(1-h^2)/(M^2*c^2*(scale)^2)]
      , cookilterm2,
      t > Sqrt[(1-h^2)/(M^2*c^2*(scale)^2)]
      ,cookilterm2,
      True, testfunction];

```

Plotting the N wave and placing it in column form.

```

Nwavefcn=pkpressure (trialfcn+cookilterm1);
Plot[Nwavefcn,{t,-time-0.1,time+0.1}, PlotRange ->
      {-pkpressure-5,pkpressure+5}];

Nwavedata=Table[Nwavefcn,{t,-time,time-duration/
      signalsamples,duration/signalsamples}];
Length[Nwavedata]
zerolist=Table[i 0,{i,1,30}];
Nwaveplot=Join[zerolist,Nwavedata,zerolist];
ListPlot[Nwaveplot,PlotJoined->True,PlotRange->All];
ColumnForm[Nwavedata]

```


Algorithm For Equal Energy N Waves

This *Mathematica* notebook presents the algorithm described in Chapter 3. It was used to calculate the underwater sound field from the experimental signatures and the equal energy N waves presented in Chapter 6.

■ Reading in the incident waveforms and predicting the underwater signatures at a specified depth

Wave1 inputs signal length, depth, Mach number, and the data file of the experimental wave then calculates the signature at the specified depth using the method described in Chapter 3. The last line of Wave1 computes the peak dB of the experimental wave.

```
$DefaultFont={"Courier",14};

Wave1[siglength_,depth_,Machno_,datafile_] := {
  datalist=ReadList[ datafile,Number];
  signalsamples=Length[datalist];
  samples=2048;
  duration=siglength;
  M=Machno;
  c=343;
  W=4.5;
  mu=Sqrt[1-(M^2/W^2)];
  z=depth;
  h=mu z;
  pref=20 10^(-6);
  fs=signalsamples/duration;
  zerosamples=Round[samples-signalsamples];
  totalduration=(duration/signalsamples)*samples;
  deltat=duration/signalsamples;
  T=totalduration/samples;
  fs1=1/T;
  deltaf=fs1/samples;
  timeaxis=Table[y,{y,0,totalduration-totalduration
/samples,
totalduration/samples}];
  zeros=Table[0 i,{i,1,zerosamples/2}];
  zeropad=Join[zeros,datalist,zeros];
  maxdata=Max[zeropad];
  normlist=zeropad/maxdata;
  transform=N[Sqrt[samples]*InverseFourier
[normlist]];
  listswitch=N[RotateRight[transform,samples/2]];
```

```

explist=N[Table[Exp[-h*Abs[(om)/(c*M)]],
{om,-Pi fs,Pi fs-(2 Pi fs)/samples,(2 Pi fs)
/samples}]];
integrand=N[explist listswitch];
switchback=N[RotateLeft[integrand,samples/2]];
invtrans=N[(2/Sqrt[samples])*Fourier
[switchback]];
finalform=maxdata*N[Chop[invtrans]];
pressmax=Max[finalform];
dBpeak=20 Log[10,pressmax/(pref Sqrt[2])];
}

```

Wave2b inputs signal length, depth, Mach number, and the data file of the equal energy N wave then calculates the signature at the specified depth using the method described in Chapter 3. The last line of Wave2b computes the peak dB of the N wave.

```

Wave2b[siglengthb_,depthb_,Machnob_,datafileb_]:=({
datalistb=ReadList[ datafileb,Number];
signalsamplesb=Length[datalistb];
samplesb=2048;
durationb=siglengthb;
Mb=Machnob;
cb=343;
Wb=4.5;
mub=Sqrt[1-((Mb)^2/(Wb)^2)];
zb=depthb;
hb=mub*zb;
prefb=20 10^(-6);
fsb=signalsamplesb/durationb;
zerosamplesb=Round[samplesb-signalsamplesb];
totaldurationb=(durationb/signalsamplesb)*samplesb;
deltatb=durationb/signalsamplesb;
Tb=totaldurationb/samplesb;
fsc=1/Tb;
deltafb=fsc/samplesb;
timeaxisb=Table[y,{y,0.2064,(totaldurationb+0.2064)
-totaldurationb/samplesb,totaldurationb
/samplesb}];
zerosb=Table[0 i,{i,1,zerosamplesb/2}];
zeropadb=Join[zerosb,datalistb,zerosb];
maxdatab=Max[zeropadb];
normlistb=zeropadb/maxdatab;
transformb=N[Sqrt[samplesb]*InverseFourier
[normlistb]];
listswitchb=N[RotateRight[transformb,samplesb/2]];

```

```

explistb=N[Table[Exp[-hb*Abs[(omb)/(cb*Mb)]],
{omb,-Pi fsb,Pi fsb-(2 Pi fsb)/samplesb,(2 Pi fsb)
/samplesb}]];
integrandb=N[explistb listswitchb];
switchbackb=N[RotateLeft[integrandb,samplesb/2]];
invtransb=N[(1/Sqrt[samplesb])*Fourier
[switchbackb]];
finalformb=maxdatab*N[Chop[invtransb]];
pressmaxb=Max[finalformb];
dBpeakb=20 Log[10,pressmaxb/(prefb Sqrt[2])];
}

```

■ Calculating the various metrics

This section calculates unweighted, C-weighted, and A-weighted sound exposure levels of the signature at the specified depth. This code is taken from Reference 13.

fftcomplex inputs a list of peak pressure values and takes the Fourier Transform.

```

fftcomplexb[list_] := {
  fftpresszb=20 N[Log[10,((Sqrt[samplesb]
*InverseFourier[list])/
(Sqrt[2] prefb))]];
  fftposb= Table[{fftpresszb[[i+1]]},
  {i,0,(Quotient[samplesb,2]-1)}];
}

```

■ C weighting, A weighting

Weighting Constants

```

f1=20.598997;
f2=107.65265;
f3 = 737.86223;
f4 = 12194.22;
f5 = 158.48932;
K1 = 2.242881 10^16;
K2 = 1.025119;
K3 = 1.562339;

```

C weighting for frequency:

```
WC[f_] := {
  10 Log[10,
    (K1 f^4) / ((f^2+f1^2)^2 (f^2+f4^2)^2)]];
```

A weighting for frequency:

```
WA[f_] :=
  10 Log[10,
    ((K3 f^4) / ((f^2 + f2^2) (f^2 +
    f3^2))) + WC[f];
```

dBAPolar and dBCPolar attenuate the magnitude of the complex numbers and create a list of polar complex numbers A or C-weighted.

```
dBcpolarb[list_] :={
  dBclistb =
  Table[
    (Abs[list[[i]]] +
    WC[(i deltafb)]) Exp[I Arg[list[[i]]]],
    {i,1,(Length[list])}];}
```

```
dBapolarb[list_] :={
  dBalistb =
  Table[
    (Abs[list[[i]]] +
    WA[(i deltafb)]) Exp[I Arg[list[[i]]]],
    {i,1,(Length[list])}];
}
```

Changing dB into pressure

```
pressfromdBb[list_] :=
  pb=N[10^(list/20) Sqrt[2] prefb];
```

Changing peak pressure into dB

```
dBvalueb[list_] :=
  dBb=20 N[Log[10, (Abs[list]/(Sqrt[2] prefb))]];
```

Changing rms pressure into dB

```

dBvaluermsb[list_] :=
  dBb=20 N[Log[10, (Abs[list]/prefb)]];

Pos2Fullb[list_] := {
  presslistb=pressfromdBb[list];
  revlistb=Reverse[presslistb];
  addlistb=Conjugate[revlistb];
  list2xformb=Join[presslistb,addlistb];
}

```

invfft takes the list of discrete values and takes the inverse fourier transform.

```

invfftb[list_] := {
  templistb=N[Abs[(Fourier[list])/Sqrt[samplesb]]];
  invfftlistb=Flatten[templistb];
}

```

SELtheorhalf uses rms pressures, and also subtracts 3 dB since we should be using only half the energy

```

SELtheorhalfb[list_] := N[10 Log[10,
  deltatb Sum[(list[[j]] / Sqrt[2])^2 / prefb^2,
    {j,1,Length[list]}]] - 3]

```

■ Calculations

These calculations are in the form of dB peak, unweighted SEL, C-Weighted SEL, then A-Weighted SEL. In order to use this, values must be substituted for the signal length, depth, local Mach number and data file. The data file name must also be placed in quotations. The For loop places the x axis in time in seconds.

Wave1 again calculates the underwater signature from the experimental wave.

```

Wave1[siglength,depth,Machno,datafile];
plot1table=Table[Null,{i,1,2*samples}];
plot1table2=Partition[plot1table,2];
plot1plot=For[i=1, i<=samples, i++,
  plot1table2[[i]]={timeaxis[[i]],finalform[[i]]}
];
plot1=ListPlot[plot1table2,PlotJoined->True];

```

Wave2 predicts the underwater signature from the equal energy N wave.

```
Wave2b[siglengthb,depthb,Machnob,datafileb];  
plot1tableb=Table[Null,{i,1,2*samplesb}];  
plot1table2b=Partition[plot1tableb,2];  
plot1plotb=For[i=1, i<=samplesb, i++,  
    plot1table2b[[i]]={timeaxisb[[i]],finalformb[[i]]}  
];  
plot1b=ListPlot[plot1table2b,PlotJoined->True];
```

array0 places the two waveforms on the same set of axes for comparison purposes.

```
array0=Show[plot1,plot1b];
```

N[dBpeak] displays the peak dB value for the equal energy N wave calculated in Wave2b.

```
N[dBpeak]
```

This routine calculates the unweighted sound exposure level for the N wave.

```
fftcomplexb[finalformb];  
Pos2Fullb[fftposb];  
invfftb[list2xformb];  
SELtheorhalfb[invfftlistb]
```

This routine calculates the C-weighted sound exposure level for the N wave.

```
dB Cpolarb[fftposb];  
Pos2Fullb[DBClistb];  
invfftb[list2xformb];  
SELtheorhalfb[invfftlistb]
```

This routine calculates the A-weighted sound exposure level for the N wave.

```
dB Apolarb[fftposb];  
Pos2Fullb[dbAlistb];  
invfftb[list2xformb];  
SELtheorhalfb[invfftlistb]
```

Appendix C.

PCBoom3 Files

The following pages contain files created from the sonic boom prediction program PC-Boom3. These files were used in the analyses of waveforms presented in Chapters 4 and 5. The files listed include an atmospheric profile, .ATT file, a trajectory, .TRJ file, a contour/isopemp file, a signature file, and a main output, .OUT file. PCBoom3 was run in DOS on a 25MHz 386. Comments are added throughout the files, therefore no prior knowledge of PCBoom3 is needed to fully understand the content.

Atmospheric Profile, .ATT File

U.S. Standard Atmosphere, No Winds

2116.

41	0	0								
0.	1.	2.	3.	4.	5.	6.	7.	8.	9.	
10.	11.	12.	13.	14.	15.	16.	17.	18.	19.	
20.	21.	22.	23.	24.	25.	26.	27.	28.	29.	
30.	31.	32.	33.	34.	35.	36.	37.	38.	39.	
80.										
59.0	55.5	51.9	48.3	44.7	41.1	37.6	34.0	30.5	26.9	
23.4	19.8	16.2	12.7	9.1	5.5	2.0	-1.6	-5.1	-8.7	
-12.3	-15.8	-19.4	-22.9	-26.5	-30.0	-33.6	-37.2	-40.7	-44.3	
-47.8	-51.4	-54.9	-58.5	-62.1	-65.6	-69.2	-69.7	-69.7	-69.7	
-69.7										

Line by line description of this file:

1. Title of the atmospheric profile.
 2. The ambient pressure at the ground in psf.
 3. The number of temperatures, number of X wind values and Y wind values. In this file, there are no wind values.
 - 4-8. Altitudes measured from sea level in kilofeet at which temperatures will be defined.
 - 9-13. Temperatures in degrees Fahrenheit at each of the altitudes defined in lines 4-8.
- If the file contained wind values, the altitudes and values for the X and Y winds would follow the temperature data.

Trajectory File, .TRJ File

Straight flight, no acceleration

.12000000476837D+01 .00000000000000D+00

0. 0. 20000. 0. .00 .00

.00000000000000D+00 .00000000000000D+00 .00000000000000D+00

.00000000000000D+00 .00000000000000D+00 .00000000000000D+00

TADVANCE

5.

TADVANCE

5.

TADVANCE

5.

TADVANCE

5.

TADVANCE

5.

TADVANCE

5.

TADVANCE

5.

Line by line description of this file:

1. Title of the trajectory file.
2. The initial Mach number and time.
3. The initial x, y position in feet, altitude in feet, latitude in degrees north, heading angle in degrees clockwise from north, and climb angle in degrees up from the horizontal.
4. The first derivative of the Mach number, heading angle, and climb angle.
5. The second derivative of the Mach number, heading angle, and climb angle.
- 6-19. Set of "advance time" specifications for which the trajectory is projected forward in time in seconds to a new location. In this case, each TADVANCE line moves the trajectory ahead 5 seconds.

Contour/Isopemp File

This file contains three distinct sections. The first information listed is the trajectory path of the aircraft. Line one lists the number .0, the number of trajectory points, another 0, and the traj states the list is a trajectory path. The numbers that follow are the x, y trajectory points in feet.

.0	24	0	traj
.0		.0	
-941.0		.0	
-1884.0		.0	
-2825.0		.0	
-3778.0		.0	
-4744.0		.0	
-5723.0		.0	
-6716.0		.0	
-7722.0		.0	
-8741.0		.0	
-9774.0		.0	
-10821.0		.0	
-11881.0		.0	
-12954.0		.0	
-14041.0		.0	
-15141.0		.0	
-16256.0		.0	
-17383.0		.0	
-18525.0		.0	
-19680.0		.0	
-20849.0		.0	
-22031.0		.0	
-23228.0		.0	
-24452.0		.0	

The next section of the contour/isopemp file lists the isopemps. The first line contains the number .0, the number of points in the particular isopemp, index of isopemp, and the pemp states the list is an isopemp. The numbers that follow are the x, y isopemp points in feet. This information is repeated for every isopemp created during the trajectory.

.0	15	9	pemp
-47031.0		8469.0	
-45584.0		7023.0	
-44460.0		5700.0	

-43600.0	4467.0
-42966.0	3299.0
-42529.0	2176.0
-42274.0	1081.0
-42190.0	.0
-42274.0	-1081.0
-42529.0	-2176.0
-42966.0	-3299.0
-43600.0	-4467.0
-44460.0	-5700.0
-45584.0	-7023.0
-47031.0	-8469.0

The final section of the contour/isopemp file lists the contours. The first line contains the contour values, the number of points in the contour, index of the contour, and the psf states the list is in pounds per square foot. The numbers that follow are the x, y contour points in feet. This information is repeated for every contour the user specified to plot.

.9	21	1	psf
-95016.4	-23455.2		
-94446.1	-24873.2		
-90420.9	-25007.5		
-61544.0	-20068.1		
-57192.1	-16709.4		
-52713.9	-13502.0		
-48746.8	-10069.7		
-47671.3	-8510.6		
-44974.2	-5726.4		
-43410.1	-3314.7		
-42595.2	.0		
-43410.1	3314.7		
-44973.9	5726.4		
-47670.9	8510.6		
-48746.3	10069.6		
-52711.9	13500.5		
-57191.1	16709.2		
-61541.9	20067.6		
-90347.6	24994.8		
-94395.3	24859.9		
-94997.3	23446.7		

Signature File

```

Tac = 20.000 sec, Phi = .00 deg, Carpet boom
Pmax, Pmin = 2.87, -2.87 psf, Tg = 57.310 sec, Xg, Yg = .00, 59.72 kf
Lpk = 136.8 dB, Lft = 123.3 dB, CSEL = 112.5 dB, ASEL = 96.8 dB
NPTS = 200      Loud = 111.7 PLdB
  Time, msec      P, psf
.5650198E+02      .0000000E+00
.6044397E+02      .2871399E+01
.7095598E+02      .2402601E+01
.7621198E+02      .2168201E+01
.8672397E+02      .1699401E+01
.9197997E+02      .1465001E+01
.9723596E+02      .1230602E+01
.1077480E+03      .7618017E+00
.1130040E+03      .5274016E+00
.1182599E+03      .2930016E+00
.1235159E+03      .5860157E-01
.1314000E+03      -.2929984E+00
.1366560E+03      -.5273985E+00
.1419120E+03      -.7617985E+00
.1524240E+03      -.1230598E+01
.1576800E+03      -.1464998E+01
.1629360E+03      -.1699398E+01
.1734481E+03      -.2168198E+01
.1787041E+03      -.2402597E+01
.1892161E+03      -.2871396E+01
.1931580E+03      .0000000E+00

```

Line by line description of this file:

1. Trajectory time, phi value, and type of sonic boom.
2. Maximum and minimum overpressure in psf, ground arrival time, and x, y arrival location of the respective ray.
- 3-4. Various metrics of the signature including C- and A- weighted sound exposure level and loudness.

The rest of the file contains a list of the signature in pressure values in psf over time in milliseconds. One point to mention concerning signature files is that more points are calculated than are given. The list that is shown is an excerpt from an existing signature file.

Main Output File, .OUT File

```

F-22 data
.50 .500 500.0 5.00 1.90
0. 0. 20000. .00 -47.00 47.00
1.2000 .0000 .0000 47.88
.0000000000D+00 .0000000000D+00 .0000000000D+00
.0000000000D+00 .0000000000D+00 .0000000000D+00
-47.00
GROUND INTERCEPT =
37108. 76491. 0. 80.779 .43516 .89700 -.07759
GROUND BOOM SIGNATURE
4
.00 .000
.00 1.714
151.32 -1.714
151.32 .000

```

Line by line description of this file:

1. Title of the case.
 2. This line contains numerical parameters that have no relevance to the present research.
 3. x, y position in feet, altitude in feet, trajectory time in seconds, and carpet bounding values of phi in degrees.
 4. Aircraft Mach number, climb angle in degrees up from the horizontal, heading angle in degrees clockwise from north, and the no-wind cutoff value of phi.
 5. First derivative of the Mach number, heading angle, and climb angle.
 6. Second derivative of the Mach number, heading angle, and climb angle.
 7. Phi value
 - 8-9. These lines list the x, y, z intersection of the ray with the ground in feet, arrival time of the ray with the ground in seconds, and the x, y, z components of the ray-direction unit vector at the ground. This is the unit vector that is used to calculate the local ground Mach number.
 - 10-15. Here, the type of sonic boom, the number of points in the signature, and lines containing the defining times in milliseconds and pressures in psf of the waveform.
- The .OUT file shown above is an excerpt from an existing file. A complete file would repeat lines 2-6 for every trajectory time and lines 7-15 for every phi value.